

**DEVELOPMENT OF PULSED FIBRE LASERS AND
SUPERCONTINUUM LIGHT SOURCE BASED ON
NONLINEAR EFFECT**

ARMAN ZAREI

**THESIS SUBMITTED IN FULFILLMENT OF THE
REQUIREMENT FOR THE DEGREE OF
DOCTOR OF PHILOSOPHY**

**DEPARTMENT OF ELECTRICAL ENGINEERING
FACULTY OF ENGINEERING
UNIVERSITY OF MALAYA
KUALA LUMPUR**

2015

UNIVERSITI MALAYA

ORIGINAL LITERARY WORK DECLARATION

Name of Candidate: ARMAN ZAREI

(I.C/Passport No: H95658835)

Registration/Matric No: KHA120034

Name of Degree: DOCTOR OF PHILOSOPHY

Title of Project Paper/Research Report/Dissertation/Thesis ("this Work"):

DEVELOPMENT OF PULSED FIBRE LASERS AND SUPERCONTINUUM LIGHT SOURCE BASED ON NONLINEAR EFFECT

Field of Study: Photonics

I do solemnly and sincerely declare that:

- (1) I am the sole author/writer of this Work;
- (2) This Work is original;
- (3) Any use of any work in which copyright exists was done by way of fair dealing and for permitted purposes and any excerpt or extract from, or reference to or reproduction of any copyright work has been disclosed expressly and sufficiently and the title of the Work and its authorship have been acknowledged in this Work;
- (4) I do not have any actual knowledge nor do I ought reasonably to know that the making of this work constitutes an infringement of any copyright work;
- (5) I hereby assign all and every rights in the copyright to this Work to the University of Malaya ("UM"), who henceforth shall be owner of the copyright in this Work and that any reproduction or use in any form or by any means whatsoever is prohibited without the written consent of UM having been first had and obtained;
- (6) I am fully aware that if in the course of making this Work I have infringed any copyright whether intentionally or otherwise, I may be subject to legal action or any other action as may be determined by UM.

Candidate's Signature

Date

Subscribed and solemnly declared before,

Witness's Signature

Date

Name:

Designation:

ABSTRACT

This thesis aims to investigate and demonstrate the generation of different types of pulse lasers and supercontinuum (SC) light based on nonlinear effects. At first, Brillouin fiber laser (BFL) is demonstrated using a long piece of Single mode fiber (SMF), Erbium-doped fiber (EDF) and highly nonlinear fiber (HNLF) as the gain medium. With 10 km long SMF, the BFL exhibits temporal characteristics where the pulse width and repetition frequency of the laser are obtained at 440 μ s and 2 kHz, respectively. The Brillouin Erbium fiber laser (BEFL) also shows a self-pulsing characteristic with repetition rates of 66.7 kHz while mode-locked BFL is obtained by replacing the SMF with a 100m-long HNLF. Several passively mode-locked and Q-switched fiber lasers are then demonstrated based on nonlinear effects inside the ring laser cavity. For instance, a nanosecond optical pulse operating in fundamental mode is successfully generated in the EDF laser (EDFL) cavity by incorporating a 100 m long HNLF based on nonlinear polarization rotation (NPR) technique. The laser operates at 1567.2 nm and produced a pulse train with a repetition rate of 1.56 MHz, pulse width of 297 ns and the maximum pulse energy of 1.4 nJ. SC generation is then demonstrated by launching Q-switched mode-locking (QML), continuous-wave mode-locking (CWML) and dark pulse trains into various nonlinear fibers. With the amplified QML laser, the SC ranging from 1350 nm and 1900 nm has been successfully generated in 100 m long HNLF. With the amplified dark pulse, SC ranging from 1200 nm to 1810 nm, 1200 nm to 1920 nm and 1480 nm to 1740 nm are produced with the use of 50 m long photonic Crystal fiber (PCF), 100 m long HNLF and 20 km long PCF, respectively. Pulsed lasers have many applications in micromachining while super-continuum light sources are very useful for spectroscopy, frequency metrology, device characterization and medical science.

ABSTRAK

Tesis ini bertujuan untuk menyiasat dan mendemonstrasi generasi pelbagai jenis laser denyut dan cahaya super-kontinum (SC) berdasarkan kesan tak-linear. Pada mulanya, laser gentian Brillouin (BFL) didemonstrari menggunakan sekeping panjang gentian SMF, gentian Erbium-didopkan (EDF) dan gentian sangat tak-linear (HNLF) sebagai medium gandaan. Dengan SMF 10 km panjang yang mempamerkan ciri-ciri BFL sementara, masing-masing lebar denyut dan frekuensi kekerapan laser yang diperolehi adalah $440 \mu\text{s}$ dan 2 kHz. Laser gentian Brillouin Erbium (BEFL) ini juga menunjukkan ciri-ciri berdenyut sendiri dengan kadar pengulangan 66.7 kHz manakala mod-kunci BFL diperolehi dengan menggantikan SMF dengan HNLF 100m panjang. Beberapa pasif mod-kunci dan gentian laser Q-suis kemudian didemonstrasi berdasarkan kesan tak-linear dalam rongga cincin laser. Sebagai contoh, satu denyutan optik nano-saat beroperasi dalam mod asas berjaya dijanakan dalam rongga laser EDF (EDFL) dengan menggabungkan HNLF 100 m panjang berdasarkan teknik putaran polarisasi tak-linear (NPR). Laser beroperasi pada 1567,2 nm dan menghasilkan rantaian denyut dengan kadar pengulangan 1.56 MHz, lebar denyut 297 ns dan tenaga denyut maksimum 1.4 nJ. Generasi SC kemudian menunjukkan dengan melancarkan Q-suis mod-kunci (QML), gelombang selanjur mod-kunci (CWML) dan rantaian denyut gelap ke dalam pelbagai gentian tak-linear. Dengan QML laser yang dikuatkan, SC terdiri daripada 1350 nm dan 1900 nm telah berjaya dijana dalam HNLF 100 m panjang. Dengan rantaian denyut yang dikuatkan, SC terdiri daripada 1200 nm hingga 1810 nm, 1200 nm hingga 1920 nm dan 1480 nm hingga 1740 nm, masing-masing dihasilkan dengan menggunakan PCF 50 m panjang, HNLF 100 m panjang dan PCF 20 km panjang. Laser berdenyut mempunyai banyak aplikasi dalam pemesinan mikro, manakala sumber cahaya super-kontinum sangat berguna untuk spektroskopi, kekerapan metrologi, peranti pencirian dan sains perubatan.

ACKNOWLEDGEMENT

I would like to express my greatest gratitude to my supervisor, Prof. Dr. Sulaiman Wadi Harun for the continuous support, motivation, patience and knowledge throughout my Ph.D study. I have been extremely lucky to have a supervisor who cared so much about my work, and who responded to my questions and queries so promptly. Besides Prof. Dr. Sulaiman Wadi Harun, I would like to thank my co-supervisor Prof. Dr. Harith Ahmad for his advices.

My special thanks should go to the member of Photonics Research Center, Tiu Zian Cheack, Dr. Ali Abdulhadi Jasim, Muneswaran Suthaskumar and all the photonics members for their assistance as well as support throughout my research.

To my wife, parents and siblings, thank you for your endless love and continuous support. I also wish to record my heartfelt thanks to my parents for showing great understanding in allowing me and supporting me all the way till I completed my research works.

Lastly, I wish to convey my heartfelt thanks to everyone who had helped me directly or indirectly with my research.

TABLE OF CONTENTS

ABSTRACT	iii
ABSTRAK	iv
ACKNOWLEDGEMENT	v
TABLE OF CONTENTS	vi
LIST OF FIGURES	ix
LIST OF TABLES	xiii
LIST OF SYMBOLS AND ABBREVIATIONS	xiv
CHAPTER 1 INTRODUCTION	1
1.1 History Overview	1
1.2 Overview of pulsed lasers and motivation of the study	3
1.3 Thesis Objectives	6
1.4 Thesis layout	6
1.5 Original Contributions	8
CHAPTER 2 LITERATURE REVIEW ON NONLINEAR EFFECTS FOR PULSED LASER AND SUPERCONTINUUM LIGHT SOURCE	10
2.1 Understanding Nonlinear Optics	10
2.2 Stimulated Brillouin Scattering (SBS)	13
2.3 Optical Kerr effect and SPM	17
2.4 Birefringence	19
2.5 Nonlinear Polarization Rotation	20
2.6 Pulsed Laser	21
2.6.1 Q-switching	22
2.6.2 Mode-locking	24
2.6.3 NPR based fiber lasers	26

2.6.4 Soliton pulse	29
2.6.5 Dark soliton	33
2.7 Supercontinuum generation	34
CHAPTER 3 INVESTIGATION OF STIMULATED BRILLOUIN SCATTERING FOR PULSE GENERATION	37
3.1 Introduction	37
3.2 SBS generation in 10 km long SMF and a few cm long microfiber	38
3.2.1 SBS in 10 km long SMF	39
3.2.2 Brillouin Scattering in microfiber	41
3.3 Spectrum and temporal characteristics of BFL	53
3.4 Brillouin Erbium fiber laser	59
3.5 Generation of nanosecond pulse with highly nonlinear fiber (HNLF) based on SBS	68
3.5.1 Configuration of the proposed mode-locked BFL	68
3.5.2 The performance of the nanosecond mode-locked BFL	69
3.6 Summary	72
CHAPTER 4 DEVELOPMENT OF PULSED LASER BASED ON NONLINEAR EFFECTS	74
4.1 Introduction	74
4.2 Harmonic mode-locked EDFL based on NPR effect in a ring laser cavity with assistance from a 10 km long single-mode fiber	75
4.3 Generation of nanosecond pulse with a HNLF	82
4.4 Q-switched EDFL with HNLF in NOLM cavity	87
4.4.1 Configuration of the proposed NOLM cavity	88
4.4.2 Q-switching performance	89

4.5 Q-switched Brillouin fiber laser with MWCNT SA	92
4.5.1 SA preparation and experimental setup	94
4.5.2 Characteristics of SA	96
4.5.3 Performance of the Q-switched BFL	99
4.6 Summary	105
CHAPTER 5 SUPERCONTINUUM GENERATION	107
5.1 Introduction	107
5.2 SC generation by a continuous wave mode-locked and Q-switched mode-locked fiber lasers	108
5.2.1 Experimental arrangement	109
5.2.2 Performance of QML and CWML EDFLs	110
5.2.3 Performance of the SC generation	116
5.3 Enhance SC generation with picosecond dark pulse	119
5.3.1 Experimental arrangement	120
5.3.2 Performance of the dark pulse and SC generations	121
5.4 Summary	125
CHAPTER 6 CONCLUSION AND FUTURE WORK	127
6.1 Conclusion	127
6.2 Future Outlooks	132
REFERENCES	133
LIST OF PUBLICATIONS	145
APPENDIX	146

LIST OF FIGURES

Figure 2. 1 Classification of nonlinear effects in optical fiber	13
Figure 2. 2 Schematic diagram of the SBS process in an optical fiber	14
Figure 2. 3 Spectrum of reflected light from a long piece of SMF when the BP wavelength is fixed at 1550 nm.	15
Figure 2. 4 Nonlinear polarization rotation of an ellipse as it propagates through a Kerr medium.	21
Figure 2. 5 Operation principle of NPR	27
Figure 2. 6 Transmittivity due to NPR with different PC settings	29
Figure 2. 7 The plot of bright soliton with $\gamma=1f$ (Jonsson, 2003)	32
Figure 2. 8 The shape of $ A(z,t) ^2$ dark soliton (Jonsson, 2003)	34
Figure 3.1: Experimental setup for generating Brillouin scattering in the backward direction. I_p and I_s denote the intensities of the pump and Brillouin signal lights, respectively.	40
Figure 3. 2 : The reflection spectrum are demonstrated in different input power. BP reflection is due to BP Rayleigh scattering whereas the Brillouin Stokes (BS) and anti-Stokes waves are generated by Brillouin scattering and degenerate four-wave mixing process, respectively.	41
Figure 3. 3: Microscopic image for the fabricated non-adiabatic microfiber.	43
Figure 3. 4: The experimental setup for investigating the generation of Brillouin Stokes signal in both adiabatic and non-adiabatic microfibres.	44
Figure 3. 5: The transmission spectra of the ASE for the three samples.	45
Figure 3. 6: The spectra of the launched BP and the back propagating Brillouin Stokes for the three microfiber samples.	46
Figure 3. 7: The fabricated IMZI structure (a) schematic diagram and (b) microscopic images for the three tapered regions of IMZI, where the images (i), (ii) and (iii) represent the 2nd tapered region, interferometer region and 1st tapered region respectively.	49
Figure 3. 8: The transmission spectra of the ASE for the IMZI.	50
Figure 3. 9: The spectra of the back propagating Brillouin Stokes for the IMZI and sample 2.	50
Figure 3. 10: The SpBS with different launched BP power.	52
Figure 3. 11: The spectra of the back propagating Brillouin Stokes for different fiber length, where the red and blue colors represent SMF with length of 200 m and 20 km respectively and the green color represent sample 2 of the non-adiabatic microfiber	52
Figure 3. 12: Schematic diagram of the BFL using a 10 km long SMF as the gain medium	54
Figure 3. 13: Output spectra of the BFL at various pump powers.	55

Figure 3. 14: The output peak power of the BFL against the BP at three different output couplers.	56
Figure 3. 15: Temporal characteristic of the BFL at different BP power (a) 1.2 dBm, (b) 1.4 dBm (c) 1.6 dBm (d) >1.8 dBm	58
Figure 3. 16: The pulse width and Stokes peak power characteristic at different ratio of BP power to the threshold pump power	59
Figure 3. 17: Configuration of the proposed BEFL	61
Figure 3. 18: Output spectrum from the BEFL and BFL	62
Figure 3. 19: a) Output spectra of the BEFL at various 1480 nm pump power. b) Inset shows the peak power of the laser against the input 1480 nm pump power.	64
Figure 3. 20: The Stokes peak power against the BP power for both BEFL and BFL	65
Figure 3. 21: The output spectrum of the BEFL at different BP wavelengths	66
Figure 3. 22: Oscilloscope trace from the BEFL and BFL	67
Figure 3. 23: Schematic configuration of the proposed nanosecond BFL	69
Figure 3. 24: Output spectra of the BFL configured with HNLF at various BP power	70
Figure 3. 25: Typical pulse train of the proposed nanosecond BFL	71
Figure 3. 26: The RF spectrum of the nanosecond pulse BFL	72
Figure 4. 1: Experimental setup of the proposed EDFL for generating harmonic nanosecond pulses.	77
Figure 4. 2: Typical pulse train at different pump powers, which produces a different orders of harmonic (a) fundamental (b) 2nd (c) 3rd	79
Figure 4. 3: RF spectrum of the generated fundamental harmonic pulse	81
Figure 4. 4: Output spectra of the nanosecond pulses at different order of harmonics.	82
Figure 4. 5: Configuration of the passively mode-locked EDFL with a HNLF	83
Figure 4. 6: Typical output spectrum of the nanosecond pulse laser	84
Figure 4. 7: Typical pulse train of the nanosecond mode-locked EDFL	85
Figure 4. 8: Single pulse envelope	86
Figure 4. 9: RF spectrum of the nanosecond mode-locking pulse showing a SNR of around 50 dB.	86
Figure 4. 10: Schematic configuration of the proposed Q-switched EDFL	88
Figure 4. 11: Q-switched pulse emission of the proposed EDFL at different pump power	90
Figure 4. 12: Output spectrum of the NOLM based Q-switched EDFL.	91
Figure 4. 13: The change of repetition rate and pulse width against pump power.	91
Figure 4. 14: Average output power and pulse energy of the laser against pump power	92

Figure 4. 15: Schematic configuration of the proposed-switched BFL	95
Figure 4. 16: FESEM image of the prepared MWCNTs-PVA film	97
Figure 4. 17: Raman spectrum obtained from the MWCNTs-PVA film	97
Figure 4. 18: Transmission spectrum of the MWCNTs-PVA film	98
Figure 4. 19: Linear transmission curve of the MWCNTs-PVA film, which shows that the saturable absorption and non saturable absorption of around 4% and 45%, respectively	98
Figure 4. 20: Output spectrum of the proposed Q-switched BFL with MWCNTs-PVA SA	100
Figure 4. 21: Output peak power of the BFL against the BP power with and without the MWCNTs-PVA SA in the laser cavity.	100
Figure 4. 22: The typical oscilloscope trace from the BFL configured without the SA at two different BP powers; 1.0 and 5.0 dBm.	102
Figure 4. 23: Typical pulse train of the Q-switched BFL at three different BP powers of 5.0, 5.5 and 6.0 dBm	104
Figure 4. 24: The RF spectrum of the Q-switched BFL at BP power of 5.5 dBm.	104
Figure 5. 1: Schematic diagram of experimental setup used for generating SC with QML EDFL. 200 m long SMF is incorporated in the ring EDFL's cavity to change the pulse train output from QML to CWML.	110
Figure 5. 2: Output spectrum of the QML laser at pump power of 145 mW.	111
Figure 5. 3: Temporal characteristic of the QML laser (a) Typical pulse train at pump power of 145 mW, showing the Q-switching repetition rate of 49 kHz (b) A single pulse envelop with mode-locking repetition rate of 9.4 MHz.	112
Figure 5. 4: Autocorrelation trace of the QML output pulse	113
Figure 5. 5: RF spectrum of the QML pulse at pump power of 145 mW.	113
Figure 5. 6: Output spectrum of the CWML pulse laser, which is obtained before being launched into EDFA.	115
Figure 5. 7: Typical pulse train of the CWML pulse.	115
Figure 5. 8: RF spectrum of the CWML pulse at pump power of 145 mW	116
Figure 5. 9: SC spectra from the QML EDFL at various pump power	117
Figure 5. 10: SC spectra from the CWML EDFL at various pump power	118
Figure 5. 11: Comparison of SC generation between QML and bright pulse at the maximum pump power of 18.0 dBm	119
Figure 5. 12: Experimental setup to investigate the SC generation with a dark pulse	121
Figure 5. 13: Typical dark pulse train obtained from the mode-locked EDFL	122
Figure 5. 14: Output spectrum from the mode-locked EDFL at pump power of 145 mW.	123

Figure 5. 15: AC Sech2 pulse curve fitting with resolution of 100 fs.	123
Figure 5. 16: RF spectrum of the dark pulse soliton at pump power of 145 mW.	124
Figure 5. 17: Supercontinuum spectra at three different gain media using the amplified dark pulse soliton.	125

LIST OF TABLES

Table 3. 1: Geometrical parameters of the microfibre samples

43

LIST OF SYMBOLS AND ABBREVIATIONS

A_{eff}	Effective area
L_{eff}	Effective length
β_2	Group velocity dispersion parameter
I	Light intensity
α	Nonlinear coefficient
n_2	Nonlinear refractive index
n	Refractive index
P_{th}	Threshold Pump
T	Transmittivity of light
λ	Wavelength
AC	Auto-correlator
ASE	Amplified Spontaneous Emission
BEFL	Brillouin Erbium Fiber Laser
BFL	Brillouin Fiber Laser
BP	Brillouin Pump
BS	Brillouin Spacing
BP	Brillouin Pump
Cir	Circulator
CW	Continuous Wave
DCF	Dispersion Compensating Fiber
DWDM	Dense Wavelength Division Multiplexing
EDF	Erbium Doped Fiber
EDFA	Erbium Doped Fiber Amplifier
FWHM	Full Width Half Maximum
FWM	Four-Wave Mixing
GVD	Group Velocity Dispersion
HNLF	Highly Nonlinear Fiber
IMZI	Inline microfiber Mach–Zehnder interferometer

NLSE	Nonlinear Schrödinger Equation
NPR	Nonlinear Polarization Rotation
NZ-DSF	Non-zero Dispersion Shifted fiber
OSA	Optical Spectrum Analyzer
OSC	Oscilloscope
OSNR	Optical Signal to Noise Ratio
OTDM	Optical Time Division Multiplexing
PCF	Photonic Crystal Fiber
RFSA	Radio Frequency Spectrum Analyzer
SA	Saturable Absorber
SBS	Stimulated Brillouin Scattering
SEM	Scanning Electron Microscope
SMF	Single Mode Fiber
SNR	Signal to Noise ratio
SOA	Semiconductor Optical Amplifier
SPM	Self Phase Modulation
SRS	Stimulated Raman Scattering
TDM	Time Division Multiplexing
TLS	Tunable Laser Source
WDM	Wavelength Division Multiplexing
XPM	Cross Phase Modulation

CHAPTER 1

INTRODUCTION

1.1 History Overview

The first laser was realized by Maiman (Maiman, 1960) based on a ruby crystal pumped by a Xenon flash discharge. It was a laser pulse with pulse duration ranging from microsecond to millisecond. Later that year, Javan(Javanet al., 2013) demonstrated the first Helium-Neon (He-Ne) laser operating in continuous wave (CW) mode. Other researchers saw the potential in Maiman's work and decided to take steps in furthering this research. They began incorporating different substrates and rare-earth ions such as Erbium, Neodymium, Ytterbium, Holmium, Praseodymium and even Uranium. This leads to the invention of the Neodymium – Yttrium Aluminum Garnet (Nd-YAG) laser in 1964 (Geusic et al., 1964).

In 1961 Hellwarth (Hellwarth, 1961) proposed the concept of Q-switching, a process in which the laser is forced to emit pulses with duration on the order of several times the round trip propagation time of light in the laser cavity. Then, the proposal of achieving shorter pulses came using the concept of mode-locking. By constructive interference, a short pulse is formed when many longitudinal modes are held in phase in a laser resonator. There are various techniques that have been employed, usually are grouped under two categories active and passive mode-locking. Active mode-locking uses a modulator inside the laser resonator, whereas passive scheme uses a saturable absorber to lock the relative phase. The first active mode-locking of He-Ne laser was demonstrated by Hargrove et. al. (Hargrove et al., 1964) in 1964. Shortly after, in 1965, Mocker and Collins (Mocker et al., 1965) showed the first passive mode-locking laser using a saturable dye in ruby laser cavity. The first pulses shorter than 1 ps were obtained by Shank and Ippen (Shank et al., 1974) in 1974. They demonstrated the first femtosecond

pulses using a tunable broad gain dye laser media in combination with a saturable dye absorber.

The concept of a fiber laser was firstly proposed and demonstrated by Snitzer in 1961 (Snitzer, 1961). Early works on fiber lasers was mainly focused on Neodymium-doped multimode fibers, which operate at 1060 nm region. Since then, fiber lasers have always been an active research area but did not really attract much attention until the late 1980s after low loss rare-earth-doped fibers were demonstrated (Poole et al., 1985). Since that time Erbium doped fiber lasers (EDFLs) have received much attention because of the lasing wavelength of 1550 nm, which coincides with the low loss window of standard fiber. The first CW EDFL was reported by Mears et. al. (Mears et al., 1986) based on a three level energy system at room temperature. They also demonstrated the first Q-switched operating of an EDFL producing 60 ns pulse using an intra-cavity acousto-optic modulator. Development in the field of EDFL has been continuously growing since the first demonstration in the mid-80s. The performance and pulse characteristics of EDFLs have been significantly improved, by employing various cavity configurations (Desurvire, 2002) and mode-locking techniques (Haus, 2000).

The achievable pulse width and energy from a fiber laser are not nearly equal to that of a Ti-Sapphire laser, however they do have many advantages that have motivated significant research over the past 20 years. Among the numerous advantages of fiber lasers are low losses and possibility of pumping with compact and efficient diodes. The fiber itself provides the waveguide; hence the need for bulk optics is minimized. These lasers are also easily mode-locked because of an enhancement of fiber nonlinearities due to high intensities and long interaction length. Fiber lasers are compact, robust and inexpensive source of ultra-short pulses with numerous applications in field of optics.

1.2 Overview of pulsed lasers and motivation of the study

Lasers operating in CW or quasi-CW mode have limited optical output power, depending on the maximum available pump power. The laser peak output power can be improved by concentrating the available energy in a single, short optical pulse, or in a periodic sequence of optical pulses as in a Q-switched fiber laser. Q-switching is a technique for obtaining energetic optical pulse at repetition rate in kHz region and pulse width in a range of microseconds to nanoseconds by sudden switching of the cavity loss. Compared to CW fiber lasers, high-peak-power Q-switched fiber lasers are practically useful in numerous applications, such as range finding, remote sensing, medical surgery and industrial processing (Kennedy et al., 2004; McGrath et al., 1998; Zajac et al., 2004). Although Q-switching does not produce the ultra-short pulses as in mode-locked lasers, it has several advantages such as inexpensive, easy to implement and efficient in extracting energy stored in upper laser level.

Mode-locking is a technique in optics by which a laser can be made to produce pulses of light of extremely short duration, on the order of nanosecond (10^{-9} s), picoseconds (10^{-12} s) or femtoseconds (10^{-15} s). The basis of the technique is to induce a fixed phase relationship between the longitudinal modes of the laser's resonant cavity. The laser is then said to be phase-locked or mode-locked. Interference between these modes causes the laser light to be produced as a train of pulses. Depending on the properties of the laser, these pulses may be of extremely brief duration, as short as a few femtoseconds.

Pulsed lasers have numerous applications in both research and industry and their uses are expected to broaden. These applications vary depending on wavelength, power and pulse width. Short pulse duration and high peak powers are the two main characteristics of ultra-short laser pulses that have been useful in the analysis of materials. They allow for time resolved experiments in which the transient response of materials

can be observed on an ultra-short pulse scale. Fabrication of passive integrated optical devices is another area in which pulse lasers are being employed. Ultra short pulse lasers have been shown to directly induce large refractive index changes in glasses and other dielectric materials. Hence they have been used for fabrication of optical devices, such as optical waveguides (Hirao et al., 1998) and Bragg grating (Kawamura et al., 2000)

With the imminent arrival of practical, compact and cost effective pulsed laser sources, real world application of ultrashort laser pulses in communications systems has become very likely. Short pulse lasers are ideal for use as sources in all optical switching based on the third order nonlinear Kerr effect, as they provide the large intensities that are required (Asobe et al., 1996). The large spectral bandwidth offered by short pulse lasers also make them an ideal light source for wavelength division multiplexed (WDM) and time division multiplexed (TDM) networks. (Mikulla et al., 1999)

There are various methods that can be adopted to generate pulsed laser to suit different applications. These include the active and passive pulsing techniques. An external modulator is required to electronically synchronize to the cavity repetition rate for the active technique while for the passive technique this external synchronization is not needed but rather uses an all optical nonlinear process in a laser resonator. The construction of active technique for Q-switching and mode-locking can be considered complex, complicated and bulky with the employment of external modulator. For passive method, the mechanism used is by generating saturable absorption action. One can use real saturable absorbers (SAs) or can also exploit the artificial SAs. Real SAs are such as semiconductors and the newly discovered carbon nanotubes (CNTs) and graphene while the most prominent artificial SA is called nonlinear polarization rotation (NPR). The benefits of passive over active mode-locking is for its simple and compact construction, cost efficiency, robustness and ultra-short pulse generation (Sotor et al., 2012).

Recently, nonlinear polarization rotation (NPR) technique has been widely used to provide an artificial SA effect especially in mode-locked fiber ring laser (ZC Luo et al., 2009). The components needed to construct NPR based oscillator are polarization sensitive element (polarizer and polarization tuning component) and a segment of nonlinear fiber to allow an intensity dependent transmission for pulse generation. The self-started mode-locking phenomenon occurs in a way similar to real SAs, where light of higher intensity undergoes less absorption loss at the polarizer upon selecting the appropriate light polarization at the polarizer. The advantage of the NPR technique is its ultra-fast response, whereby it can produce ultra-short femtosecond pulse (Deng et al., 2009) in the stretched pulse region. Wu et al. reported on the generation of nanosecond pulses directly from a mode-locked erbium-doped fiber laser (EDFL) with NPR technique (Wu et al., 2009) .

Moreover, NPR techniques are flexible and can be applied in all-fiber configurations, as polarizing fiber isolators and fiber polarization controllers are widely available. However, most of the fiber lasers generate bright pulses. Besides the bright pulses, there are also the dark pulses, which having a temporary drop in laser intensity with respect to the laser background level (H. Zhang et al., 2009). Recently, these pulses have also attracted the attention of researchers who strive to understand the mechanism of laser pulse oscillation and evolution from their unconventional behavior. Furthermore, dark pulses display other advantages such as being less affected by intra pulse-stimulated Raman scattering, less sensitive to fiber loss than bright pulses, and having better stability in long-distance communications with respect to the Gordon–Haus jitter (Kivshar et al., 1994).

This PhD work is intended to explore several passive pulsing approaches based on nonlinear effects to generate different Q-switching and mode-locking pulse profiles. In this thesis, at first, we demonstrate self-pulsing characteristic in a Brillouin fiber lasers

(BFL). We also demonstrate various bright and pulse emissions in EDFL based on NPR technique. The newly developed Q-switched and mode-locked fiber lasers are then employed to generate super-continuum (SC) light source using various nonlinear fibers as the gain medium. The SC generation is defined as an extreme spectral broadening induced by the coupling of a high peak power pulse laser in a nonlinear optical fiber. It has been a hot topic in recent years due to its potential applications in a variety of areas such as surgery (Zajac et al., 2004), optical communication (Palais, 1988) and sensing (Kaminski et al., 2008).

1.3 Thesis Objectives

As discussed in the previous section, pulsed fiber lasers and supercontinuum light sources are indeed important devices for optical communication, sensor industries and medical diagnostics. There is great incentive to develop a new generation of pulse lasers and super-continuum light that are compact, robust and easy to operate. The main objective of this thesis is realize and study practical pulsed fiber lasers and super-continuum light source by utilizing various nonlinear effects in optical fibers. To achieve this, several objectives have been outlined to guide the research direction:

1. To study SBS effect for generating pulsed laser.
2. To demonstrate both Q-switched and mode-locked fiber lasers based on nonlinear effects such as SBS and NPR techniques.
3. To generate super-continuum using various type of pulse profiles such as the Q-switched mode-locking, nanosecond and dark soliton pulses, which were obtained based on NPR technique.

1.4 Thesis layout

Although several interesting concepts were investigated and many experiments carried out in the laboratory, only the issues directly related to the objective of the project

will be discussed, therefore limiting the writing to six brief chapters. This thesis aims to comprehensively demonstrate the generation of pulsed laser and super-continuum generation based on nonlinear effects.

Chapter 2 provides a brief discussion of laser theory, various nonlinear effects in optical fibers, principle of NPR, NPR based fiber lasers and principle of SC generation. These literatures are relevant to the experimental part of the thesis. The stimulated Brillouin scattering (SBS) effect in optical fibers and self-pulsing characteristic in Brillouin fiber lasers are presented.

In Chapter 3, at first, we investigate on the SBS phenomenon in both single mode fiber and microfiber. The temporal characteristic of both Brillouin fiber laser (BFL) and Brillouin Erbium fiber laser (BEFL) is then demonstrated. A nanosecond mode-locked BFL is also demonstrated using an SBS effect in a highly nonlinear fiber (HNLF).

In Chapter 4, several passively mode-locked and Q-switched fiber lasers are demonstrated based on nonlinear effects inside the ring laser cavity. At first, the NPR based mode-locked EDFL with three switchable operation states is proposed and demonstrated by incorporating a 10 km long SMF in the ring cavity. Then, a nanosecond optical pulse generation is demonstrated in EDFL by using a 100 m long HNLF instead of the SMF. The HNLF plays an important role to induce Kerr effect in the cavity, which allows the polarization rotation occur in the cavity. This allows a mode-locking pulse is generated based on NPR technique. A Q-switched EDFL is also demonstrated based on nonlinear optical loop mirror (NOLM) cavity. The NOLM is used in the laser cavity to generate the intensity dependent transmission so that it functions as a saturable absorber. Finally, a Q-switched BFL is demonstrated using multi-walled carbon nanotubes (MWCNTs) embedded in polyvinyl alcohol (PVA) film as a passive saturable absorber. The performances of these lasers (NPR-based EDFL and BFL) are compared in terms of threshold pump power, pulse stability, complexity of cavity and ease of implementation.

Chapter 5 focuses on generating SC spectrum using various type of pulse profiles, which are obtained using the newly developed mode-locked fiber lasers. A mode-locked EDFL with dark pulse output is also proposed and demonstrated for realizing a simple optical fiber-based supercontinuum source. Finally, chapter 6 summarizes the findings for this PhD work.

1.5 Original Contributions

The major contributions of this research work are summarized below:

1. Demonstration of SBS effect in both SMF and microfiber.

It is found that the microfiber geometry, which determines the amount of acoustic modes' irritation inside the device, plays an important role in both SBS generation and gain bandwidth broadening. Nevertheless, the short length of non-adiabatic microfibers (in millimeters) retains the relative advantages of design simplicity and lower cost in generation of SBS.

2. Development of a new type of pulsed laser based on SBS self-pulsing:

BFL and BEFL behave as a pulsed laser when the pump power is set slightly above the SBS threshold power due to relaxation oscillation. As the pump power increases, it transforms from pulsed laser to continuous wave (CW) laser. A BFL with a mode-locking characteristic is also demonstrated using a HNLF as a Brillouin gain medium in conjunction with relaxation oscillation technique.

3. Demonstration of NPR fiber laser using a long SMF and short HNLF.

A nanosecond harmonic pulse laser source operating with ultra-low repetition rate was demonstrated by inserting a 10 km long SMF in the ring cavity. The SMF plays an important role to induce Kerr effect in the cavity, which allows the polarization rotation occur in the cavity. This allows a mode-locking pulse is generated based on NPR technique. Then, a nanosecond optical pulse generation was demonstrated in the

similar EDFL cavity by replacing the SMF section with a 100 m long HNLF. The laser operated at 1567.2 nm and produced a pulse train with a constant repetition rate of 1.56 MHz and pulse width of 297 ns.

4. Demonstration of Q-switching NPR fiber laser.

To improve the pulse energy, a Q-switched EDFL was also demonstrated based on NOLM cavity. The NOLM was used in the laser cavity to generate the intensity dependent transmission so that it functions as a saturable absorber.

5. Development of a Q-switched BFL.

A Q-switched BFL was successfully demonstrated using MWCNTs embedded in PVA film as a SA. The SA was obtained by sandwiching the developed MWCNTs–PVA film between two FC/PC fiber connectors after depositing index matching gel onto the fiber ends.

6. Demonstration of SC generation.

The performance of SC generation in QML and CWML EDFLs, which was amplified by an EDFA as pump source was investigated. A SC generation based on dark pulse was also demonstrated in three different fiber spools in a passively mode locked EDFL.

CHAPTER 2

LITERATURE REVIEW ON NONLINEAR EFFECTS FOR PULSED LASER AND SUPERCONTINUUM LIGHT SOURCE

2.1 Understanding Nonlinear Optics

Nonlinear optics deals mainly with various new optical effects and novel phenomena arising from the interactions of intense coherent optical radiation with matter. A light wave consists of electric and magnetic fields varying sinusoidally at high frequencies (Buck, 2004). When light propagates through matter it induces motion of the charged particles that constitute the material. In a dielectric medium the charges are bound together and will start to oscillate in the applied electric field; they form oscillating electric dipoles. The contribution from the magnetic field part of the light and from electric quadruples is much weaker and is usually neglected. This is called the electric dipole approximation. The oscillating dipoles add up to a macroscopic polarization P which is used to describe the response of the material. For low light intensities, i.e. small amplitudes of the electric field E , the charges can follow the field almost exactly and the relationship between E and P is essentially linear. For larger amplitudes the motion of the particles will be distorted and nonlinear terms will become important. The origin of nonlinear optics can be uncovered by recalling Maxwell's equations, which are a set of laws governing light-matter interaction (Boyd, 2003; Buck, 2004; Jackson et al., 1962).

$$\nabla \cdot \vec{D} = \rho_f \quad (2.1)$$

$$\nabla \cdot \vec{B} = 0 \quad (2.2)$$

$$\nabla \times \vec{E} = -\frac{\partial \vec{B}}{\partial t} \quad (2.3)$$

$$\nabla \cdot \vec{H} = \vec{J}_f + \frac{\partial \vec{D}}{\partial t} \quad (2.4)$$

where \vec{D} and \vec{B} are electric and magnetic flux densities, \vec{E} and \vec{H} are electric and magnetic field vectors, ρ_f is the free charge density, and \vec{J}_f is the current density vector. In a non-magnetic medium ($\mu = \mu_0$), the magnetic flux densities is related to the magnetic field vector according to $\vec{B} = \mu_0 \vec{H}$, where μ_0 is the permeability of free space. The electric displacement field can be expressed in terms of the electric field and the induced polarization \vec{P} according to

$$\vec{D} = \epsilon_0 \vec{E} + \vec{P} \quad (2.5)$$

where ϵ_0 is the electric permittivity of free space.

These equations can be used to drive the wave equation by first taking the curl of both sides of Eq. (2.3). The left hand side of the resulting equation can be simplified using the following identity

$$\nabla \times (\nabla \times \vec{E}) = \nabla(\nabla \cdot \vec{E}) - \nabla^2 \vec{E} \quad (2.6)$$

and assuming the free charge density to be zero. The right hand side of the resulting equation can be simplified by recalling the relationship between the magnetic induction and the magnetic in free space and invoking equation (2.4). The free current density is assumed to zero. Using Eq. (2.5) and noting that although the divergence of the electrical field is not identically zero, it is nearly so, the wave equation for a dielectric medium then takes following form

$$\nabla^2 \vec{E} - \mu_0 \epsilon_0 \frac{\partial^2 \vec{E}}{\partial t^2} = \mu_0 \frac{\partial \vec{P}}{\partial t^2} \quad (2.7)$$

The electric field can also be used in conjunction with the susceptibility tensors $\chi^{(n)}$ to define the induced polarization as follows (Boyd, 2003);

$$\vec{P} = \epsilon_0(\chi^{(1)} \cdot \vec{E} + \chi^{(2)} : \vec{E}\vec{E} + \chi^{(3)} : \vec{E}\vec{E}\vec{E} + \dots) \quad (2.8)$$

The order of each susceptibility tensor is denoted by the superscript n . The first order susceptibility tensor $\chi^{(1)}$ is associated with several of the linear properties of a material, including the index of refraction and absorption. While the second order susceptibility $\chi^{(2)}$ is the lowest nonlinear susceptibility responsible for second-order nonlinear effects such as second harmonic generation and sum-frequency generation. The third order nonlinear susceptibility tensor $\chi^{(3)}$ is connected to many other optical phenomena, including stimulated Raman scattering (SRS), stimulated Brillouin scattering (SBS), and self-phase modulation (SPM)(Boyd, 2003).

Fig. 2.1 shows the classification of nonlinear effects in optical fibers. It is divided into two main effects: nonlinear refractive index and elastic scattering effects. Fiber nonlinearity along transmission path causes inter mixing of the optical subcarriers and it has three different effects, namely four-wave mixing (FWM), cross-phase modulation (XPM) and SPM. The two main nonlinear effects in the inelastic scattering are SBS and SRS. These scattering causes the optical field to transfer a part of its energy to the nonlinear medium. They can be explained quantum-mechanically as scattering of an incident light photon to a lower energy photon called Stokes photon by generating an acoustic phonon in SBS and optical phonon in SRS with energy equal to the energy reduction of the initial photon. The main difference between the two is the type of interval mode involved. SRS involves non propagating collective modes as optical phonons in the medium whereas SBS involves low frequency propagating acoustic wave phonons in the medium. Another fundamental difference is that SBS occurs only in the backward direction which is the opposite direction with respect to the incident light. However, SRS is able to occur in both forward and backward directions although it dominates in the

forward direction where it is in the same direction as the incident light. The other difference is that the downshifted scattered light is about 10 GHz for SBS but 13 THz for SRS with respect to the incident light frequency in SMF. Finally, the Brillouin gain spectrum is less than 100 MHz bandwidth which is very narrow in comparing with Raman gain spectrum bandwidth which is more than 20 to 30 THz (Bloembergen, 1996).

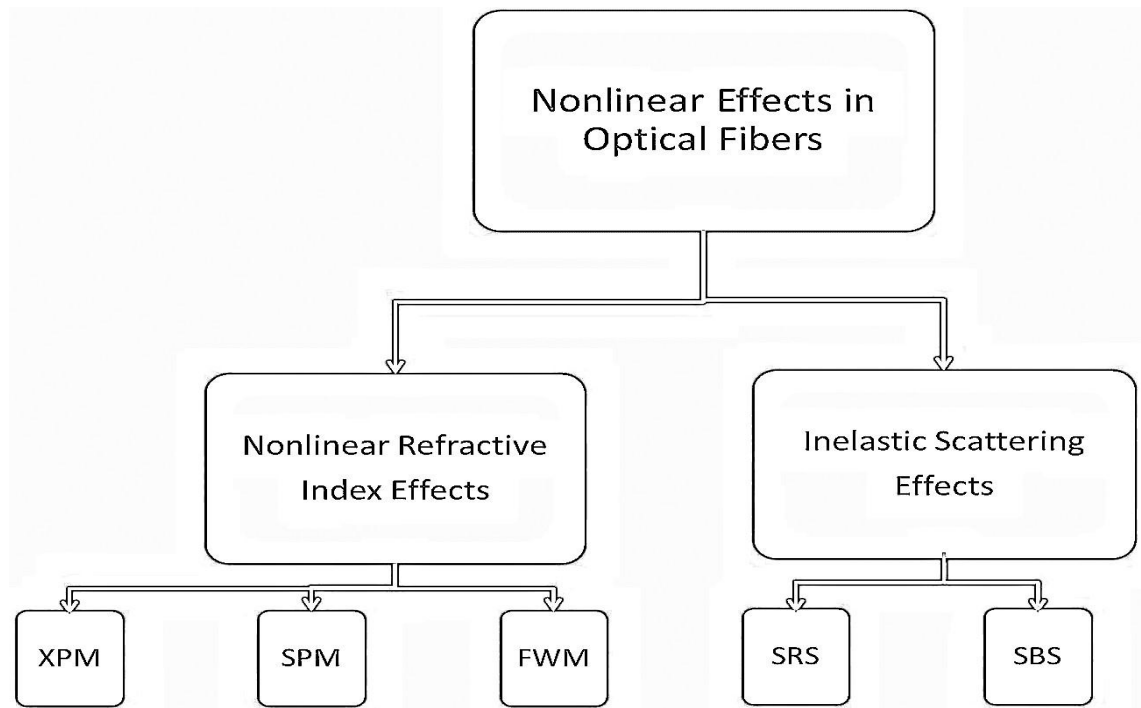


Figure 2. 1 Classification of nonlinear effects in optical fiber

2.2 Stimulated Brillouin Scattering (SBS)

When a narrow line width laser radiation is propagated through a long piece of optical fiber, a part of the light is seen to scatter in the backward direction when the power exceeds a certain limit (G. P. Agrawal, 2007). This nonlinear phenomenon is referred Stimulated Brillouin Scattering (SBS) (Ruffin, 2004) and it occurs at power as low as a few *mW* in the small core of a single-mode fiber (SMF). As the pump power reaches the threshold level, it generates acoustic vibration in a nonlinear medium or optical fiber. The acoustic wave generated by the optical power affects the density of the material and thus changes its refractive index. This refractive index fluctuation can scatter light to generate

a Stokes wave whose frequency is downshifted from an incident pump light by the amount set by the nonlinear medium. The scattered light is downshifted in frequency, because of the Doppler shift associated with a grating moving at the acoustic velocity (Cotter, 1983). The working principle of SBS can be explained as illustrated in Fig. 2.2.

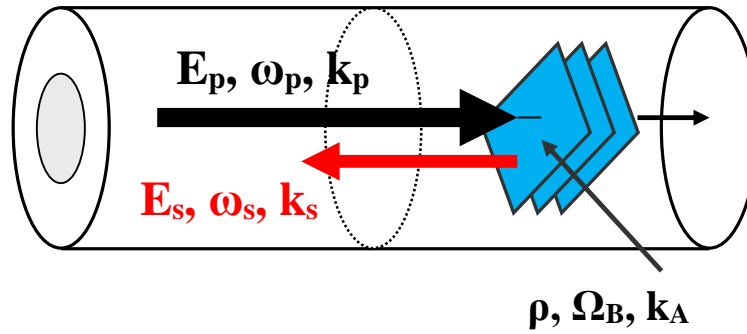


Figure 2. 2 Schematic diagram of the SBS process in an optical fiber

As shown in Fig. 2.2, the characteristic of SBS is strongly on the density ρ , frequency Ω_B and the wave vector k_A of the acoustic wave. Since the energy and momentum are conserved during the scattering events, the frequencies and wave vectors of the pump light, scattered light, and acoustic fields are given by following equations;

$$k_A = k_P - k_S \quad (2.9)$$

$$\Omega_B = \omega_P - \omega_S \quad (2.10)$$

where ω_P and ω_S are the frequencies, and k_P and k_S are the wave vectors, of the pump and Stokes waves, respectively. The frequency Ω_B and the wave vector k_A of the acoustic wave satisfy the standard dispersion relation

$$\Omega_B = v_A |k_A| \approx 2v_A |k_p| \sin(\theta/2), \quad (2.11)$$

where v_A is the speed of sound in the medium and θ is the angle between the pump and Stokes fields. However, in a single-mode fiber the relevant θ values are 0 and π . Hence, SBS occurs only in the backward direction with the Brillouin shift given by

$$v_B = \Omega_B / 2\pi = 2nv_A / \lambda_p \quad (2.12)$$

where n is the modal index or refractive index of fiber core at the pump wavelength λ_p (G. P. Agrawal, 2007; Mills, 1991).

Since the scattering occurs in backward direction, the angle θ is π . By using $v_A = 5.96 \text{ km/s}$ and $n = 1.45$ as typical values for silica fibers, the shift is found to be 11 GHz or 0.08 nm at 1550nm region based on Equation (2.12). Fig. 2.3 shows the example of the SBS signal reflected from a long piece of silica fiber. The peak at the lower wavelength is a reflected BP signal, which is caused by the combination of Rayleigh scattering as well as the spurious reflections from connectors and splice joints. The Stokes signal due to the SBS is obtained at a longer wavelength, which is 0.08 nm shifted from the BP signal. Anti-Stokes is obtained in the shorter wavelength as shown in Fig. 2.3.

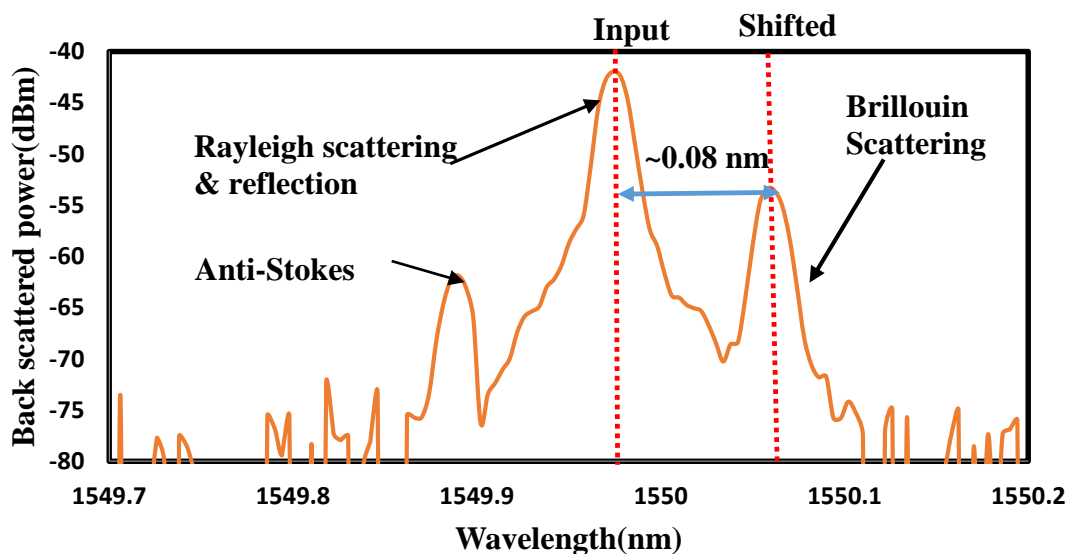


Figure 2. 3 Spectrum of reflected light from a long piece of SMF when the BP wavelength is fixed at 1550 nm.

The Brillouin gain spectrum, $g_B(\nu)$, which has a Lorentzian spectral shape can be also determined by (G. P. Agrawal, 2007; Mills, 1991);

$$g_B(\nu) = \frac{(\Delta\nu_B/2)^2}{(\nu - \nu_B)^2 + (\Delta\nu_B/2)^2} g_B(\nu_B) \quad (2.13)$$

where $\Delta\nu_B$ is the 3dB spectral bandwidth that is related inversely to the decay time of acoustic phonons (~ 100 ns). The peak value of the Brillouin gain coefficient at $\nu = \nu_B$ can be evaluated using the following equation,

$$g_B(\nu_B) = \frac{2\pi n^7 p_{12}^2}{c \lambda_p^2 \rho_0 v_A \Delta\nu_B} \quad (2.14)$$

where p_{12} is the longitudinal electro-optic coefficient, ρ_0 is the density of the material and λ_p is the pump wavelength. The typical value of g_B for pure silica core fibre is $g_B = 5 \times 10^{-11} \text{ m/W}$. Both the Brillouin shift ν_B and the gain bandwidth $\Delta\nu_B$ can vary from fiber to fiber because of the presence of dopants in the fiber core (G. P. Agrawal, 1997).

The development of SBS in optical fibers is governed by a set of two coupled equations as follows (G. Agrawal, 2001):

$$\frac{dI_s}{dz} = \alpha_s I_s - g_B(\Omega) I_p I_s \quad (2.15)$$

$$\frac{dI_p}{dz} = -(\alpha_p I_p + g_B(\Omega) I_p I_s) \quad (2.16)$$

where the absorption coefficients α_s and α_p account for the fiber loss at the Stokes and pump frequencies, respectively. Two simplifications can be made because of the fact that the Brillouin shift is relatively small, as $\omega_p \approx \omega_s$ it follows that $\alpha_p \approx \alpha_s = \alpha$. We also assume that the Stokes and pump are co-polarized. If we assume that the pump is so intense compared with the Stokes, the pump depletion is neglected. Hence, the Stokes

intensity inside the fibre is found to grow exponentially in the backward direction where I_0 is the pump intensity at $z = 0$ according to the relation.

$$I_s(0) = I_s(L) \exp(g_B P_0 L_{eff} / A_{eff} - \alpha L) \quad (2.17)$$

We used $P_0 = I_p(0)A_{eff}$, where P_0 and L are the input pump power and length, respectively. In Eq. (2.14) the Stokes signal incident at $z = L$ grows in the backward direction as a result of SBS. In the case of a pump laser with a Lorentzian spectral profile, the Brillouin threshold can be written (G. P. Agrawal, 2007) as,

$$P_{th}(mW) \cong \frac{21A_{eff}}{g_B(\nu_B)L_{eff}} \left(1 + \frac{\Delta\nu_p}{\Delta\nu_B}\right) \quad (2.18)$$

where $\Delta\nu_p$ is the frequency linewidth of the pump, $\Delta\nu_B$ is the spontaneous Brillouin linewidth. However, the Brillouin threshold, by a good approximation, is summarized by;

$$g_B(\nu_B)P_{th} \frac{L_{eff}}{A_{eff}} \approx 21 \quad (2.19)$$

Using $g_B = 5 \times 10^{-11}$ m/W and $A_{eff} = 50 \mu m^2$ as typical values, the threshold power P_{th} for the SBS onset can be as low as 1 mW for CW signals in the wavelength region near 1.55 μm (Abedin, 2005).

2.3 Optical Kerr effect and SPM

Most of the nonlinear effects in optical fibers originate from nonlinear refraction, a phenomenon that refers to the intensity dependence of the refractive index. This effect is known as the optical Kerr effect. The intensity dependent refractive index derives from the third order susceptibility and is given by (2.8)

$$n(I) = n_0 + n_2 I \quad (2.20)$$

where n_0 is the linear refractive index, $I \sim |E|^2$ is the optical intensity and n_2 is the nonlinear coefficient (the optical Kerr coefficient). Many phenomena arise from the linear variation of refractive index with intensity; one of particular interest to the work in this thesis is SPM.

The intensity dependent refractive index has a direct effect on the spectrum of any optical pulse, because the pulse has a time varying intensity (G. P. Agrawal et al., 1989). The propagation of a pulse described by the slowly varying amplitude approximation is given by

$$E(L, t) = \frac{1}{2} [A(L, t) e^{j(\omega_0 t - KL)}] \quad (2.21)$$

where $A(L, t)$ is the slowly varying envelope and L is the length of the Kerr medium.

Further $KL = \frac{2\pi(n_0 + n_2 I(t))}{\lambda_0} L = \frac{2\pi n_0 L}{\lambda_0} + \frac{2\pi n_2 I(t) L}{\lambda_0}$; the second term represents the nonlinear phase shift caused by SPM.

SPM is a phenomenon that leads to spectral broadening of optical pulses as a result of the time dependent nonlinear phase shift. A temporally varying phase implies that the instantaneous optical frequency differs across the pulse. The time dependence of the different frequencies can be viewed as a frequency chirp. The chirp is induced by SPM and increases in magnitude with propagation distance (Lamminpää, 2003). In other words, new frequency components are continuously being generated as the pulse propagates down the fiber. These generated frequency components broaden the spectrum over its initial width. The maximum nonlinear phase shift experienced by a pulse is given by

$$\phi_{NL}^{max} = \frac{2\pi n_2 I_0 L}{\lambda_0} \quad (2.22)$$

where L is the propagating distance, λ_0 is the center wavelength, and I_0 is the peak intensity of the pulse. The maximum amount of spectral broadening for a pulse of duration τ_0 is given by (Boyd, 2003)

$$\delta\omega_{max} \cong \frac{\phi_{NL}^{max}}{\tau_0} \quad (2.23)$$

Phase modulation can be converted into intensity modulation, for example by using a difference between self modulated phase of two polarization components as a wavelength retarder placed between crossed polarizers.

SPM is often accompanied by cross phase modulation (XPM), a phenomenon that leads to coupling between two or more incident waves or modes through the fiber nonlinearity. This occurs because the effective refractive index of a wave depends not only on the intensity of that wave but also on the intensity of other co-propagating waves (G. P. Agrawal, 2007).

2.4 Birefringence

A single mode fiber is not truly single mode; even a perfectly cylindrical single mode fiber supports two degenerate polarization modes. Small departures from a perfect cylindrical geometry or small fluctuations in the material anisotropy results in these modes becoming slightly non-degenerate. Therefore, in practice a fiber supports two direction. Mathematically, the mode-propagation constant become a slightly different for modes polarized in the X and Y directions. This is referred to as modal birefringence. The degree of modal birefringence B is defined by (G. P. Agrawal, 2007)

$$B = K_0 |n_x - n_y| \quad (2.24)$$

where $K_0 = 2\pi/\lambda$, n_x and n_y are the effective mode indices in the two orthogonal polarization states. The axis along which the effective mode index is smaller is called the

fast axis, as the group velocity is larger for light propagating in that direction. Similarly the axis with the larger mode index is called the slow axis.

The relative strength of the birefringence is described by the beat length. The length of period in which the polarization state is reproduced. The beat length is given by Eq. (2.25) and for standard SMF fiber this length is approximately 2 – 10 *m* at 1550nm.

$$L_B = \frac{2\pi}{B} \quad (2.25)$$

Elliptically polarized light can be resolved into its right and left hand circulator polarization components of different intensities. If the light input to a fiber is elliptically polarized, XPM induces nonlinear coupling between *X* and *Y* electric field components creating nonlinear birefringence, which changes the state of polarization. This phenomenon is referred to as nonlinear ellipse rotation since it is manifested as a rotation of the polarization ellipse (Duling III, 2006).

2.5 Nonlinear Polarization Rotation

Since the refractive index depends on the intensity of light, elliptically polarized light sees an induced birefringence the index is slightly higher for polarization along the major axis of the ellipse. This holds back the phase of that component of the E-field, and alters the ellipse slightly. The effect is to tilt the major axis of the ellipse slightly as shown in Fig. 2.4. The effect is continuous, since there is now a new birefringence along a new major axis. The net effect is that high intensity elliptically polarized light in a Kerr medium experiences a continuous rotation of the major axis of the ellipse. This is called Kerr ellipse rotation or nonlinear polarization rotation (NPR).

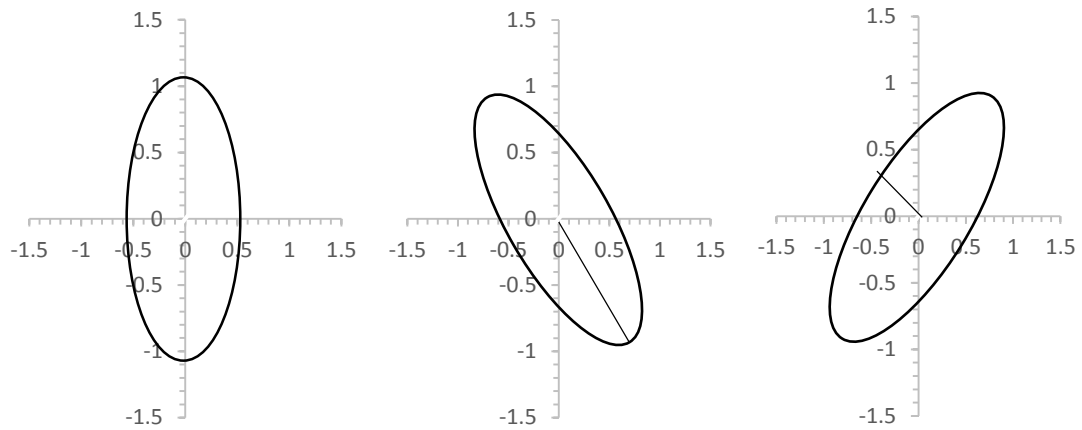


Figure 2. 4 Nonlinear polarization rotation of an ellipse as it propagates through a Kerr medium.

Another way to look at this is in terms of the right and left hand circularly polarized light. Consider an elliptically polarized light made up of a strong right-hand circular light and somewhat weaker left-hand circular light. The right circular light will see a slightly larger index of refraction than the left, thus the right circular component will steadily drop back in phase, relative to the left circular component. The result is a slow rotation of the polarization ellipse as the light propagates (Boyd, 2003).

2.6 Pulsed Laser

Lasers can be classified into two categories based on its operating conditions. A continuous wave (CW) laser is where its output power runs continuously over time while the output power of a pulsed laser is due to light emission in the form of optical pulses. In a CW laser, the laser modes usually oscillate in random phase and have unbalanced amplitudes. Generally, there are two common methods to produce pulsed laser which are Q-switching and mode-locking. Depending on the wavelength requirements such as pulse duration, pulse repetition rate and pulse energy, different methods to generate various types of pulses. Details of these techniques are presented in the following sub-sections.

2.6.1 Q-switching

One of the common practices to produce pulsed laser is Q-switching. Q-switched laser is a device to which the technique of active or passive Q-switching is applied, so that it emits high-energy pulses (Spühler et al., 1999). In Q-switching, cavity losses are high in the beginning until the gain medium has stored high energy by increasing input pump power. After that the losses in the cavity are reduced to extremely low values which enables the cavity to increase the power of laser radiation and thus pulsed laser is generated (Siegman, 1986) . By decreasing the optical loss, Q-factor of the cavity will be increased.

$$Q = 2\pi\nu_0 \left(\frac{W}{\text{Energy lost per second}} \right) \quad (2.26)$$

where ν_0 is the central frequency of the laser and W is the energy stored in the cavity. Energy loss per second is given by $\frac{\delta W C}{nL}$, where δ is the energy loss rate for single path propagation of light in the cavity, L is the length of the resonator, n is refractive index of the medium and c is the light velocity. Thus, the equation (2.26) can be simplified as

$$Q = 2\pi\nu_0 \frac{W}{\delta W c/nL} = \frac{2\pi nL}{\delta \lambda_0} \quad (2.27)$$

where λ_0 laser central wavelength in the vacuum. From equation (2.27) it is clearly observable that the Q value is inversely proportional to the resonator loss (δ) when the value of λ_0 and L are definite. The conditions for light oscillations in the laser cavity can be summarized as follows:

- a) If the loss (δ) is high, the Q value will be low and will require a higher threshold, which in turn makes it difficult for oscillation to be initiated.

b) If the loss (δ) is small, the Q value which is inversely related to the loss (δ) will be higher and thus requires a lower threshold, thereby oscillation will be easily initiated. It is also evident from equation (2.27) that to change the threshold of the laser, we could change the Q value or the loss (δ) will be higher and thus require a low threshold, oscillation will be easily initiated.

Active Q-switching uses external means to control the loss or Q-factor inside the laser cavity. In active Q-switching, the losses of the laser are modulated by employing acousto optic modulator (AOM) (Delgado-Pinar et al., 2006) or electro optic modulator (EOM)(El-Sherif et al., 2003). By inserting the external control element, the output characteristics of the generated pulsed can be controlled. Recently, Huang (Huang et al., 2011) had demonstrated a hybrid technique using AOM and semiconductor saturable absorber (SESAMs) in generating Q-switched pulse laser. They reported an improvement of output pulse in comparison to purely passive Q-switched and purely active Q-switched operation.

In a passively Q-switched laser, no external modulator is needed where the cavity loss is modulated by saturable absorber. Saturable absorber can be exhibited artificially by polarization effect such as nonlinear polarization rotation (NPR)(Degnan, 1995) or real saturable absorber by means of transition metal doped crystals (Pan et al., 2007), SESAMs (Nodop et al., 2007), SWCNTs (Dong et al., 2011; Harun et al., 2012), grapheme (Zhengqian Luo et al., 2010; Popa et al., 2010), graphene oxide (GO)(Lee et al., 2013) and reduced graphene oxide (rGO)(Sobon et al., 2012). The saturable absorber transmission or reflection depends on the light intensity where the low light intensity will be absorbed by the material and the high light intensity will be released depending on the material recovery time.

Compared to mode-locking, Q-switching requires less control of cavity parameters and efficient in terms of cost, operation and implementation. Recently,

tunable fiber laser have been demonstrated using graphene (Popa et al., 2010) and SWCNTs (Zhou et al., 2009) which enable simultaneous wavelength tuning with pulse laser.

2.6.2 Mode-locking

Mode-locking is a powerful technique for obtaining ultra-short pulses ranging from picoseconds to femtoseconds. It is a process in which the longitudinal modes of a laser are forced into phase synchronism. The different modes add constructively in such a way that the laser produces a train of pulses (Siegman, 1986). The numbers of longitudinal modes that can simultaneously lase are dependent on the gain linewidth, $\Delta\nu_g$ and the frequency separation between modes. Under sufficiently strong pumping, we can expect that the number of modes oscillating in the cavity is given by:

$$M = \frac{\Delta\nu_g}{c/2L} = \frac{2L}{c} \Delta\nu_g \quad (2.28)$$

where c is the speed of light and L is the length of a linear cavity. The shortest duration that we can expect to obtain by a given gain linewidth is

$$\tau_{min} = \tau_M = \frac{2L}{cM} = \frac{1}{\nu_g} \quad (2.29)$$

From (equation 2.29) we can conclude that the shortest pulse that can be obtained is a reciprocal of gain linewidth (in Hz) (Milonni et al., 2010)

The laser cavity arrangement for mode-locked laser needs careful design because the dynamics of ultrashort pulse is usually much more complicated than Q-switched pulse as it involves dispersion, SPM, XPM etc. The repetition rate of the laser pulses is determined by the length of the laser cavity, and for laser with ring cavity the relation is given by:

$$\Delta f = \frac{c}{nL} \quad (2.30)$$

where Δf is the repetition rate(Hz), c is the velocity of light in vacuum, n is the refractive index and L is length of cavity. As the round-trip time, T_R , is the inverse of repetition rate, therefore, T_R is given as;

$$T_R = \frac{Ln}{c} \quad (2.31)$$

Depending on the cavity type, under certain conditions, the repetition rate can be some integer multiple of the fundamental repetition rate. In this case, it is called harmonic mode-locking. Typically the repetition rate is in the range of megahertz with shorter pulse width compared to pulse generation by Q-switching method. Mode locking methods can be divided into two main categories: active and passive.

Active mode-locking requires an active element driven by an external electronic signal to modulate the loss inside the fiber cavity. There are two type types of modulators which is amplitude modulation (AM) and frequency modulation (FM). The use of modulator is to provide a high speed pulse train that is an order higher than the fundamental repetition rate. In AM mode locking, the loss cavity is periodically modulated and the pulse is built up at the position having minimum loss in the fiber cavity. The repetition rate reported by applying AM for mode locking is as high as 3.77 GHz (Gupta et al., 2002) FM mode locking is carried out by repeated up or down frequency chirping. After many round trips the pulse is built up and shortened because the chirped light is swept out of the gain bandwidth of the laser. By applying FM to mode locked, the reported repetition rate is about 40 GHz (Nakazawa et al., 1998), with a shorter pulse width compared to AM mode locking.

Passive mode locking is a method that does not require any external trigger when nonlinear element is part of the laser cavity. The characteristic of the output pulse is achieved by using saturable absorber or artificial saturable absorber such as Kerr lens

mode-locking, NPR and additive pulse mode-locking. They are two types of saturable absorbers, which is artificial saturable absorber or real saturable absorber. Apart from the above mentioned techniques, self-pulsing with relaxation oscillation induced by SBS can also seed mode-locking (G. P. Agrawal, 2007). Details on mode-locking techniques that are applied in this study are presented in the following sub-sections.

2.6.3 NPR based fiber lasers

NPR is a phenomenon that is caused by the changes in the polarization direction of light inside the laser cavity due to SPM and XPM as well as to some birefringence of the fiber. It exploits the nonlinear effects in optical fiber, which causes rotation of light in fiber to enable intensity modulation mechanism in the laser cavity. Through appropriately selecting the orientation of the polarizer or the length of the fiber, an artificial saturable absorber effect with ultra-fast response could then be achieved in a fiber laser cavity. The NPR based fiber laser relies on the Kerr effect in an Erbium doped fiber (EDF) in conjunction with an optical isolator to produce a pulse by setting the initial polarization state to elliptical. This elliptical state can be resolved into right and left-hand circular polarization components of different intensities. As a result, an elliptically polarized pulse will have its x and y components experience different phase shifts, thus rotating the polarization ellipse. Since this is a nonlinear process, the polarization rotation depends on the intensity.

The transmission path of NPR is shown in Fig. 2.5, which can be used to explain the working principle of the NPR-based fiber laser. As a linear polarized light leaves the polarizer, it becomes elliptically polarized light after propagating through the polarization controller (van Saarloos et al.). The light can then be resolved into two orthogonal polarized lights, that is E_x and E_y . After passing through the fiber, both E_x and E_y accumulate nonlinear phase shift due to the SPM and XPM effects in the fiber. The angle

of polarization can be changed from α_1 to α_2 as it the light propagates through the fiber. Here, α_1 is the angle between the polarization direction of the input signal and the fast axis of the fiber and α_2 is the angle between the fast axis of the fiber and the polarization direction of the polarizer. Both α_1 and α_2 angles can be adjusted by PCs.

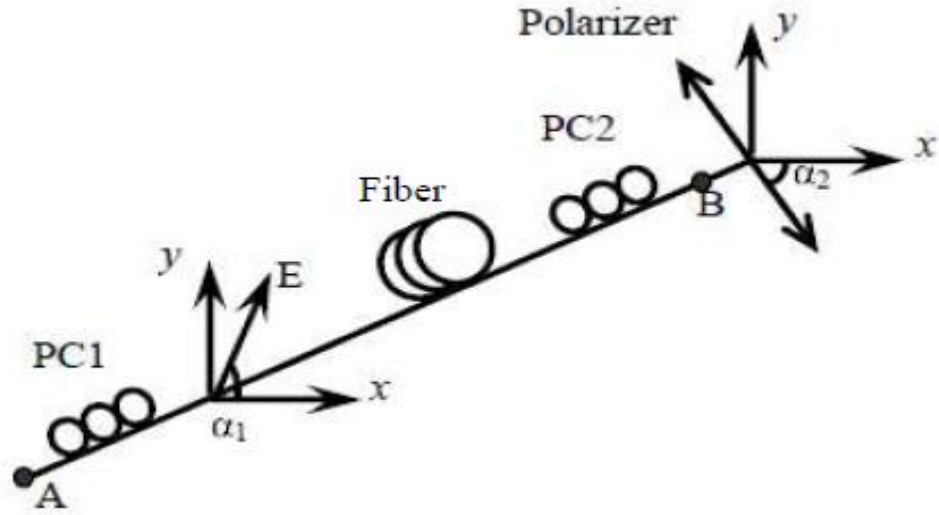


Figure 2. 5 Operation principle of NPR

The light transmission is described using the following equation (Feng et al., 2006; ZC Luo et al., 2009):

$$T = \cos^2\alpha_1\cos^2\alpha_2 + \sin^2\alpha_1\sin^2\alpha_2 + \frac{1}{2}\sin 2\alpha_1\sin 2\alpha_2 \cos(\Delta\varphi_L + \Delta\varphi_{NL}) \quad (2.32)$$

where $\Delta\varphi_L$ is the linear phase shift from modal birefringence and is the nonlinear phase shift contributed by both SPM and XPM effects. $\Delta\varphi_L$ and $\Delta\varphi_{NL}$ are represented by:

$$\Delta\varphi_L = \frac{2\pi L}{\lambda}(n_y - n_x) \quad (2.33)$$

$$\Delta\varphi_{NL} = \frac{2\pi n_2 LP}{3A_{eff}\lambda} \cos 2\alpha_1 \quad (2.34)$$

where n_y and n_x are the refractive indexes of the respective fast and slow axes of the optical fiber, L is the fiber length, λ is the operating wavelength, n_2 signifies the nonlinear refractive index, P is the instantaneous peak power of the input signal while A_{eff} is the effective core area. The angles of α_1 and α_2 can be manipulated by rotating the PC.

When the light transmission (T) is plotted against power (P), two regions of transmittivity, namely region A and region B are obtained as illustrated in Fig. 2.6. Region A is the region where transmittivity increases with power. The combination of PC-fiber-PC-polarizer acts as an artificial saturable absorber that is responsible for mode-locking. PC is adjusted so that only the high intensity light leaves the polarizer while the propagation of low intensity light is prevented. Subsequently, this leads to the formation of train of pulses. In contrast, there is also another region where transmittivity decreases with power (region B). In this region, higher intensity light experiences higher losses. The inhomogeneous loss encountered by the high intensity in region B can be used to suppress mode competition in EDF, thereby allowing generation NPR-based stable multi-wavelength laser with uniform spacing. As can be observed from Eq. (2.33), the transmittivity of system also oscillates with operating wavelength. By adjusting the PC, the polarization of light varies for different wavelengths. As the polarizer only allows certain light polarizations to pass through, the combination of PC-fiber-PC-polarizer provides wavelength dependent loss which permits the laser to oscillate at more than one wavelength at the same time. Additionally, wavelength switching can also be executed by controlling the wavelength dependent loss through the rotation of PC. Fig. 2.6 shows the transmittivity due to different settings of PC.

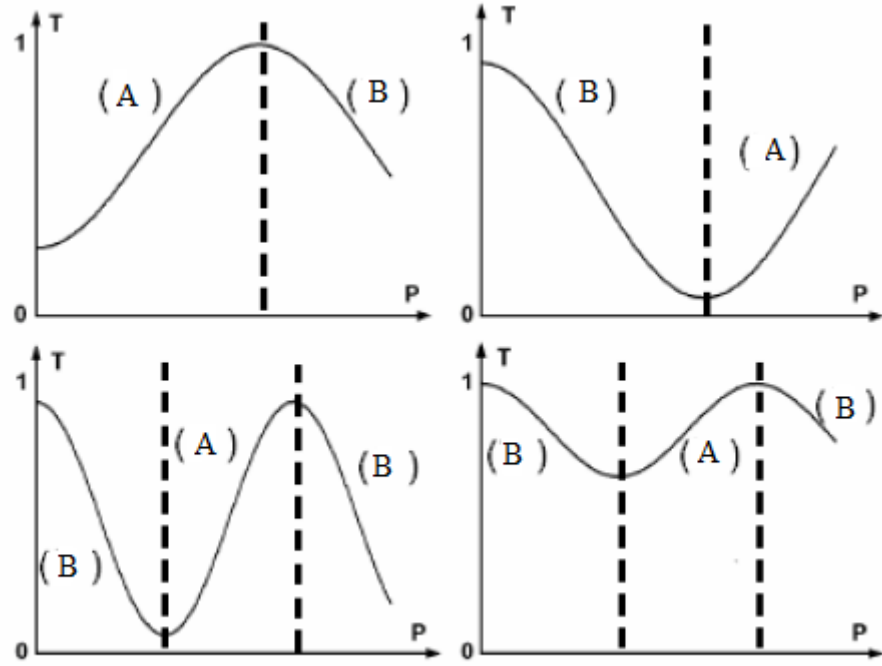


Figure 2. 6 Transmittivity due to NPR with different PC settings

2.6.4 Soliton pulse

Pulse width is influenced by group velocity dispersion (GVD) and SPM. When SPM and GVD (β_2) are balanced, a pulse can propagate in a nonlinear medium without changes in shape. This type of pulse is addressed as the soliton pulse and it is produced under negative cavity GVD ($\beta_2 < 0$). A soliton pulse laser is a promising laser source since its pulse shape is unaltered due to the chirping of both the dispersion and nonlinearity cancelling out each other during propagation. Pulsed laser in a nonlinear dispersive medium, is described by the nonlinear Schrödinger equation (NLSE) as follows (Ghatak et al., 1998):

$$-i \left(\frac{\partial A}{\partial Z} + \frac{1}{v_g} \frac{\partial A}{\partial t} \right) - \frac{\beta_2}{2} \frac{\partial^2 A}{\partial t^2} + \gamma |A|^2 A = 0, \quad (2.35)$$

where

$$\frac{1}{v_g} = \left. \frac{dk}{d\omega} \right|_{\omega=\omega_0} \quad (2.36)$$

$$\beta_2 = \left. \frac{d^2k}{d\omega^2} \right|_{\omega=\omega_0} \quad (2.37)$$

$$\gamma = \frac{1}{2} \omega_0 \epsilon_0 n_0 n_2 \quad (2.38)$$

where γ is responsible for SPM. It is often easier to write Equation (2.35) in a frame moving at the group velocity by making the substitution

$$T = t - \frac{z}{v_g}, \quad (2.39)$$

in which case Eq. (2.35) becomes

$$-i \frac{\partial A}{\partial Z} - \frac{\beta_2}{2} \frac{\partial^2 A}{\partial T^2} + \gamma |A|^2 A = 0, \quad (2.40)$$

In the case of CW radiation, the amplitude A is independent of T at the input end of the fiber at $z = 0$.

Assuming $A(z, t)$ remains time independent during propagation inside the fiber, Eq. (2.40) can be solved to obtain the steady-state solution

$$\bar{A} = \sqrt{P_0} \exp(i\Phi_{NL}) \quad (2.41)$$

where P_0 is the incident power and $\Phi_{NL} = \gamma P_0 z$ is the nonlinear phase shift induced by SPM. Equation 2.41 implies that a CW light is unchanged when it propagates through the fiber, except for acquiring a power-dependent phase shift and for reduction in power due to fiber losses.

A slight perturbation is then introduced to the steady state solution as shown below.

$$A = (\sqrt{P_0} + \alpha)\exp(i\phi_{NL}) \quad (2.42)$$

Examining the evolution of the perturbation $\alpha(z, T)$ using a linear stability analysis by substituting Eq. (2.42) in Eq. (2.40) and linearizing it, we obtain

$$-i \frac{\partial A}{\partial Z} = \frac{\beta_2}{2} \frac{\partial^2 A}{\partial T^2} - \gamma P_0 (\alpha + \alpha'), \quad (2.43)$$

This linear equation can be easily solved in the frequency domain, nevertheless, because of the α' term in the above equation, the Fourier components at frequencies Ω and $-\Omega$ are coupled. Then, we obtain,

$$\alpha(z, T) = a_1 \exp/[iKz - \Omega T] + a_2 \exp/[iKz - \Omega T] \quad (2.44)$$

where K is the wave number of perturbation. Eq. (2.43) and Eq. (2.44) provide a set of two homogenous equations for a_1 and a_2 . This set has a non-trivial solution only when K and Ω satisfy the following dispersion relation

$$K = \pm \frac{1}{2} |\beta_2 \Omega| [\Omega^2 + \text{sgn}(\beta_2) \Omega_c^2]^{1/2} \quad (2.45)$$

where $\text{sgn}(\beta_2) = \pm 1$ depending on the *sign* on β_2 ,

$$\Omega_c^2 = \frac{4\gamma P_0}{|\beta_2|} = \frac{4}{|\beta_2| L_{NL}} \quad (2.46)$$

The nonlinear length L_{NL} is defined as $L_{NL} = 1/\gamma P_0$.because of the factor $\exp(i(\beta_{0z}\omega_0 t))$ have been factored (previously) in

$$E(r, t) = \frac{1}{2} \hat{x}\{F(x, y)A(z, t) \exp[i(\beta_0 z - \omega_0 t)] + c. c\} \quad (2.47)$$

The actual wave number and the frequency of perturbation are $\beta_0 \pm k$ and $\omega_0 \pm \Omega$ respectively. Therefore, the two terms in the equation represent two different frequency components, $\omega_0 + \Omega$ and $\omega_0 - \Omega$, that are present simultaneously.

The dispersion relation shows that steady state stability depends critically on whether light experiences normal or anomalous GVD inside the fiber. The plot of bright soliton with $\gamma = 1$ is shown in Fig. 2.7. In the case of normal GVD ($\beta_0 > 0$), the wave number K is real for all Ω , and the steady state is stable against small perturbations. In the case of anomalous GVD($\beta_0 < 0$), K becomes imaginary for $|\Omega| < \Omega_c$, and the perturbation $\alpha(z, T)$ grows exponentially with z as seen from Equation (2.47) (Dennis et al., 1994; Nelson et al., 1997). As a result, the CW solution Eq. (2.47) is inherently unstable for $\beta_0 < 0$. This instability is referred to as modulation instability. It leads to spontaneous temporal modulation of the CW beam and transforms it into a pulse train (G. P. Agrawal, 2007)

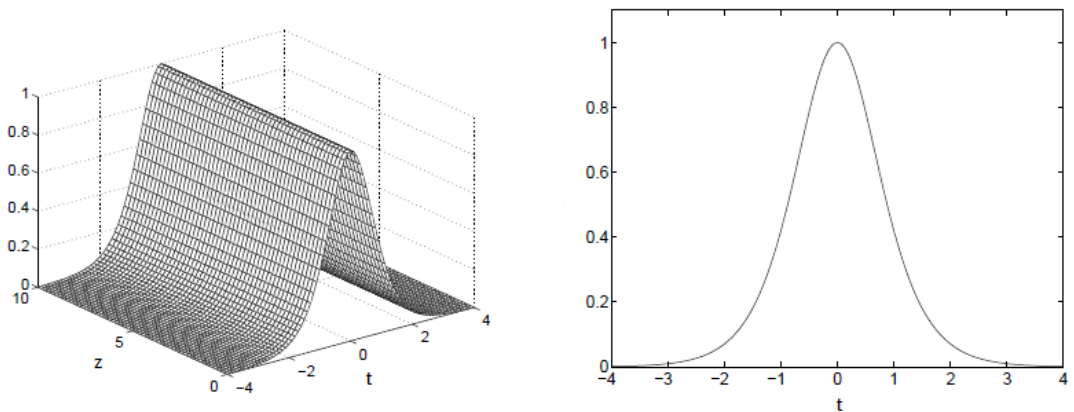


Figure 2. 7 The plot of bright soliton with $\gamma=1$ f (Jonsson, 2003)

2.6.5 Dark soliton

Soliton pulses discussed in the previous sub-section are reported to operate in the bright pulse region. In addition to the bright pulse, fiber lasers can also generate dark solitons that are also a solution of the nonlinear Schrödinger equation (NLSE)(Zakharov et al., 1973). Similar to the case of bright solitons, the inverse scattering method can be used to find dark-soliton solutions of Equation (2.40)

$$\left(-i \frac{\partial A}{\partial Z} - \frac{\beta_2}{2} \frac{\partial^2 A}{\partial T^2} + \gamma |A|^2 A = 0 \right)$$

by imposing the boundary condition that $|A(z, t)|$ tends toward a constant nonzero value for large values of $|t|$. Dark solitons can also be obtained by assuming ($\beta_0 > 0$) for the first order ($\gamma = 1$) (G. P. Agrawal, 2007; Jonsson, 2003):

$$A(z, t) = \tanh(t) e^{iz} \quad (2.48)$$

The shape of $|A(z, t)|^2$ dark soliton is shown in Fig. 2.8. For higher order solitons ($\gamma > 1$) the following closed form expression is used:

$$A(t, z = 0) = \gamma \tanh(t) \quad (2.49)$$

It is a soliton, in the sense that it propagates without changing its shape, but it is not generated by a normal bright pulse. Rather, it is due to lack of energy in a continuous time beam. The intensity is constant, but for a short time during which it jumps to zero and back again, thus generating a “dark pulse”. These solitons can actually be generated to introduce short dark pulses in much longer standard pulses.

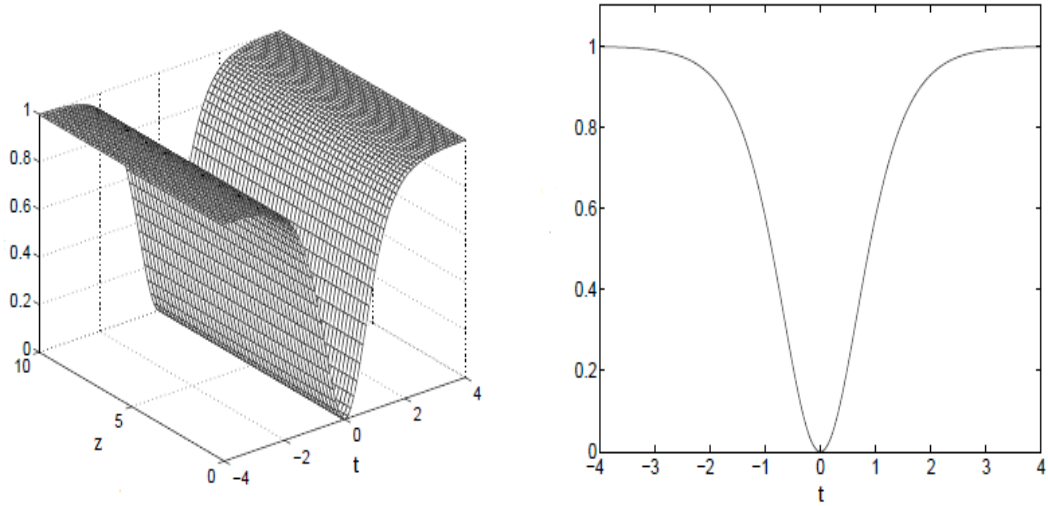


Figure 2. 8 The shape of $|A(z,t)|^2$ dark soliton (Jonsson, 2003)

2.7 Supercontinuum generation

A supercontinuum (SC) is an extreme spectral broadening induced by the coupling of a high peak power pulsed laser in a long nonlinear optical fiber. The interaction between dispersion and nonlinearity exhibits novel phenomena that are responsible for new frequency generation. Microstructure fiber can provide a nonlinearity for a supercontinuum generation. There are several different types of microstructure fibers being used to produce supercontinuum. The most commonly used is highly nonlinear fiber (HNLF), micro fiber and photonic crystal fiber (PCF). It has generated great interest in recent years due to its potential applications in spectroscopy, frequency metrology, device characterization and surgery (Shi, 2007; Wood et al., 2012). Many works have been performed to understand the phenomenon as well as to construct the intended practical devices. The SC generation is dependent on both the pump pulse and the fiber characteristics. A SC can be generated using femtosecond to nanosecond pulses, or even a continuous wave pump where spectral broadening is initiated in the so-called “long pulse” region (Shahabuddin et al., 2012). The dominant nonlinear effects occurring in the generation of a supercontinuum include SRS, FWM and SPM. The

spectral broadening is due to the effect of SPM in cavity, which is significantly enhanced by the incorporation of nonlinear fiber. When a pulse travels into the nonlinear fiber, higher light intensity of the pulse undergoes higher refractive index change compared to its lower light intensity part. The varying refractive index will produce nonlinear phase changes in optical pulse, leading to a change in the pulse frequency spectrum. The Raman self-frequency shift transfers energy from the shorter to longer wavelengths (by about 13 THZ) as the pulse propagates. The FWM process generates new frequency components due to interaction of the primary frequencies. The supercontinuum generation process can be studied by solving the generalized nonlinear Schrödinger equation (NLSE) (G. P. Agrawal, 2007; Kaminski et al., 2008) as shown below;

$$\begin{aligned} & \frac{\partial A}{\partial z} + \frac{1}{2} \left(\alpha + i\alpha_1 \frac{\partial}{\partial t} \right) A + \sum_{m=2}^M i^{m-1} \frac{\beta_m}{m!} \frac{\partial^m A}{\partial t^m} \\ & = i \left(\gamma + i\gamma_1 \frac{\partial}{\partial t} \right) \left(A(z, t) \int_0^\infty R(t') |A(z, t - t')|^2 dt' \right) \end{aligned} \quad (2.50)$$

,where α is the fiber loss and β_m are the coefficients of Taylor-series expansion of the propagation constant β and m represents the order up to which dispersive effects are included. The $m = 1$ term has been removed from Eq. (2.50) by assuming that t represents time in a frame moving at the group velocity of the input pulse. The loss terms can be neglected for a short fiber. The approximation $\gamma_1 \approx \gamma/\omega_0$ is often employed in practice but its use is not always justified. The response function, $R(t)$, may be written as:

$$R(t) = (i - f_R)\delta(t) + f_R h_R(t) \quad (2.51)$$

where $h_R(t)$ is the Raman response function and $\delta(t)$ is frequency shift. Eq. (2.51) has gained successful in modeling most features of supercontinuum spectra observed experimentally by launching ultrashort optical pulses into HNLF (Abeeluck et al., 2004)

CHAPTER 3

INVESTIGATION OF STIMULATED BRILLOUIN SCATTERING FOR PULSE GENERATION

3.1 Introduction

The field of nonlinear fiber optics has gained a tremendous interest since 1990s and has grown considerably recently. It has led to a number of advances important from the fundamental as well as the technological point of view. Nonlinear effects in optical fibers occur due to the interaction of intense light with dielectric material (G. P. Agrawal, 2007). These effects can be classified into two categories. The first category arises due to the interaction of light waves with phonons which causes inelastic scattering phenomenon such as stimulated Raman scattering (SRS) and stimulated Brillouin scattering (SBS). The intensity of scattered light grows exponentially if the incident power exceeds a certain threshold value. The difference between Brillouin and Raman scattering is that the Brillouin generated phonons (acoustic) are coherent and give rise to a macroscopic acoustic wave in the fiber, while in Raman scattering the phonons (optical) are incoherent and no macroscopic wave is generated. The second category is due to the change in the refractive index of the medium with optical intensity, which is responsible for the Kerr-effect. Depending upon the type of input signal, the Kerr-nonlinearity manifests itself in three different effects such as Self-Phase Modulation (SPM), Cross-Phase Modulation (XPM) and Four-Wave Mixing (FWM).

Stimulated Brillouin scattering (SBS) is a nonlinear effect arising from the interaction between the intense pump light and acoustic waves in a medium, giving rise to backward-propagating, frequency-shifted light (G. P. Agrawal, 2007; Shirazi et al., 2008). The thermally excited acoustic waves generate an index grating that co-propagates with the pump light at the acoustic velocity in the medium. This moving grating reflects

the pump light and causes a frequency downshift in the backscattered light due to the Doppler effects. Although this scattering creates problems for some nonlinear signal processing applications that involve using a strong continuous wave (cw) pump (Chraplyvy, 1990), stimulated Brillouin scattering (SBS) can however be used for amplification of light propagating in a direction opposite to the pump light. This has led to many applications, such as in Brillouin amplifiers, lasers, and microwave signal processors (Ahmad et al., 2010; Chraplyvy, 1990).

In this chapter, a SBS in single mode fiber and microfiber is investigated. The Brillouin fiber laser is then demonstrated using a 10 km long SMF, Erbium-doped fiber (EDF) and highly nonlinear fiber. The temporal characteristics of these BFLs are also investigated.

3.2 SBS generation in 10 km long SMF and a few cm long microfiber

SBS is a nonlinear phenomenon which takes place in optical fiber through a nonlinear interaction between the pump (input) and Stokes field through an acoustic wave. It arises when the pump light interacts with the acoustic waves inside an optical fiber thus generates a backward propagating frequency shifted light (G. P. Agrawal, 2007; Shirazi et al., 2008). SBS will be initiated in the backward propagating direction when the pump power reaches a crucial value, which is regarded as the SBS threshold. SBS threshold is defined as the input power where the Stokes power increases exponentially (Shee et al., 2009). When the pump power is beyond this SBS threshold, majority of the pump power is transferred to the Stokes wave and the pump power becomes depleted. One of the important parameters that characterize SBS is its threshold. Low SBS threshold is desirable especially for multi-wavelength Brillouin fiber laser applications whereby more Stokes lines can be produced. In this section, Brillouin Stokes generation

is investigated in two gain media; 10 km long single mode fiber (SMF) and SMF based microfiber structures.

3.2.1 SBS in 10 km long SMF

Figure 3.1 shows the experimental setup to examine the SBS effect in a piece of 10 km long SMF. As shown in the figure, a tunable laser source (TLS) is used as the Brillouin pump (BP) with maximum peak power approximately 6 dBm at the wavelength of 1550 nm. The maximum BP power is launched into the 10 km SMF through the ports 1 and 2 of the optical circulator (OC). The reflection is detected through the port 3 of the OC by using the optical spectrum analyzer (OSA) with the resolution of 0.02 nm. As described in many literatures (Harun et al., 2010), the acoustic phonons involved in the Brillouin scattering and the interactions occurs typically over a narrow order of tens of MHz of Brillouin gain linewidth, such as 35 MHz for fused silica (Shibata et al., 1988; Smith, 1972). Fig. 3.2 shows back-propagating Brillouin when the BP is fixed at 1550.4 nm. The anti-Stokes, the BP Rayleigh reflection and the Brillouin Stokes for 0 dBm input power are observed in the reflection spectrum with the peak power of about -66.4 dBm, -46 dBm, and -65.14 dBm, respectively.

As shown in Fig. 3.2, the Brillouin Stokes light wavelength is shifted upward by 0.088 nm, which is equivalent to the downshifted frequency of around 11 GHz from the BP signal. The shift is determined by the velocity of the acoustic grating along the fibre and is therefore dependent on the mechanical properties of the fibre such as the elasto-optic coefficient, applied strain and ambient temperature (Nikles et al., 1996; Yoshizawa et al., 1993). SBS provides gain in the opposite direction of the direction of the BP wave source. The pump power is depleted to be converted to a potentially strong Brillouin Stokes wave propagating backward to the pump direction. The Brillouin Stokes distorts

communication signal in optical communication systems, which may harmful in some cases. Therefore, an optical isolator is normally deployed in the system to eliminate the back-propagating signals.

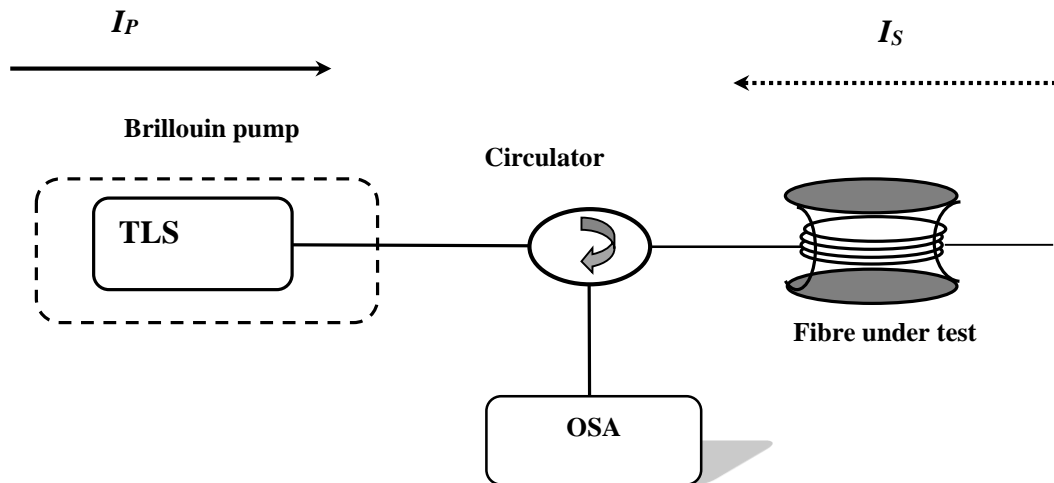


Figure 3.1: Experimental setup for generating Brillouin scattering in the backward direction. I_p and I_s denote the intensities of the pump and Brillouin signal lights, respectively.

The Brillouin Stokes is obtained due to the interactions between the gain media and BP. According to the SBS theory, the beat frequency between the Brillouin scattered wave and the incident BP light is equal to the frequency of the acoustic wave. As long as the Brillouin laser pump and the Brillouin Stokes wave interactions reinforce the acoustic waves, it amplifies the scattered Brillouin Stokes wave so that the stimulated Brillouin scattering (SBS) occurs. Rayleigh scattering in the fibre causes some portion of BP is reflected back as shown in the Fig. 3.2. The anti-Stokes signal is also observed in the reflection spectrum where its wavelength is shifted downward by 0.088 nm from the BP wavelength. The anti-Stokes is caused by the degenerate four-wave mixing effect which happening between the BP and Brillouin Stokes waves.

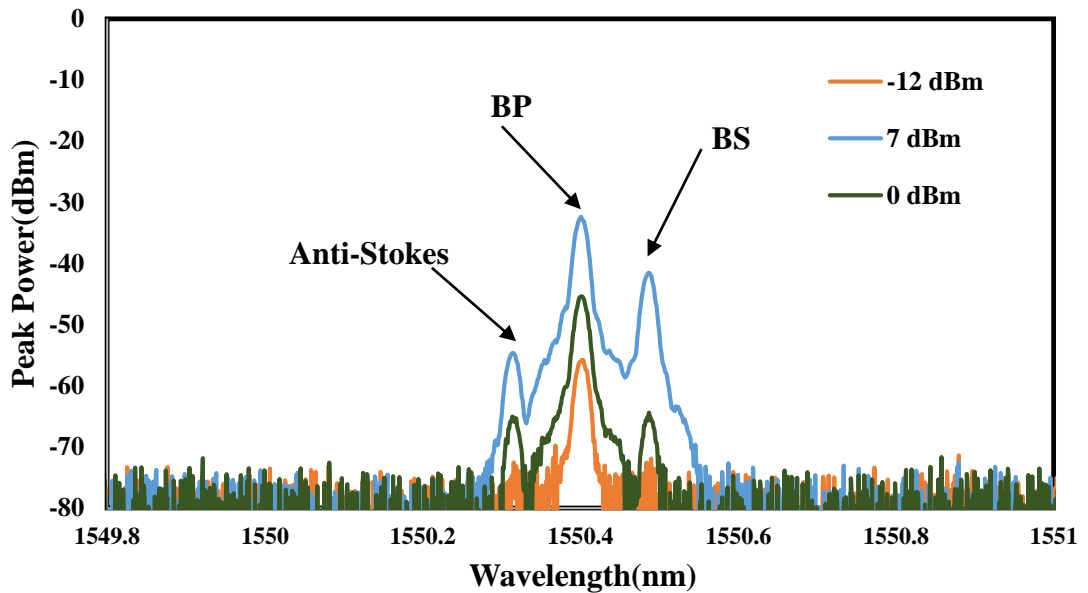


Figure 3. 2 : The reflection spectrum are demonstrated in different input power. BP reflection is due to BP Rayleigh scattering whereas the Brillouin Stokes (BS) and anti-Stokes waves are generated by Brillouin scattering and degenerate four-wave mixing process, respectively.

3.2.2 Brillouin Scattering in microfiber

Microfibres have attracted considerable interests in recent years, as they exhibit a number of exciting properties such as large evanescent field and strong confinement light which light is confined in a very small area over long length allowing it to observe the nonlinear interactions. These properties are advantageous for a wide range of applications including lasing systems, sensing devices and nonlinear optics. Their high nonlinearity was often used to generate ultra-broad supercontinuum light (Cordeiro et al., 2005). Microfibres may be divided into two distinct categories which are adiabatic and non-adiabatic. The microfiber is considered as an adiabatic type when a large portion of the power remains in the fundamental mode and does not couple to higher order modes as it propagates along the microfiber. To avoid coupling between the fundamental and higher order modes, the microfiber local length scale is designed to be so much larger than the coupling length between these two modes. In other words, the relative local change in the taper radius or angle has to be very small (Lacroix et al., 1988; Muhammad et al., 2013). The non-adiabatic fibre tapers occurs when an abrupt change in tapering angle can be

made so that coupling occurs primarily between the fundamental mode and the higher order modes. This phenomenon causes interference between the fundamental mode HE_{11} and its closest higher order mode HE_{12} while an increase in the insertion loss is also observed due to the large difference in the refractive index (RIs) of air and glass. Therefore, the non-adiabatic tapered microfiber is normally not suitable to be used in the fabrication of microfiber based resonators and interferometers devices.

Recently, spontaneous and stimulated Brillouin scattering have been extensively investigated and demonstrated using various gain media such as photonic crystal fibres (PCF) (Woodward et al., 2014) and a hybrid chalcogenide-PMMA microwire, which exhibit an ultra-high Kerr nonlinearity (Beugnot et al., 2013). The microfiber with a small diameter, surrounded by air, has similar acoustic and optical properties to the PCFs, due to the confinement light in a small core (Dainese, Russell, Wiederhecker, et al., 2006; Kang et al., 2008). In this section, we demonstrate the generation of spontaneous Brillouin scattering (SpBS) in a non-adiabatic microfiber and inline microfiber Mach-Zehnder interferometer (IMZI) or microfiber based MZI (MMZI) for the first time. Both devices are fabricated based on flame brushing technique from a standard silica fibre.

At first, three microfiber samples are fabricated from a standard telecom single-mode fibre (SMF) using a flame brushing technique. We use the similar fabrication technique as explained in reference (Jasim et al., 2012). Table 3.1 summarizes the geometrical characteristic of the microfiber samples used in this work. Sample 1 is an adiabatic type of microfiber, which has a total length of 70 mm and waist diameter of 4.6 μm . Samples 2 and 3 are fabricated by making an abrupt tapering angle at the transition part of one end of the microfiber as shown in Fig. 3.3. This type of microfiber is referred to a non-adiabatic type. Sample 2 has a total tapered length of 50 mm and waist diameter of 4.9 μm while the sample 3 has shorter length of 40 mm with a waist diameter of larger waist diameter of 6.5 μm . The abrupt change in taper angle of the non-adiabatic

microfibre allows the fundamental mode of the un-tapered fibre couples into two modes of the microfibre which one mode propagating in the core of the waist and another extend through the cladding–air interface, due to the large difference of the refractive indices of air and glass, the microfibre normally supports more than one mode. The back and forth coupling between the single mode of the fibre and the two (or more) modes of the microfibre produces an interference spectral response at the output of the microfibre.

Table 3. 1: Geometrical parameters of the microfibre samples

	Sample 1	Sample 2	Sample 3
Type of tapered device	Adiabatic (uniform)	Non-adiabatic (abrupt)	Non-adiabatic (abrupt)
Taper length (mm)	70	50	40
Waist diameter (μm)	4.6	4.9	6.5

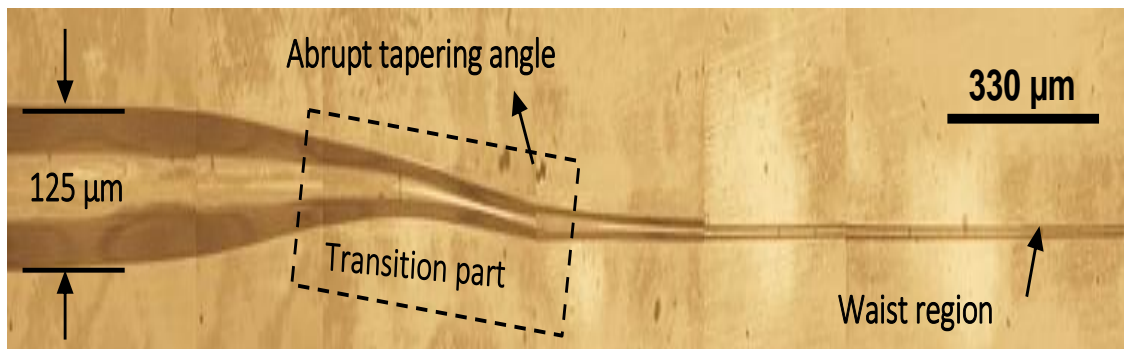


Figure 3. 3: Microscopic image for the fabricated non-adiabatic microfibre.

Fig. 3.4 shows the experimental setup for demonstrating the SpBS effect in the fabricated microfibre. It consists of three main components; Brillouin pump (BP), 3-ports optical circulator (Ahmad et al.) and microfibre sample. The BP is assembled by an external TLS and erbium doped fibre amplifier (EDFA), where the input laser from the TLS is amplified by the EDFA to achieve the maximum BP power of 24 dBm. The BP is then launched into the microfibre through port 2 of the OC to investigate the backward propagating Brillouin Stokes signal, which is generated based on the SpBS process. The Brillouin scattering was monitored through port 3 of the OC by using an optical spectrum

analyzer (OSA) with resolution of 0.02 nm. Two samples of fabricated non-adiabatic microfibres and one adiabatic microfibre sample with varied waist diameters and tapering length are used in this experiment to investigate the Brillouin scattering. The total length for each sample including fibre pigtailed and the tapered section is estimated to be around 80 cm.

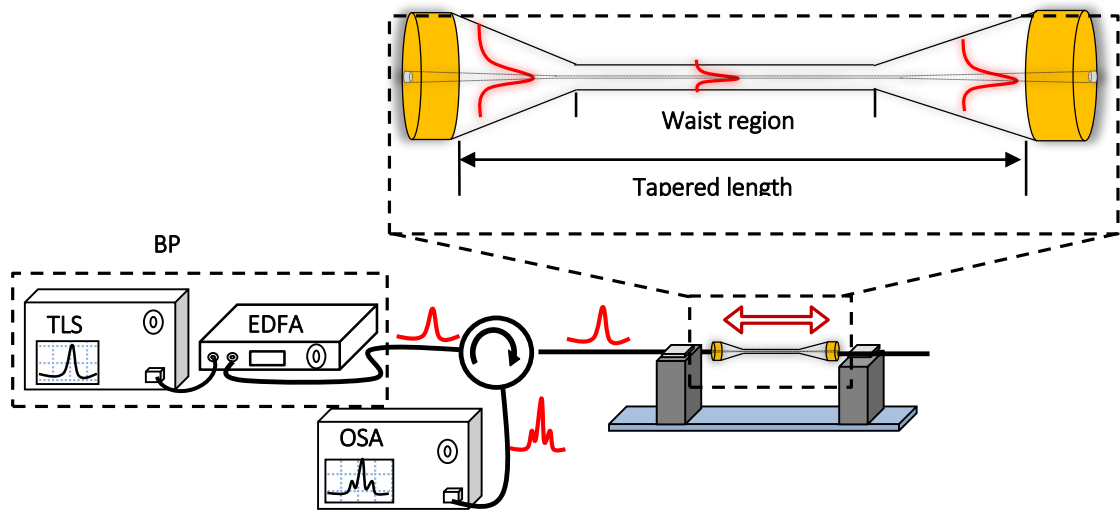


Figure 3. 4: The experimental setup for investigating the generation of Brillouin Stokes signal in both adiabatic and non-adiabatic microfibres.

During the fabrication of the microfibres, a broadband amplified spontaneous emission (ASE) light source is launched into the microfibre and the loss and spectral response are monitored using an OSA at the output end of the microfibre. Fig. 3.5 shows the transmission spectra of all the microfibres used in the experiment. As shown in the figure, sample 1 produces a uniform spectrum without any interference, which indicates that the fabricated microfibre has a low loss with adiabatic tapering characteristic. As expected, the output spectra for samples 2 and 3 exhibit interference fringes with extinction ratio of 7.6 dB and 6.7 dB at 1533 nm respectively, due to the beating between the modes. The highest loss is observed with sample 3, which has the shortest taper length. This is due to

the abrupt change in tapering angle, which increase the leakage loss. The bending at the transition region allows more photons to escape from the fibre due to scattering effect.

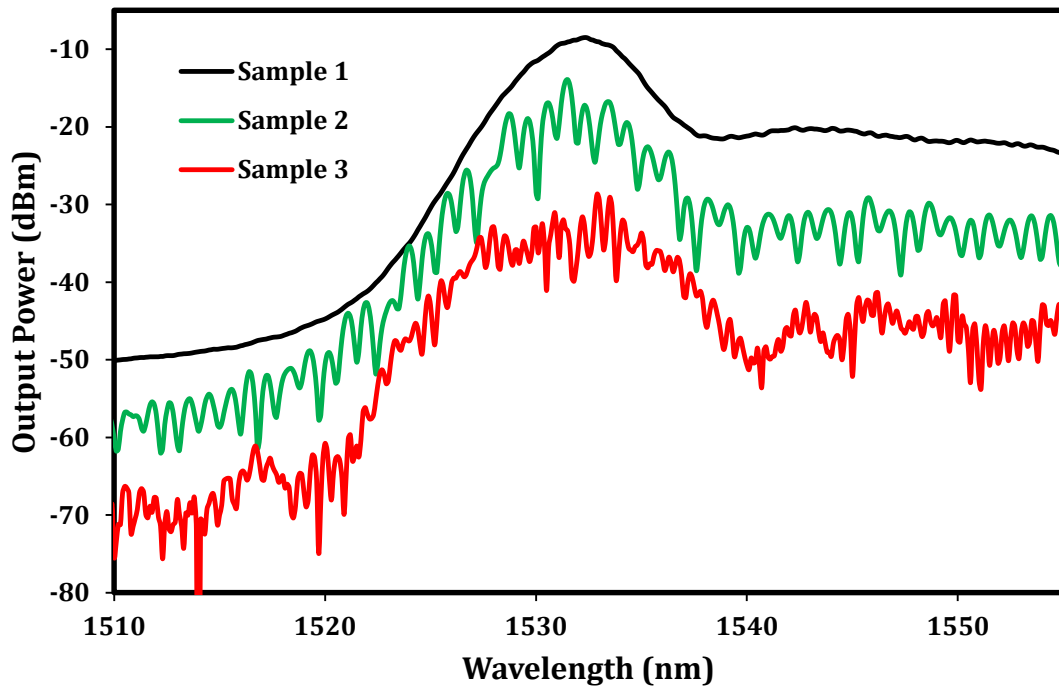


Figure 3. 5: The transmission spectra of the ASE for the three samples.

Fig. 3.6 shows the reflected light spectra from the three microfibre samples as the BP operating at 1558 nm is launched into the microfibre via an optical circulator (as illustrated in Fig. 3.4). The reflected light spectrum from an un-tapered fibre is also shown for comparison purpose. As shown in Fig. 3.6, Brillouin Stokes and anti-Stokes are generated in both non-adiabatic microfibre of samples 2 and 3. This is attributed to the nonlinear beating between the incident light (BP) and Stokes fields creating a moving interference pattern that induces an acoustic wave via the electrostriction effect, resulting in so-called the spontaneous Brillouin scattering (G. P. Agrawal, 2007; Bernini et al., 2002). SpBS is manifested through the generation of a backward-propagating Stokes wave whose frequency is downshifted from that of the pumping field by an amount set by the nonlinear medium. As shown in figure 4, the Brillouin Stokes light wavelength is

shifted upward by 0.088 nm (10 GHz) from the BP wavelength and the anti-Stokes wavelength is downshifted by the same spacing for both samples. On the other hand, the spectrum of the sample 1 shows no Stokes and it is quite similar to the spectrum of the launched BP before tapering the fibre.

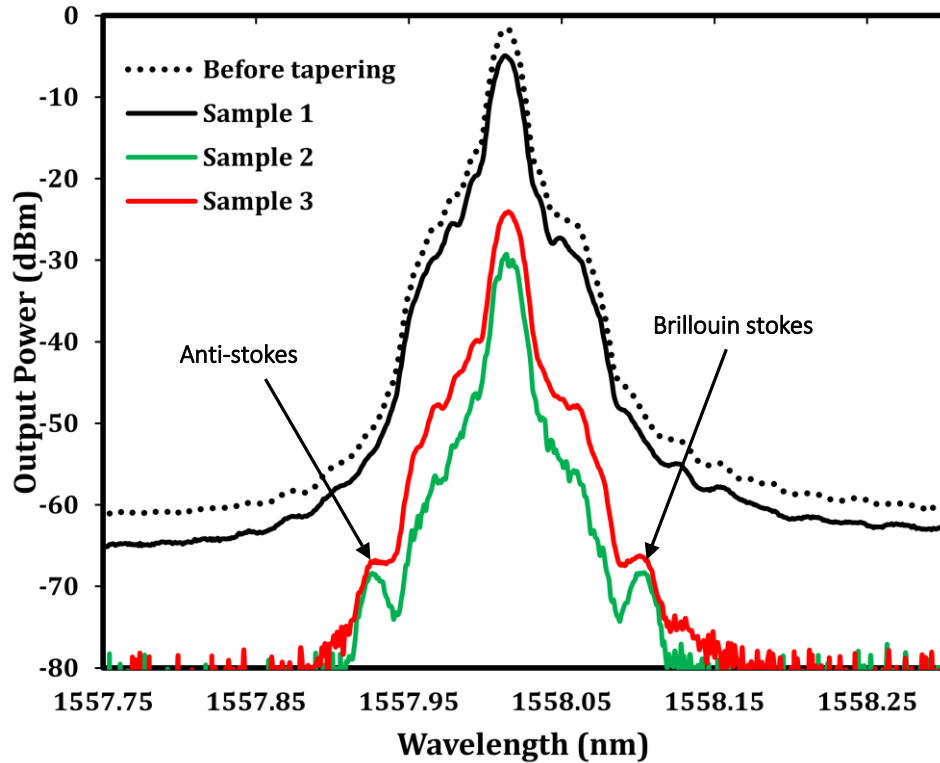


Figure 3. 6: The spectra of the launched BP and the back propagating Brillouin Stokes for the three microfiber samples.

The reason for such result is due to the abrupt and asymmetric shape of tapering where the non-adiabatic microfibres plays as a key effect in irritation the acoustic modes inside the microfiber due to the great contrast of the refractive indices of air and glass caused by changing density of a glass during tapering (Bernini et al., 2002). The complex geometry and “hard” boundaries provide strong acoustic reflections can be guided in the core (Russell, 2006). This periodic perturbation of the refractive index of the fibre associated with the acoustic wave can reflect the pump field by Bragg diffraction, thus make SpBS occurs with the Brillouin shift given by (Nikles et al., 1997) :

$$v_i = 2n_{eff}V_a^i/\lambda, \quad (3.1)$$

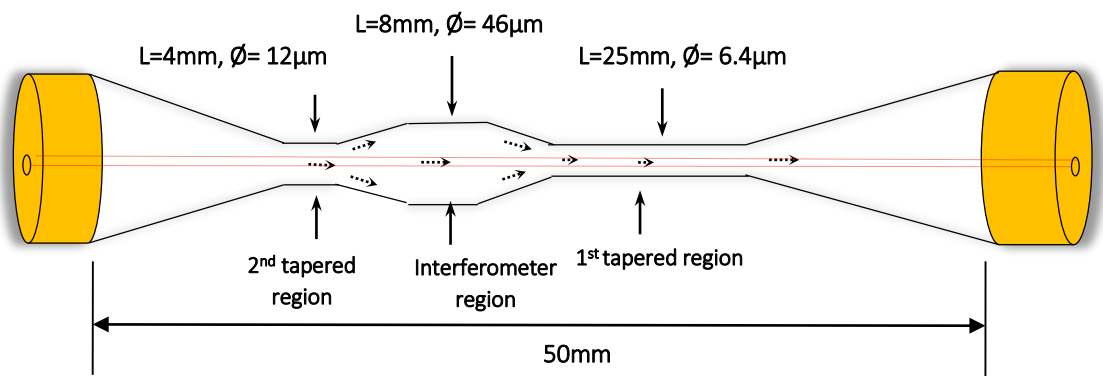
where n_{eff} is the the effective refractive index of the fibre optical, V_a^i is the effective acoustic velocity of the i -th order acoustic modes and λ is the wavelength in vacuum. It is worth noting that the Brillouin shift which caused by the periodic perturbation of the acoustic mode velocity along the fibre is dependent on the the mechanical properties of the fibre such as the elasto-optic coefficient, applied strain and ambient temperature (Nikles et al., 1997). From Fig. 3.6, it also observed that the magnitude of the Brillouin-gain spectra of sample 3 is higher than that magnitude of sample 2, where the three peaks of Brillouin stokes, BP Rayleigh backscattering and anti-stokes of the sample 2 is observed at the power of around -68dBm, -30dBm and -68.5dBm repectively; while the three peaks for the sample 3 is observed at -66.3 dBm, -24.6 dBm and -66.9dBm respectively. The explanation of that is because the waist diameter for the sample 2 is thinner than the waist diameter of the sample 3 which partially makes a multiple excitation to the acoustic modes (Dainese, Russell, Joly, et al., 2006). The magnitude and shape of the Brillouin gain spectrum is corresponding to the different acoustic modes in the fibre since each mode has a different acoustic velocity V_a^i which is strongly influenced by the fibre geometry (G. P. Agrawal, 2007). The fibre geometry as well can make factual effect to the bandwidth of the Brillouin-gain where the inhomogeneities of the fibre-core cross can broadening the bandwidth.

As seen in Fig. 3.6, the bandwidth of the reflection spectrum of sample 3 is broader than the bandwidth of the sample 2 owing to the inhomogeneities shape of the sample. This sample has a stronger inhomogeneities compared to that of sample 2. In order to investigate the effect of the fibre geometry on the Brillouin gain bandwidth broadening, we fabricated another non-adiabatic microfibre structure so-called inline Mach-Zehnder Interferometer (IMZI). This structure is fabricated by re-tapering both

transition regions of the microfibre to realize the IMZI structure of Fig. 3.7. The total length of the fabricated IMZI was about 50 mm where the length of the first tapered region, second tapered region and the interferometer region are 25 mm, 4 mm and 8 mm while the waist diameters are 6.4 μ m, 12 μ m and 46 μ m respectively. The IMZI allows the input light to split into two or more modes at the entrance of the interferometer region. These modes are defined as guided and unguided modes. The guided mode keeps travelling in the core and the unguided mode propagates through the cladding-air interface. An interference signal occurs when the two modes are recombined at the exit part of the interferometer region. The phase difference between the core and cladding modes can be expressed as:

$$\varphi = \left(\frac{2\pi(\Delta n_{eff})L}{\lambda} \right) \quad (3.2)$$

where Δn_{eff} is defined as $(n_c^{eff} - n_{cl}^{eff})$ which is the difference of the effective refractive indices of the core and the cladding modes, L is the length of the interferometer region and λ is the input wavelength.



(a)

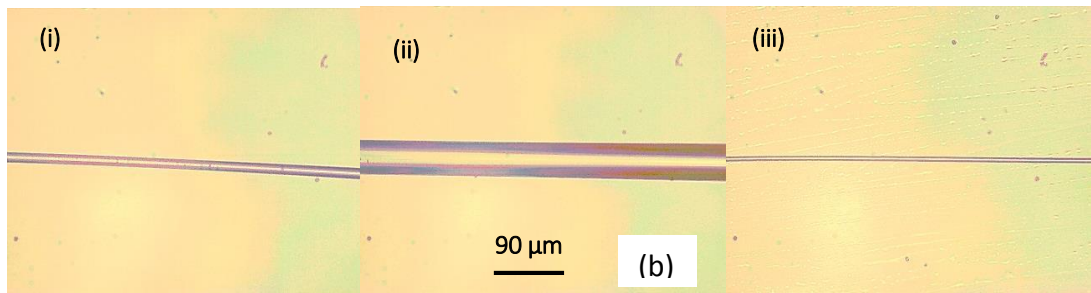


Figure 3. 7: The fabricated IMZI structure (a) schematic diagram and (b) microscopic images for the three tapered regions of IMZI, where the images (i), (ii) and (iii) represent the 2nd tapered region, interferometer region and 1st tapered region respectively.

Fig. 3.8 shows the transmission spectrum of the fabricated IMZI, which was obtained by using an ASE spectrum from EDFA as a light source. The transmission spectrum before the fabrication of the IMZI structure is also included for comparison purpose. As shown in Fig. 3.8, the IMZI produces interference fringes with extinction ratio of approximately 15 dB due to the mode interferences in the device. The insertion loss of fabrication inline MMZI is measured to be approximately 9 dB. When the IMZI is incorporated into the experimental setup of figure 2 for generating Brillouin scattering, the Brillouin Stokes and anti-Stokes are observed as shown in Fig. 3.9. Fig. 3.9 compares the back propagating Brillouin signal for the sample 2 and the IMZI when the BP is fixed at 1558 nm. It is found that the Brillouin Stokes wavelength is shifted upward by 0.088 nm (10 GHz) from the BP wavelength and the anti-Stokes wavelength is downshifted by the same spacing. As seen in Fig. 3.9, the magnitude of the Brillouin-gain spectra for the IMZI is higher than that magnitude of the sample 2, where the three peaks of Brillouin Stokes, BP Rayleigh backscattering and anti-Stokes of the sample 2 is observed at the power of around -66.7dBm, -28.9dBm and -66.9dBm respectively. This is due to the IMZI structure, which allows a stronger multimode interference and thus improves the SpBS generation in the fibre. Also observed from Fig. 3.9, the bandwidth of the dominant gain for the IMZI is broader than the bandwidth of the sample 2 owing to the

inhomogeneities shape of the fabricated IMZI. This shows that the microfibre geometry plays an important role in the SpBS generation.

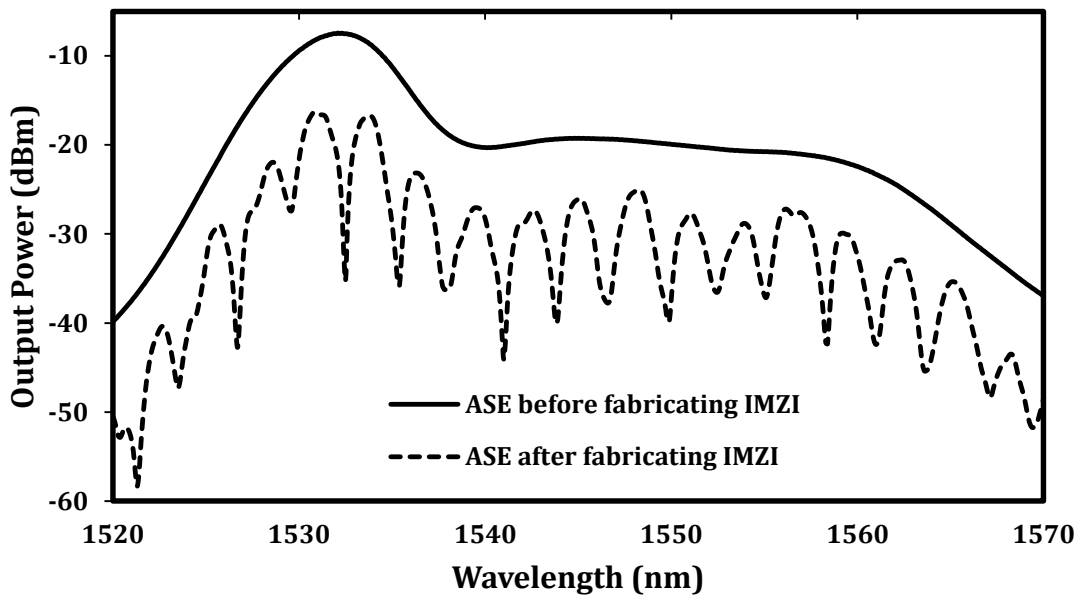


Figure 3. 8: The transmission spectra of the ASE for the IMZI.

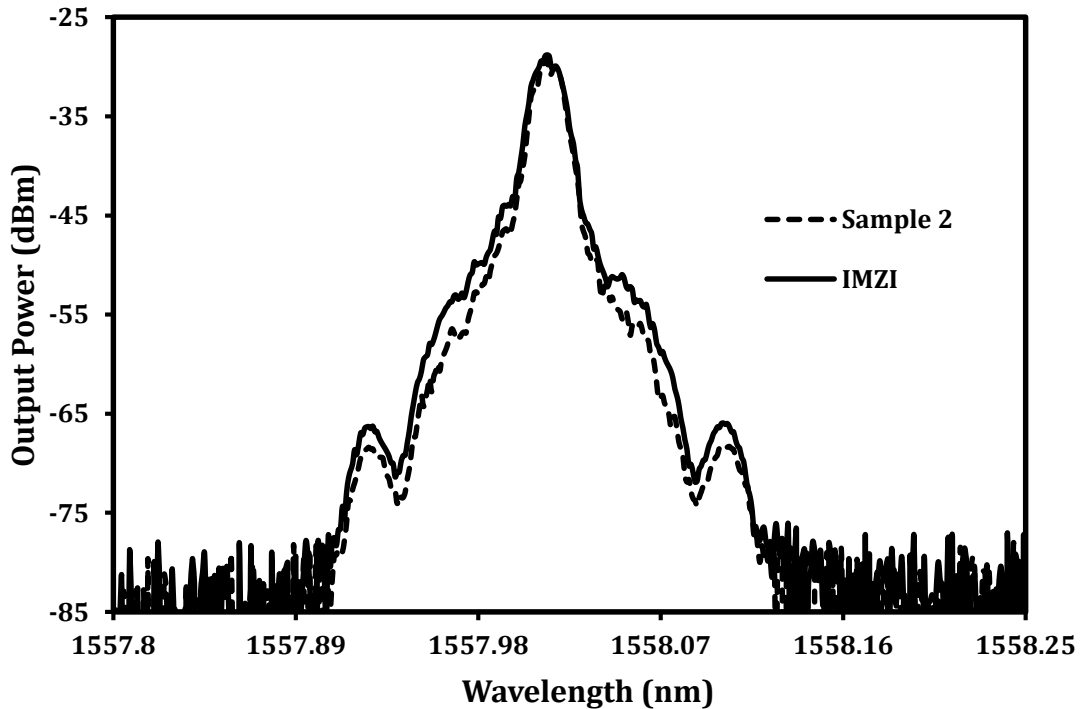


Figure 3. 9: The spectra of the back propagating Brillouin Stokes for the IMZI and sample 2.

Fig. 3.10, shows the SpBS process by increasing the launched BP power to the non-adiabatic microfibre. From Fig. 3.10, it can clearly observed that the Brillouin Stokes

and anti-stokes started to appear at the launched BP power of $39.8 \text{ mW} \approx 16 \text{ dBm}$; and the intensity of these signals are slightly improved by increasing the BP power to the $50.1 \text{ mW} \approx 17 \text{ dBm}$ and $63 \text{ mW} \approx 18 \text{ dBm}$. It can be also observed from Fig. 3.10 that the peak power of the BP Rayleigh backscattering and the Brillouin gain bandwidth are reducing by increasing the BP power, owing to the improving of the Brillouin Stokes. Such results indicated that the SpBS based on non-adiabatic microfiber will require a high BP power to be stimulated strongly, as well as an increase of the tapered length and a decrease the diameter of the waist regions. Such measures should enhance the nonlinearity of the non-adiabatic microfibres, and thus lead to Brillouin Stokes being affected significantly with increasing BP power. Nevertheless, the short length of non-adiabatic microfibres (in millimeters) retains the relative advantages of design simplicity and lower cost in generation of Brillouin Stokes. Whereas, when the non-adiabatic microfiber (sample 2) replaced by 200 meter of non-tapered standard SMF, the Brillouin Stokes could not be observed even at the maximum BP power of 24 dBm as shown in Fig. 3.11. However, by using much longer length of SMF of 20 km , the Brillouin Stokes could stimulate at lower BP power of $0.79 \text{ mW} \approx -1 \text{ dBm}$, due to enhancement of the nonlinearity in the long fibre. Still, the non-adiabatic microfibres based SBS generations retain the key advantage of shortness fibre length, showing a much greater potential for stimulating Brillouin Stokes than that long length of SMF based SBS generations.

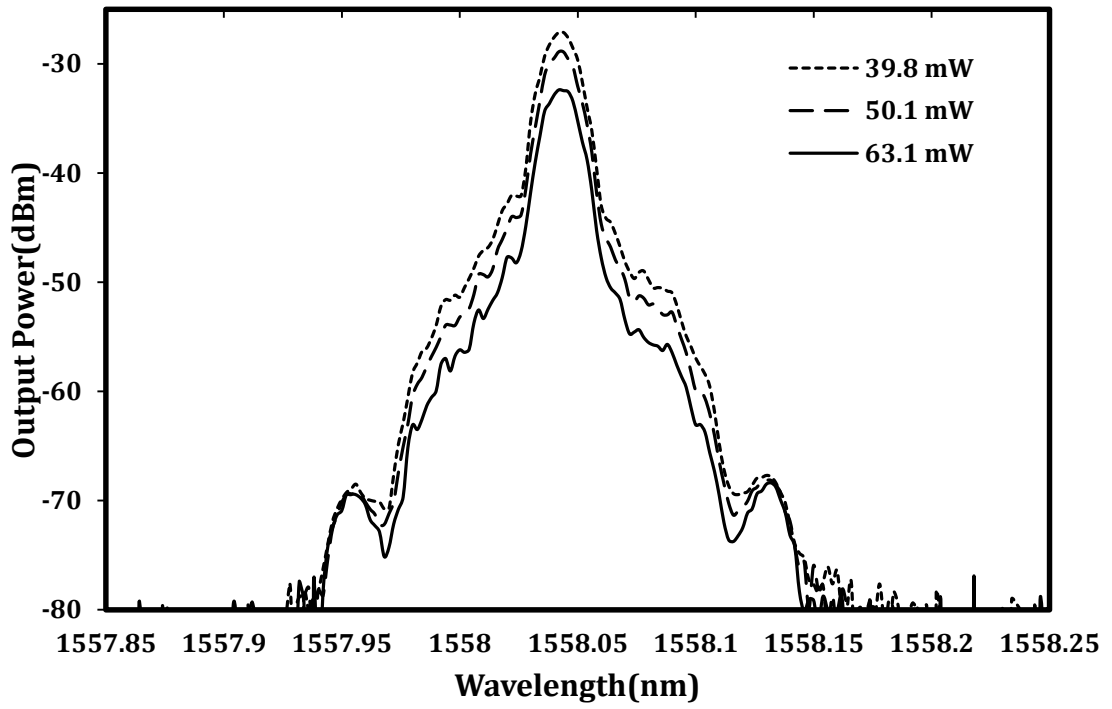


Figure 3. 10: The SpBS with different launched BP power.

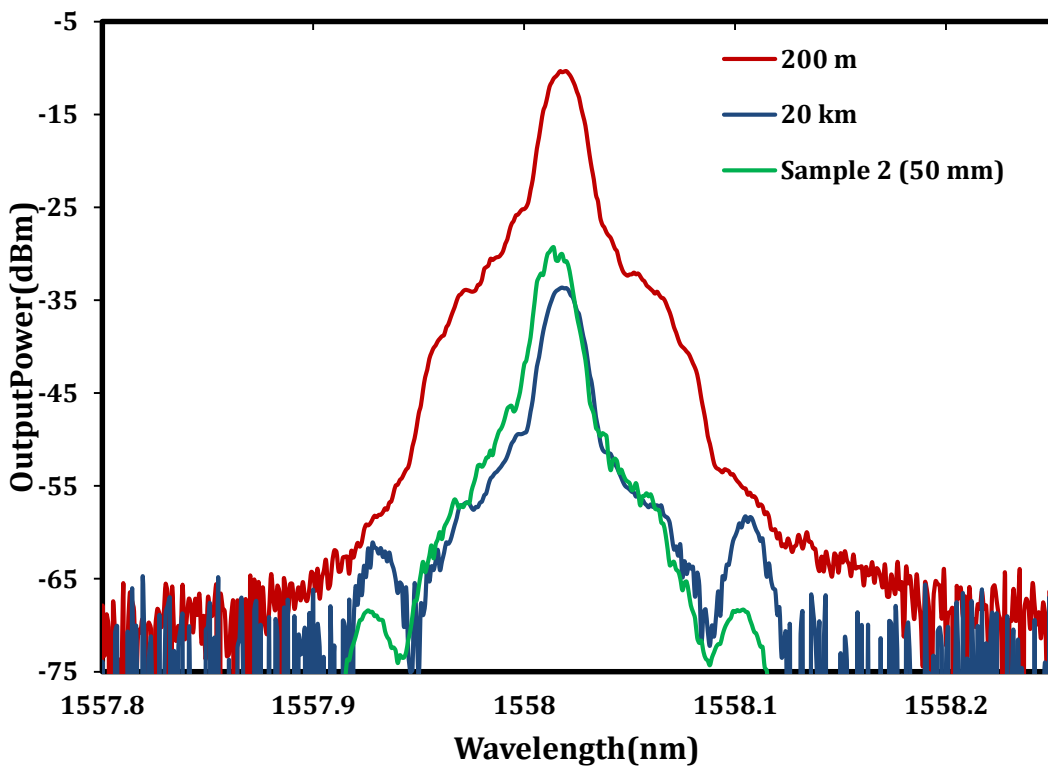


Figure 3. 11: The spectra of the back propagating Brillouin Stokes for different fiber length, where the red and blue colors represent SMF with length of 200 m and 20 km respectively and the green color represent sample 2 of the non-adiabatic microfiber

3.3 Spectrum and temporal characteristics of BFL

This section demonstrates a Brillouin fiber laser (BFL) generation using a 10 km long SMF as the gain medium in a ring configuration and investigates the spectrum and temporal characteristics of the laser. The configuration of BFL is based on the conventional ring set-up as illustrated in Fig. 3.12. It consists of an optical circulator, polarization controller (van Saarloos & Hohenberg), an output coupler and a 10 km long SMF. The SMF has a cut-off wavelength of 1161 nm, a zero dispersion wavelength of 1315 nm and a mode field diameter of 9.36 μm at 1310 nm. The BP is an external cavity TLS with a maximum power of approximately 6 dBm and a linewidth of about 15 MHz. It is injected into the SMF from port 1 through port 2 of the optical circulator in a clockwise direction. The BP wavelength is fixed at 1550 nm in this experiment. The BP is launched through the optical circulator to generate a backward propagating SBS, which oscillates inside the resonator to generate the laser at wavelength downshifted by 0.088 nm from the BP wavelength. The backward-propagating SBS generated oscillates inside the resonator in anti-clockwise direction to generate the Brillouin laser, which is coupled out using a coupler. The optical circulator which protects the TLS from any BP reflection is also used to force the unidirectional operation of the laser in the cavity although SBS in the SMF propagates only in the backward direction due to the SBS feature. The laser output spectrum is characterized using the optical spectrum analyzer (OSA, Yokogawa, AQ6370B) with a spectral resolution of 0.015 nm whereas the oscilloscope is used to observe the output temporal characteristics emission via a 1 GHz bandwidth photo-detector.

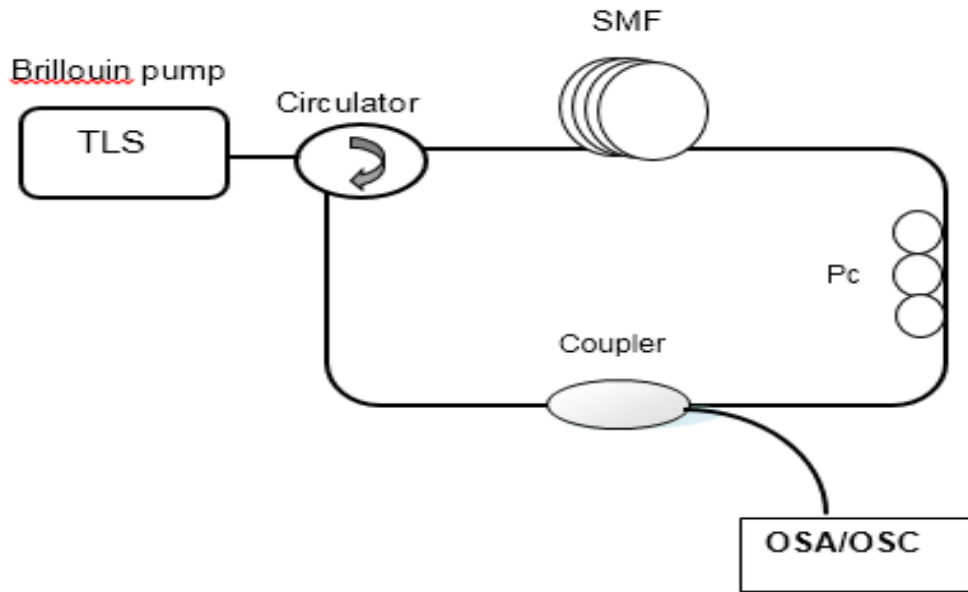


Figure 3. 12: Schematic diagram of the BFL using a 10 km long SMF as the gain medium

The threshold power of the BPL is defined as the BP power at the point where the resonator starts to generate laser via SBS. At the BP threshold power, a sudden jump of the BFL's peak power should be observed. Below this threshold power, only spontaneous scattering emission is oscillating in the resonator and thus the output Stokes power is low. The BFL output power characteristic is investigated at various BP power in order to determine the threshold BP power for the proposed BFL. Fig. 3.13 shows the output spectra of the BFL at three different BP powers. In the experiment, the 10/90 output coupler is used where 90% of the light is allowed to oscillate in the ring cavity. As shown in the figure, the resonator generates a Brillouin Stokes at around 1550.088 nm, which is 0.088 nm longer than the BP wavelength. The Stokes peak power increases with the increment of the BP power and exceeds the residual BP power, which indicates the generation of BFL at pump power of 1 dBm or above. The anti-Stokes signal is also observed at a shorter wavelength due to four-wave mixing between the BP wave and the Brillouin Stokes wave. The 3-dB bandwidth of the Stokes line is observed to be less than 0.02 nm, limited by the OSA resolution. Fig. 3.14 shows the output peak power of the

Brillouin Stokes against the input BP power at the different output coupler ratios. In the experiment, the BP power is varied from 0 to 6 dBm while the BP wavelength is fixed at 1550 nm. As shown in the figure, at 0 dBm pump power, a spontaneous Brillouin scattering is generated, which the power increases with the pump power.

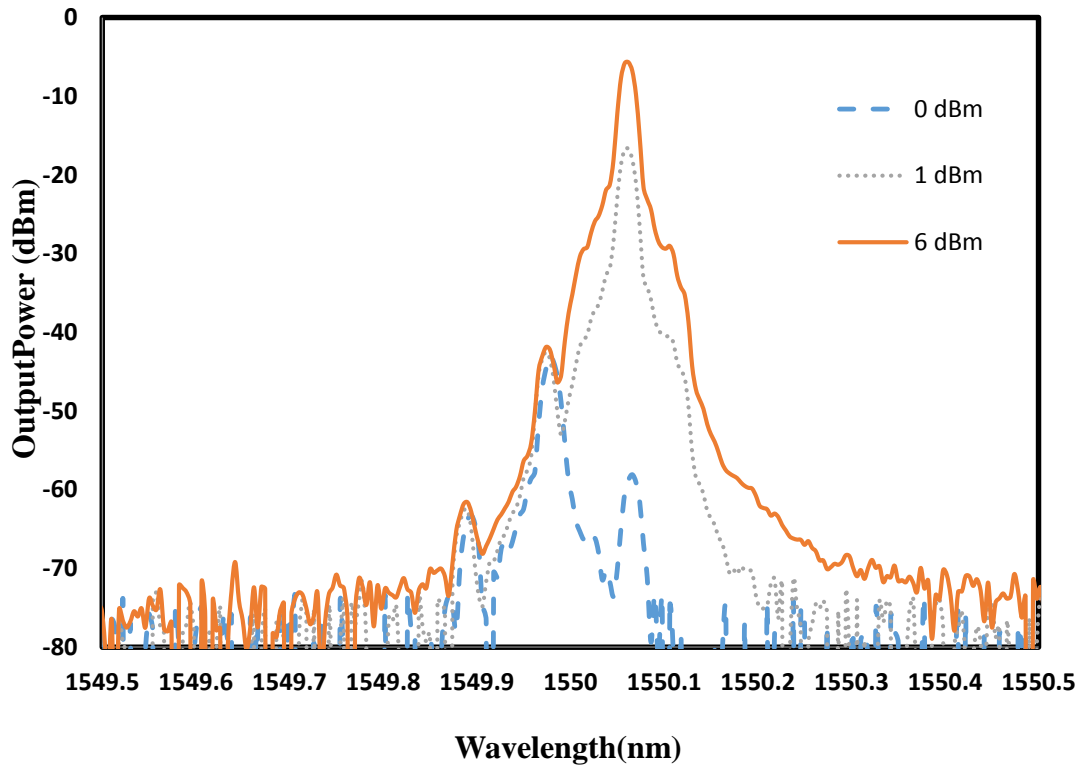


Figure 3. 13: Output spectra of the BFL at various pump powers.

As the BP is increased above a certain threshold, we observe a sudden increase in Stokes peak power due to the SBS process, which initiate the Brillouin Stokes lasing. The threshold BP powers for the BFL are obtained at 1.2, 1.5, 2.2 dBm for the laser cavity configured with 10/90, 20/80, and 50/50 output coupler, respectively. It is found that the threshold BP power increases with the use of higher output taper ratio, which increases the cavity loss. After the threshold, the peak power exponentially increases with the 1550 nm BP power. It is also observed that the maximum output power increases with the increment of the output coupler ration. For instance, the maximum laser's peak power of -3.12 dBm is obtained for the BFL configured with 50/50 coupler. The incorporation of

optical circulator in the cavity ensures the unidirectional operation of the BFL and suppresses the residual BP. This also reduces the four-wave mixing effect in the cavity and thus the generation of anti-Stokes was suppressed.

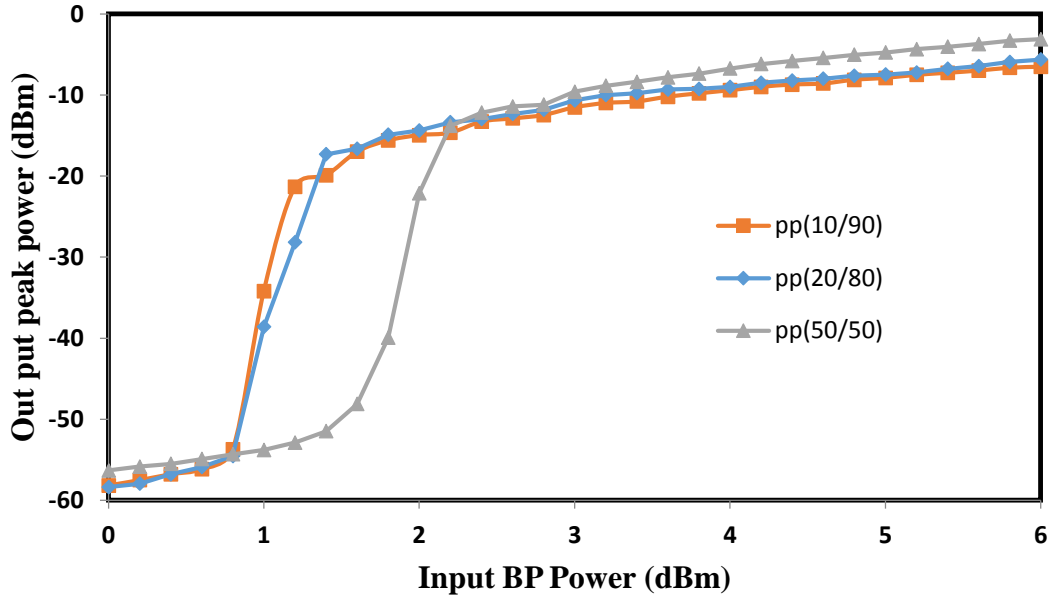
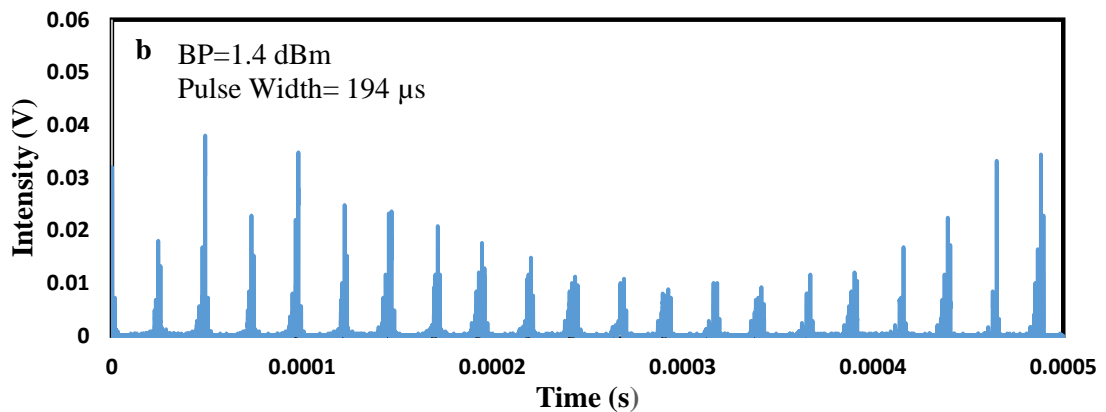
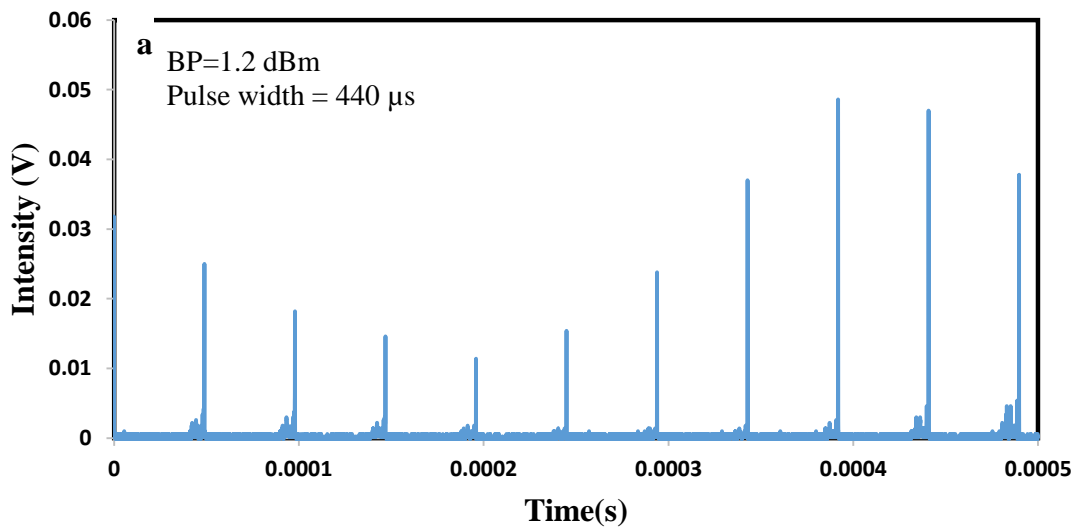


Figure 3. 14: The output peak power of the BFL against the BP at three different output couplers.

The temporal characteristics of the BFL configured with 10/90 coupler are also investigated and the result is shown in Fig. 3.15. When the BP power reaches the threshold, the laser outputs stable pulse array in periods. At a threshold pump power of 1.2 dBm, the pulse width and repetition frequency of the laser are obtained at 440 μ s and 2 kHz, respectively as shown in Fig. 3.15 (a). As the pump power increases, the pulse width becomes shorter while the repetition rate increases. For instance, the pulse width reduces from 440 to 40 μ s and the repetition rate increases from 2 kHz to 19.7 kHz as the BP power increases from 1.2 dBm to 1.6 dBm. This Q-switching or pulsing behavior is due to the relaxation oscillation, a natural trait of fiber laser, which occurs around the laser threshold as the SBS grows. Physically, the origin of relaxation oscillation can be explained as follows: rapid growth of the Stokes power near the input end of the fiber depletes the pump. This reduces the gain until the depleted portion of the pump passes

through of the fiber. The gain then builds up, and process repeats itself. In other word, the relaxation oscillation and instabilities happen due to the gain, which reacts too slowly to the light field and the stimulated lifetime, which is too long compared with the cavity decay time. However, the pulsing behavior becomes unstable and the pulse periodicity becomes so infinitesimal that the periodicity disappears as the BP is increased above 1.8 dBm as shown in Fig. 3.15 (d). This can be explained by that the backwards Stokes get more energy in center longitudinal mode frequency, and the direct current part amplitude of oscillation get higher at mean time, the other part of the longitudinal mode energy get less. When the direct current part is big enough that the longitudinal mode in the range of non-uniform line width disappears because of the absence of pump energy, then the laser's output is a stable value.



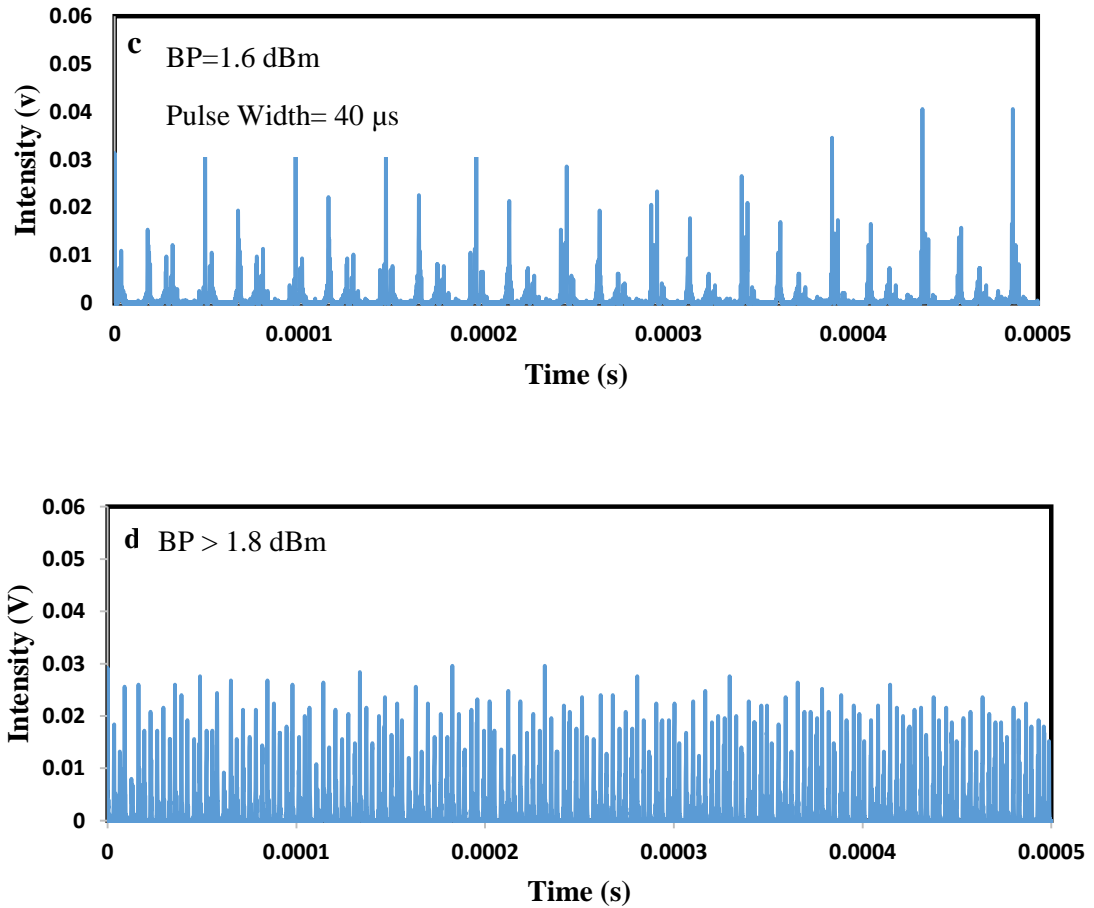


Figure 3. 15: Temporal characteristic of the BFL at different BP power (a) 1.2 dBm, (b) 1.4 dBm (c) 1.6 dBm (d) >1.8 dBm

Fig. 3.16 shows the pulse width and Stokes peak power against the increase of the pump power. We use a ratio of BP power to the threshold pump power to represent the x –axis as shown in Fig. 3.16. As shown in the figure, the width of pulse array decreases as the ratio of pump power to the threshold power is increased. In the nonlinear process of converting pump power to Stokes wave, the multilevel SBS effect and the pump exhaust of Brillouin generate under the effect of gain saturation and pump exhausts, As increase of multilevel SBS increase with the increase of pump power, and then the peak power of the output laser pulse increases gradually and the width decreases gradually.

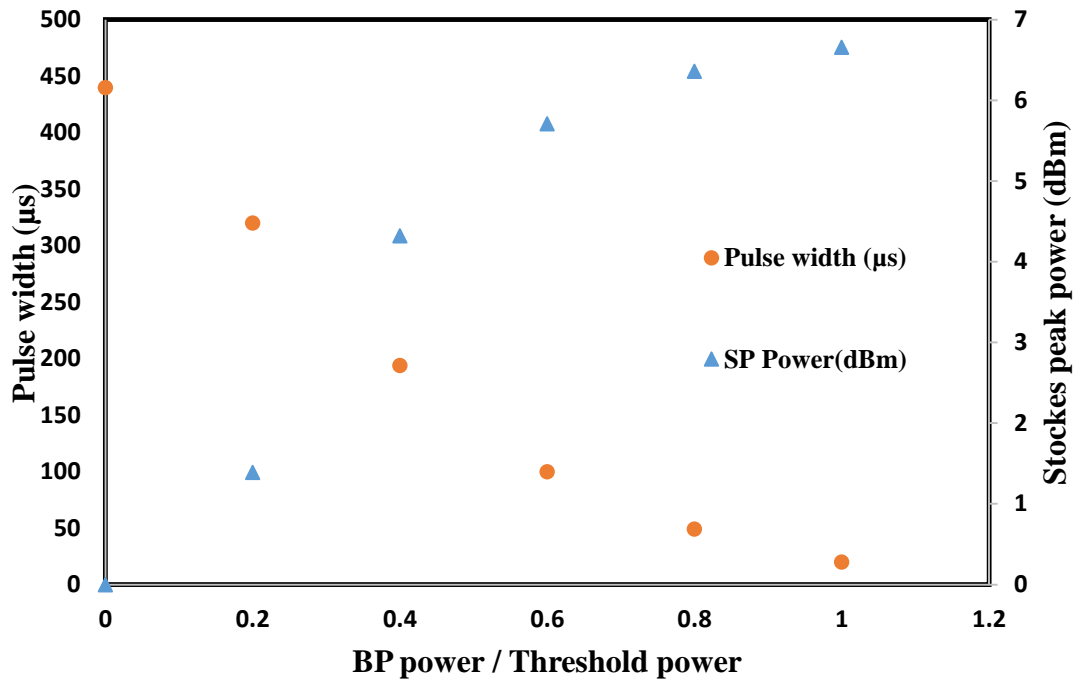


Figure 3. 16: The pulse width and Stokes peak power characteristic at different ratio of BP power to the threshold pump power

3.4 Brillouin Erbium fiber laser

Brillouin Erbium fiber laser (BEFL) is demonstrated under a new approach using an EDF with very high fiber nonlinearity as both linear and nonlinear gains medium. The Stokes is generated in the EDF by the injection of a narrow linewidth Brillouin pump. With the use of 1480 nm pumping on the EDF, the generated Brillouin Stokes is amplified to generate a BEFL. The EDF has also a high Erbium dopant concentration and thus it can be used to realize a compact BEFL. The temporal characteristic of the BEFL is investigated in this study. The performance of the BEFL is then compared with the conventional BFL.

A configuration of the BEFL is shown in Fig. 3.17, which the resonator consists of a circulator, a WDM coupler, 3 m long EDF, an isolator and 80/20 output coupler. The EDF has a cutoff wavelength of 945 nm, core diameter of 4 μm and a numerical aperture of 0.23. Since the core diameter of the fiber is small, the fiber nonlinearity is expected to

be reasonably high in this EDF compared to the standard EDF with core diameter of around 8 μm . The absorption of the EDF is 11.9 and 17.5 dB/m at 979 and 1531 nm, respectively. It is forward pumped using a 1480nm laser diode to generate amplified spontaneous emission (ASE) in 1550 nm region. The ASE oscillates in the ring cavity to generate a random laser as well as to provide a linear gain for assisting in Brillouin laser generation. A 1480/1550 nm WDM is used to combine the 1480nm pump and the oscillating signal in the ring cavity. The EDF is also pumped by an external cavity tunable laser source (TLS) with a linewidth of approximately 20 MHz and a maximum power of approximately 5 dBm to generate a nonlinear gain or Stokes, which is injected into the ring cavity via optical circulator.

The injected BP generates backward propagating Brillouin Stokes, which is amplified by the linear EDF gain and oscillates in the loop to generate a BEFL in a counter clockwise direction. An optical isolator is inserted inside the loop to block the BP from oscillating in the loop. By using a single fiber for the linear amplification and Brillouin Stokes generation, we are simultaneously amplifying the BP and Brillouin signal in this cavity. This allows shorter length of active fiber to be used for the BEFL generation, which in turn reduces a total cavity loss and increase the output power. A 20% output coupler is used to extract BEFL output, which is characterized using an optical spectrum analyzer (OSA). Oscilloscope and RF spectrum analyser are used to analyse the temporal characteristic of the laser via a 460 kHz bandwidth photo-detector (Thor lab, PDA50B-EC). The performance of the conventional Brillouin fiber laser, which is obtained by replacing the WDM coupler and EDF with a 20 km long a standard SMF is also investigated.

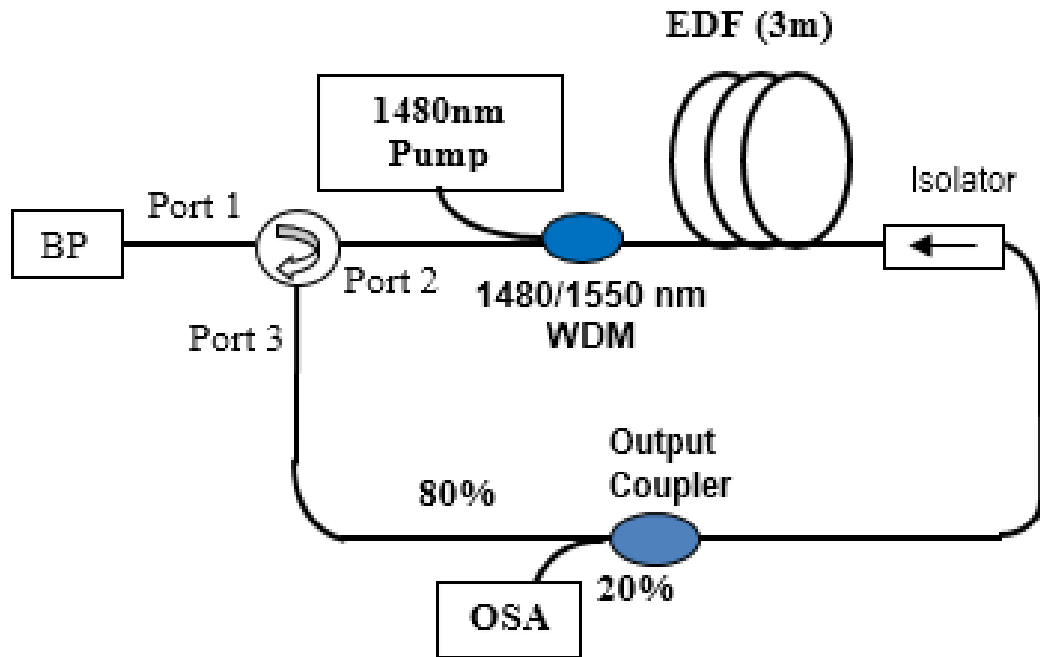


Figure 3. 17: Configuration of the proposed BEFL

Without the BP, the proposed EDFL produces a random laser with a spectrum of few peaks at wavelength region of 1561 nm. As the BP with the operating wavelength close to these peaks is injected into the laser cavity, the BEFL is generated. Figure 3.18 compares the output spectrum of the generated BEFL with the conventional BFL configured with a long length of standard SMF as the gain medium. In the experiment, the BP and 1480 nm pump power is fixed at 5 dBm and 34 mW, respectively. As shown in Figure 3.18, both lasers operate at wavelength that is shifted by 0.08 nm from the BP. The peak power of the proposed BEFL is 5 dB higher than the conventional BFL due to the stimulated emission from the Erbium ion, which provides additional gain in the cavity. However the spontaneous emission from the Erbium ion increases the noise level of the laser. The side mode suppression ratios (the difference between the Brillouin laser peak and the residual BP power) are measured to be around 5 dB and 30 dB for the BEFL and BFL, respective

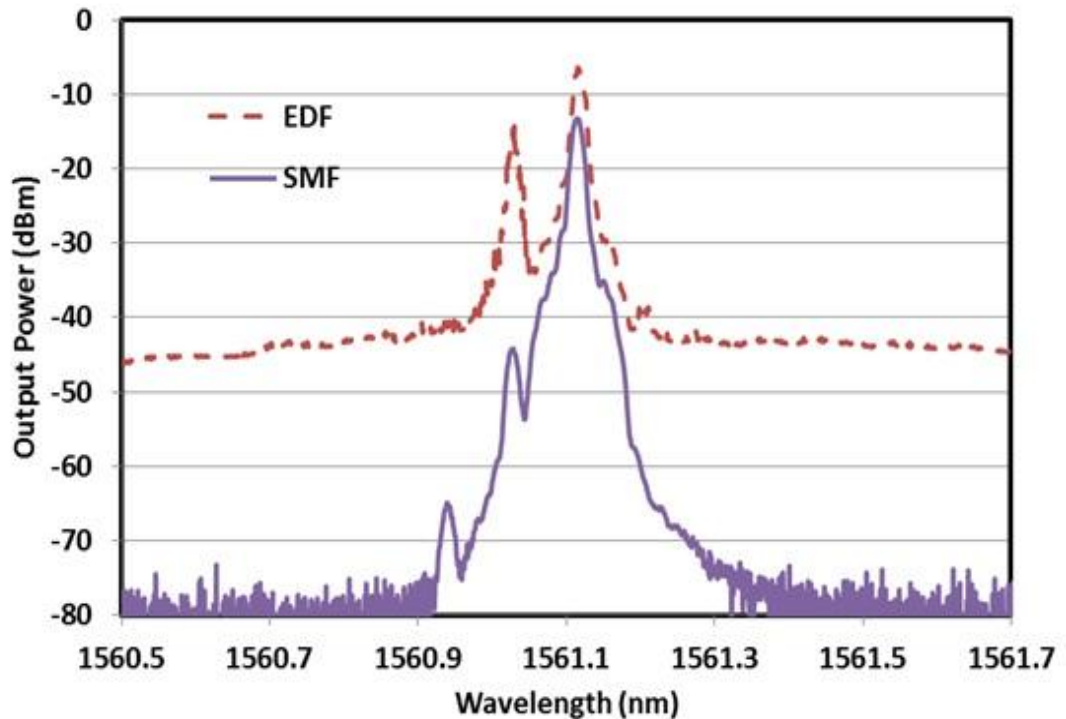
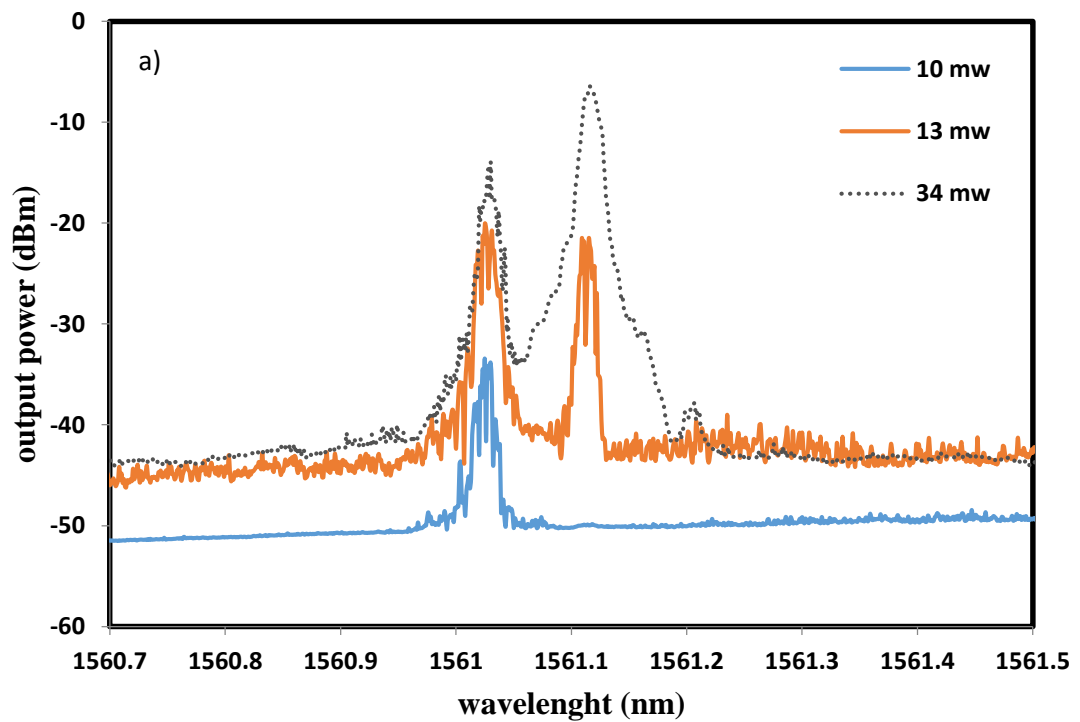


Figure 3. 18: Output spectrum from the BEFL and BFL

The performance of BEFL was studied for different 1480nm pumping power. The BP power is fixed at 5 dBm. Fig. 3.19 shows the output spectrum of the BEFL. As shown in the figure, a BEFL wavelength component at separation of 0.08 nm at longer wavelength could be easily observed when the 1480nm pump power exceeded ~13 mW, and peak power grew up to -5 dBm as the pump power was raised to 34 mW. As shown in the figure, the 1480 nm pump power threshold is approximately within 13 mW. Below this pump power, the erbium gain is very low and cannot sufficiently compensate for the loss inside the laser cavity and thus no Stokes is observed. The generated BEFL power is observed to increase as the 1480nm pump power increases, which is attributed to the increment of the erbium gain with pump power. This situation provides sufficient signal power for SBS to generate Stokes, which is then amplified by the erbium gain.

Inset of Figure 3.19 shows the relationship between the peak power and the injected 1480 nm pump power when the BP power is fixed at 5 dBm. The Brillouin Stokes

laser starts to lase at pump power of 13 mW and drastically increased by 8 dB as the pump power increased to 16 mW. After that the peak power exponentially increases with the 1480 nm pump power with the rate of 0.55 dB/mW. At the maximum 1480 nm pump power of 34 mW, the BEFL has a peak power of -5 dBm and a side mode suppression ratio (SMSR) of more than 5 dB. The incorporation of both optical isolator and circulator in the cavity ensure the unidirectional operation of the BEFL and suppresses the residual BP. These suppresses the four-wave mixing effect in the cavity and thus the generation of anti-Stokes was avoid.



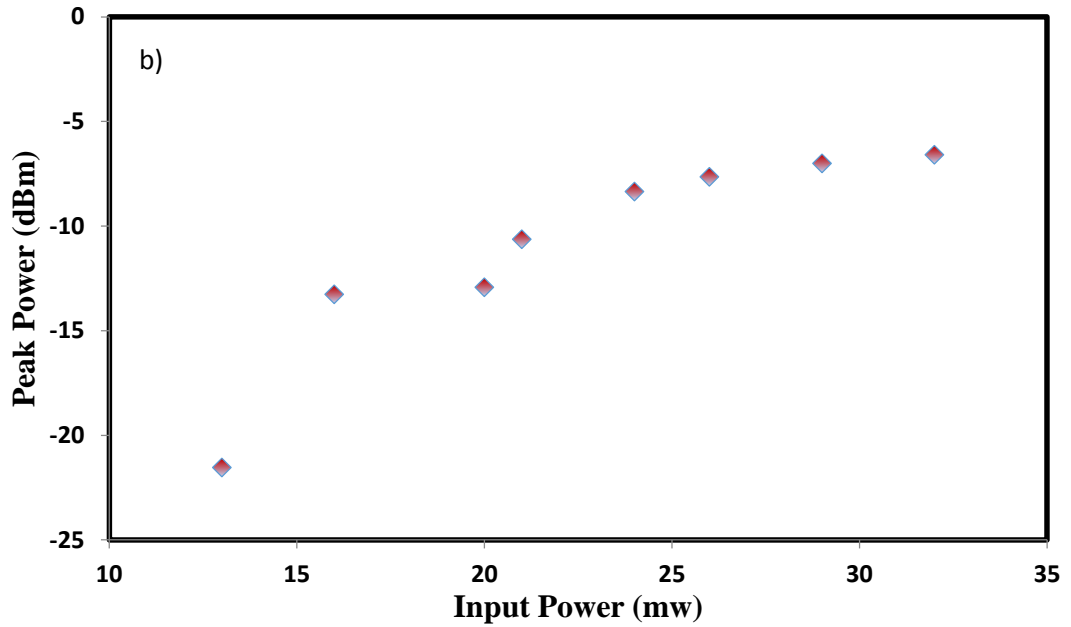


Figure 3. 19: a) Output spectra of the BEFL at various 1480 nm pump powers. b) Inset shows the peak power of the laser against the input 1480 nm pump power.

The performance of the BEFL was also studied for different input powers and wavelengths of the BP. Fig. 3.20 shows the relation between the BEFL peak power and the BP power. In the experiment, the 1480 nm pump power and BP wavelength is fixed at 34 mW and 1561 nm, respectively. The result for the conventional BFL is also included in Fig. 3.20 for comparison purpose. It is observed that the threshold BP power, which is required to initiate SBS in the EDF is about 2 dBm and the output power of the BEFL does not change much as the BP is further increased.

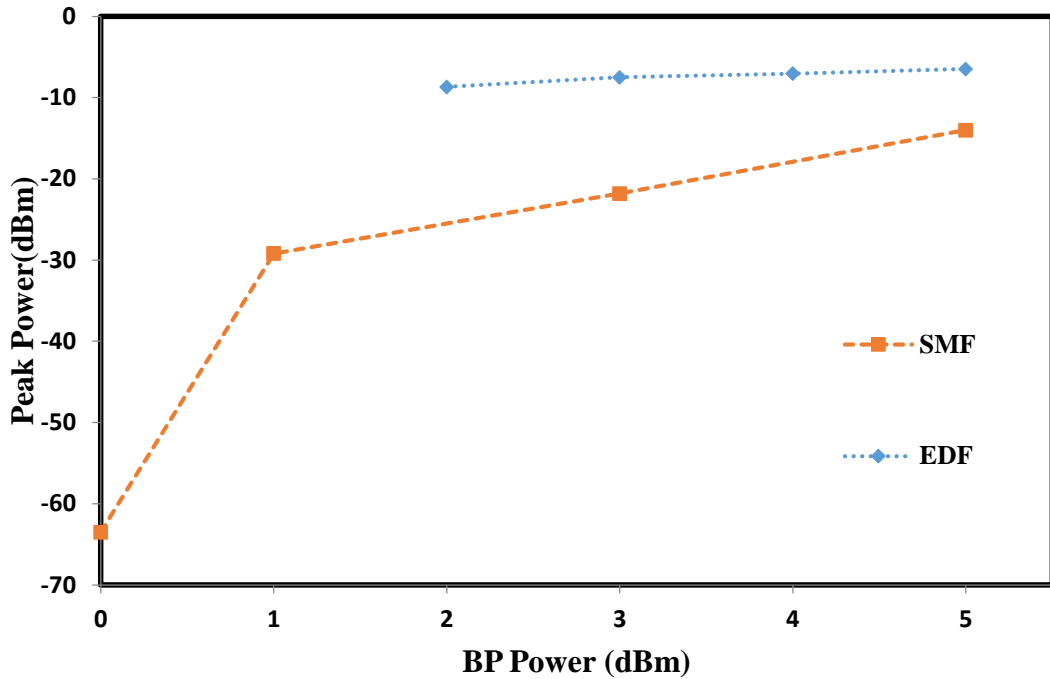


Figure 3. 20: The Stokes peak power against the BP power for both BEFL and BFL

This is attributed to the Brillouin gain which is too small and thus the output power is mainly contributed by higher Erbium gain. On the other hand, the threshold BP power is slightly lower in the conventional BFL (1 dBm). After the threshold, the output power of the BFL linearly increases with the BP power. It is also observed that the output power of the laser is reasonably lower than that of the BEFL because it only depends on Brillouin gain. Fig. 3.21 shows the output spectrum of the BEFL at various BP wavelengths. In this experiment, the BP and 1480nm pump power is fixed at 5 dBm and 34 mW, respectively. As shown in the figure, the BP can be tuned from 1560.6 to 1562.6 nm with peak power variation of less than 4.7 dB.

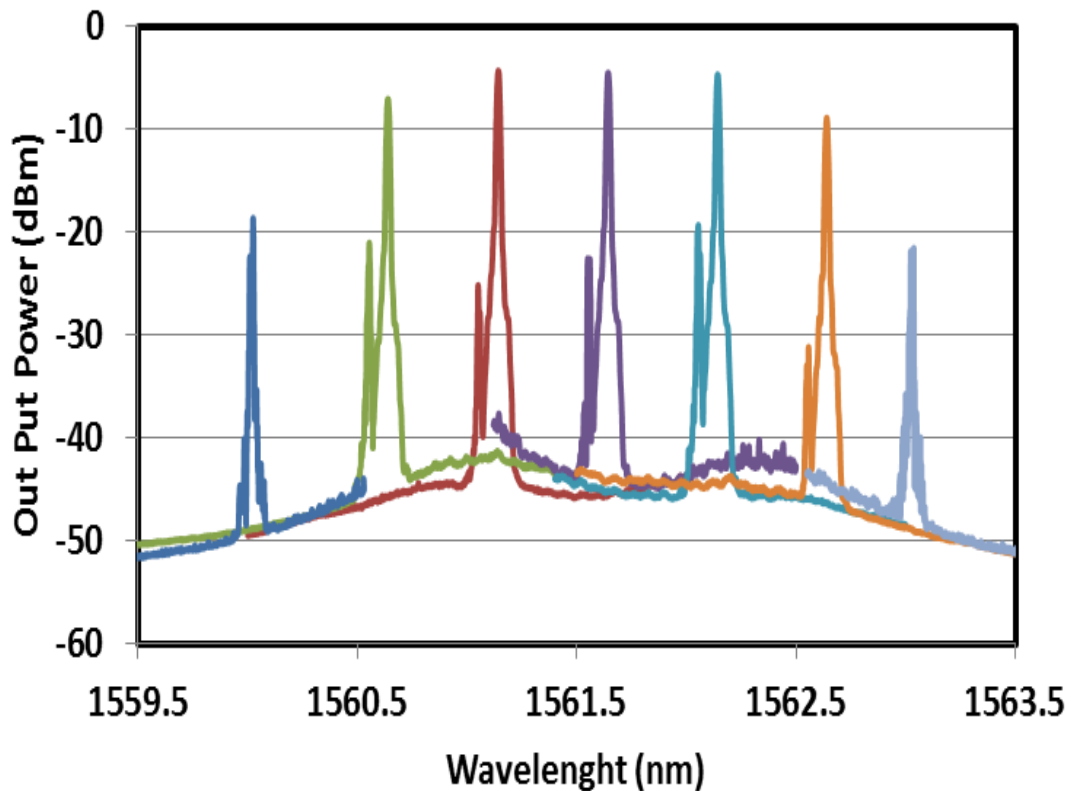


Figure 3. 21: The output spectrum of the BEFL at different BP wavelengths

The temporal characteristic could be observed in both BEFL and BFL as the Stokes is generated. A stable self pulsing behavior is observed in the BEFL as the 1480 nm pump power is set within 13 mW to 20 mW. As the pump power is increased further, the Stokes generation process stabilizes and the pulse generation disappears. In case of the BFL, the self pulsing is obtained when the BP power is set within 1 to 2 dBm. Figure 3.22 shows the oscilloscope trace of the BEFL and BFL at the threshold pump power settings. Both BEFL and BFL show a self pulsing characteristic with repetition rates of 66.7 kHz and 102.0 kHz respectively. The self-pulsing behavior is due to the relaxation oscillation, a natural trait of fiber laser which occurs around the laser threshold as the SBS grows. Physically, the origin of relaxation oscillation can be explained as follows; rapid growth of the Stokes power near the input end of the fiber depletes the pump. This reduces the gain until the depleted portion of the pump passes through of the fiber. The gain then builds up, and process repeats itself. In other word, the relaxation oscillation

and instabilities happen due to the gain which reacts too slow to the light field and the stimulated lifetime which is too long compared with the cavity decay time. As shown in Fig. 3.22, the self-pulsing characteristic is more pronounced in BFL, which has longer cavity length than that of BEFL. This is due to the longer cavity length that exhibits a higher instability and thus a pulse train can be easily produced based on nonlinear and spectral hole burning effects. This result shows that a stable CW Brillouin laser with low threshold can be realized in BEFL with low loss ring cavity.

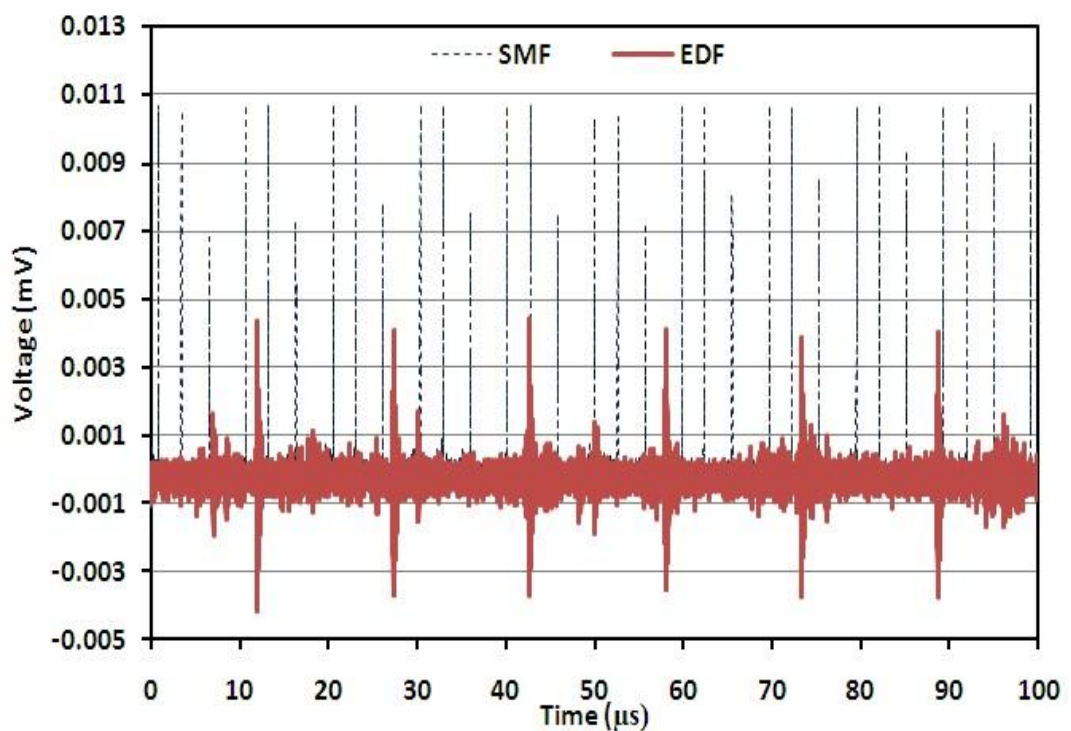


Figure 3. 22: Oscilloscope trace from the BEFL and BFL

3.5 Generation of nanosecond pulse with highly nonlinear fiber (HNLF) based on SBS

Recently, nanosecond pulse lasers attracted broad attention from scientists due to their potential applications in various fields such as medical surgery and sensing (Englander et al., 1992). Compared to the conventional picosecond or femtosecond pulses, nanosecond laser exhibits higher pulse energy. Besides, the nanosecond mode-locked fiber lasers can operate in higher frequency (Megahertz) compared to typical Q-switched laser, which operates in kilohertz region. In this section, a nanosecond mode-locked BFL is demonstrated using an SBS effect in a highly nonlinear fiber (HNLF). The BFL is based on mode locking process, which is a self-starting and does not require an intra-cavity modulator. The occurrence of pulses is also found to be highly stable.

3.5.1 Configuration of the proposed mode-locked BFL

The configuration of the BFL is shown in Fig. 3.23, which consists of a BP, Erbium-doped fiber amplifier (EDFA), an optical circulator, 100 m long HNLF and a 95/5 output coupler. The HNLF exhibits loss coefficient, dispersion slope and nonlinear parameter of 1531 nm, 0.73 dB/km, 0.007 ps/nm²km and 11.5 W⁻¹km⁻¹ respectively. The BP is an external cavity TLS with a line width of approximately 20 MHz, which is amplified by an EDFA to provide the maximum output power of 15 dBm and operated in 1560 nm. The BP output is launched into the HNLF through an optical circulator to generate a backward propagating SBS, which oscillates inside the resonator to generate the laser at a wavelength which is downshifted by 0.08 nm from the BP wavelength. The optical circulator is also used to induce unidirectional operation of the laser in the cavity. The counter-clockwise oscillating laser is extracted from the resonator via the 5 % coupler and examined by an OSA with a wavelength resolution of 0.02nm. Besides, a 350 MHz

oscilloscope in conjunction with a 1.2 GHz bandwidth photo-detector is used to analyze the temporal characteristic.

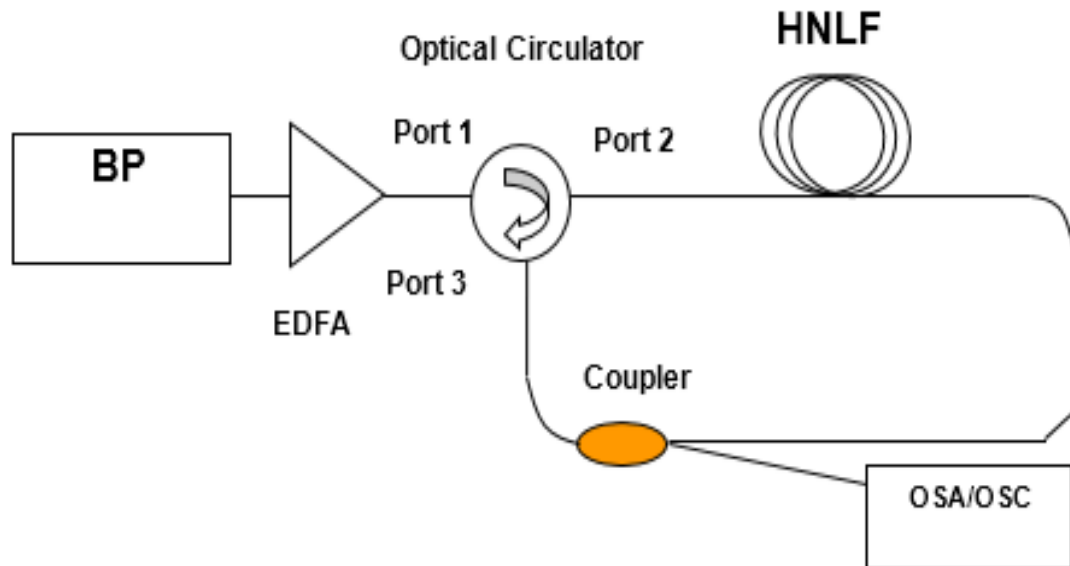


Figure 3. 23: Schematic configuration of the proposed nanosecond BFL

3.5.2 The performance of the nanosecond mode-locked BFL

Fig. 3.24 shows the output spectrum of the proposed nanosecond pulsed BFL with a HNLF as the gain medium at different BP powers. It is observed that a Brillouin Stokes is generated at a wavelength shifted by 0.08nm from that of the BP as the BP power reaches 10.5 dBm and above. The Stokes peak power increases with the increment of the BP power and exceeds the residual BP power, which indicates the generation of BFL at pump power of 10.9 dBm. A slight spectral broadening is also observed for the Stokes signal, which is most probably due to the self-phase modulation (SPM) effect. The HNLF has a zero dispersion wavelength at 1531 nm and the fiber laser is estimated to operate in the normal dispersion regime.

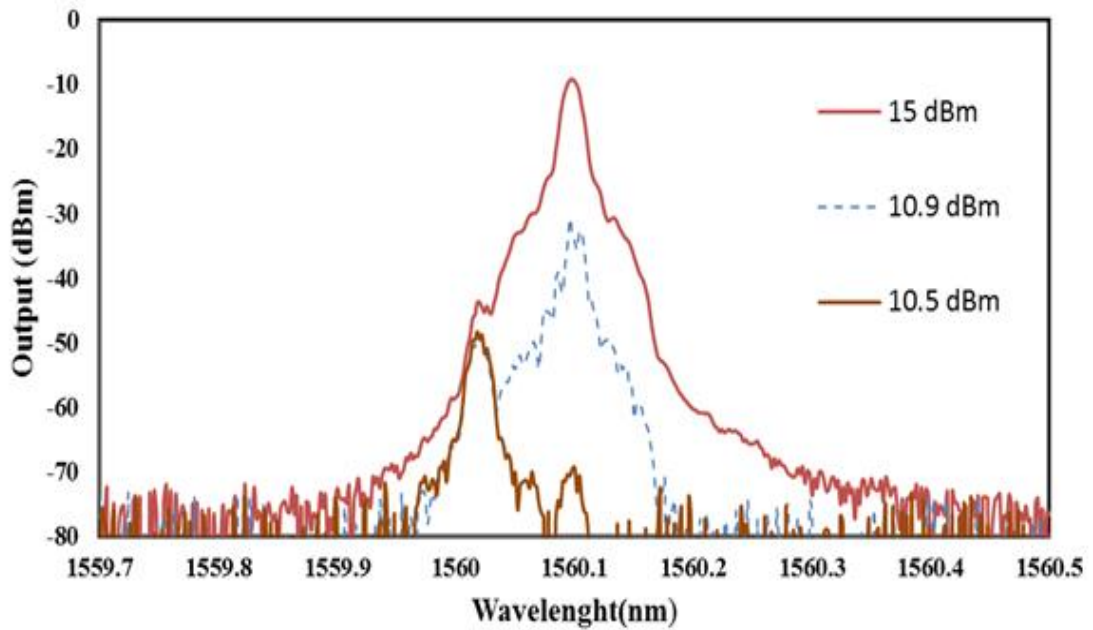


Figure 3. 24: Output spectra of the BFL configured with HNLf at various BP power

Fig. 3.25 shows a typical pulse train of the mode-locked laser at threshold of BFL. It is observed that the laser operates at repetition rates of 1.76 MHz at pump power of 10.9dBm. The corresponding pulse widths are 270 ns. The development of the short pulse is attributed to the onset of SBS, which creates a traveling high reflector in the HNLf and thereby depletes the energy stored in the gain medium through mode-locking process (Jusoh et al., 2013). This mode-locking behavior is due to a nonlinear self-pulsing mechanism based on inherent instability of the BFL. The origin of this instability lies in the relaxation oscillation, a natural trait of fiber laser which occurs around the laser threshold that causes a series of avalanche processes. The Stokes power generated by the BP does not approach its steady state value monotonically but exhibits relaxation oscillations with a period of $2T_r$, where $T_r = L/v_g$ the transit time for a fiber of length L and v_g is the group velocity. In the presence of external feedback, the relaxation oscillations can be turned into a stable oscillation where both pump and Stokes wave can develop self-induced intensity modulation. Even though the group velocity v_g is nearly the same for the pump and the Stokes wave, their relative speed is $2v_g$ because of their

counter propagating nature. Relaxation oscillations occur as a result of this group velocity mismatch. Unlike the conventional mode-locking fiber lasers, in which the pulse duration is proportional to the photon lifetime in the resonator, the short pulses generated by the SBS do not depend on the photon lifetime in the resonator but rather on the dynamics of the nonlinear process. It is found that the fundamental repetition rate fits the free-spectral range of longitudinal modes in the cavity. This is attributed to the relaxation oscillation, which allows the proposed BFL to generate Stokes pulses with a repetition rate nearly equal to the longitudinal mode spacing.

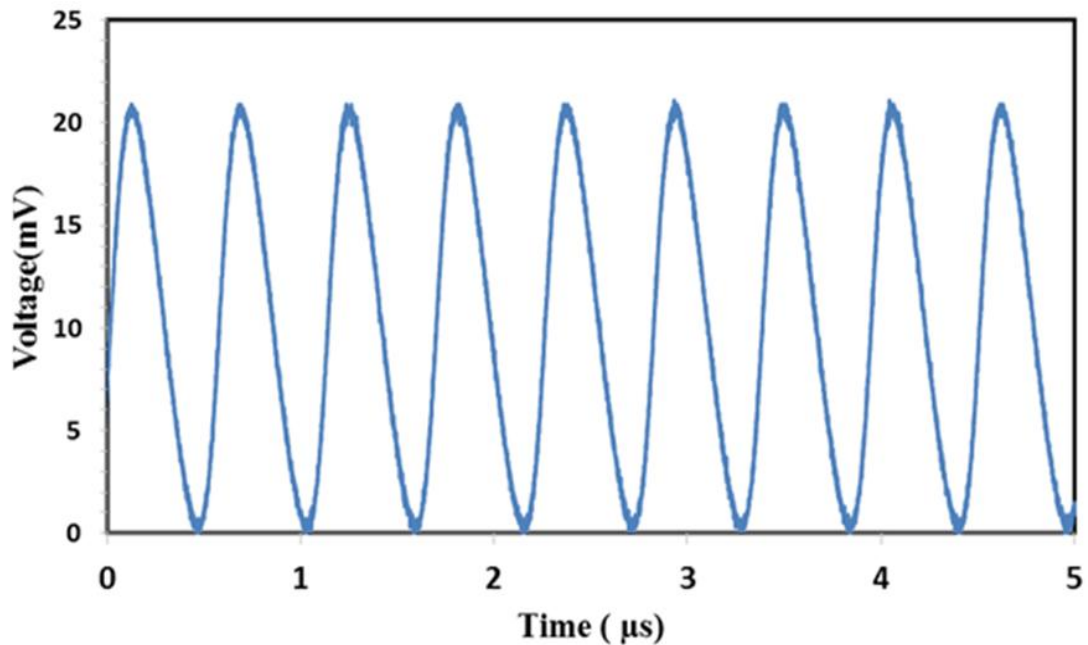


Figure 3. 25: Typical pulse train of the proposed nanosecond BFL

The output frequency spectrum of the laser is also analyzed with the RF spectrum analyzer as shown in Fig. 3.26. The signal to noise ratio (SNR) obtained is about 38 dB, which confirms the stability of the pulses. However, the obtained SNR is still lower compared to other techniques based on saturable absorber, which has an SNR more than 40 dB similar mode (Ahmad et al., 2013). These results show that the SBS can serve as a passive mode-locker inside the fiber laser resonator to generate nanosecond pulses. The proposed BFL is capable of producing nanosecond pulses with extensive wavelength

tunability, which has many potential applications such as telecommunication applications.

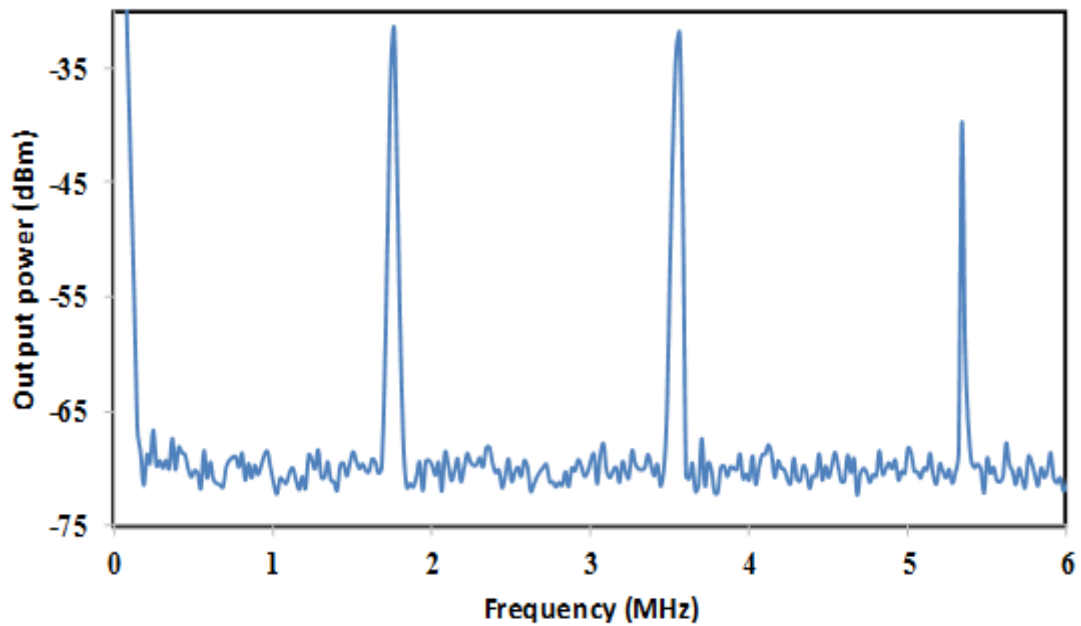


Figure 3. 26: The RF spectrum of the nanosecond pulse BFL

3.6 Summary

A SBS in both SMF and microfiber structures such as non-adiabatic microfiber and IMZI have been investigated. It was observed that the Stokes wavelength is up-shifted by 0.088 nm (10 GHz) from the BP wavelength while the anti-Stokes wavelength is downshifted by the same spacing. It was found that the IMZI can produce higher spontaneous Brillouin scattering Stokes and anti-Stokes powers due to its stronger multimode interference effect compared to the non-adiabatic microfiber. However, both microfiber structures cannot produce the SBS with our current facilities. Therefore, the BFL was then demonstrated using a long piece of SMF, EDF and HNLF as the gain medium. With 10 km long SMF, the threshold BP powers for the ring BFL were obtained at 1.2, 1.5, 2.2 dBm for the laser cavity configured with 10/90, 20/80, and 50/50 output coupler, respectively. The maximum laser's peak power of -3.12 dBm is obtained for the

BFL configured with 50/50 coupler. At a threshold pump power of 1.2 dBm, the BFL exhibited temporal characteristic where the pulse width and repetition frequency of the laser are obtained at 440 μ s and 2 kHz, respectively. As the pump power increases, the pulse width becomes shorter while the repetition rate increases. This Q-switching or pulsing behavior is due to the relaxation oscillation, a natural trait of fiber laser, which occurs around the laser threshold as the SBS grows. With 3 m long EDF, the BEFL was realized to operate at 1561.5nm region with a peak power of -5dBm and an SMSR of more than 5 dB when the BP and 1480nm pump powers were fixed at 5dBm and 34mW, respectively. The BEFL also showed a self-pulsing characteristic with repetition rates of 66.7 kHz but the amplitude of the pulse was significantly lower than the previous BFL. With 100 m long HNLF, the BFL produced a self-starting mode-locking pulse train with a repetition rate of 1.76 MHz at BP power of 10.9 Bm. The pulse width of the laser was maintained at around 270 ns.

CHAPTER 4

DEVELOPMENT OF PULSED LASER BASED ON NONLINEAR EFFECTS

4.1 Introduction

Passively pulsed fiber lasers are attractive for many applications because of their simplicity, compactness, efficient heat dissipation, and ability to generate high-quality pulses (G. P. Agrawal, 2007). For instance, mode-locked Erbium-doped fiber lasers (EDFLs), which are capable of generating ultra-short pulses in the telecommunication wavelength of about $1.55\mu\text{m}$, are promising for use in the next generation telecommunication applications (Dinu et al., 2003). Generation of ultra-short pulses has also attracted considerable attention in other areas of physics such as the ultrafast physics and nonlinear optics. The fundamental of the pulsed lasers is highly related to various type of nonlinearity. For instance, nonlinear polarization rotation (NPR) implementation can easily tune the phase shift in a laser cavity and to achieve different type of fix phase condition in a laser cavity (Xu et al., 2004).

In the previous chapter, the potential of Stimulated Brillouin Scattering (SBS) for generating pulse was investigated. A nanosecond mode-locked pulse train was successfully realized by using a highly nonlinear fiber (HNLF) as a Brillouin gain medium in a ring configuration. In this chapter, several passively mode-locked and Q-switched fiber lasers are demonstrated based on nonlinear effects inside the ring laser cavity. At first, the NPR based mode-locked EDFL with three switchable operation states is proposed and demonstrated by incorporating a 10 km long SMF in the ring cavity. Then, a nanosecond optical pulse generation is demonstrated in EDFL by using a 100 m long HNLF instead of the SMF. The HNLF plays an important role to induce Kerr effect in the cavity, which allows the polarization rotation occur in the cavity. This allows a

mode-locking pulse is generated based on NPR technique. A Q-switched EDFL is also demonstrated based on NOLM cavity. The NOLM is used in the laser cavity to generate the intensity dependent transmission so that it functions as a saturable absorber. Finally, a Q-switched Brillouin fibre laser (BFL) is demonstrated using multi-walled carbon nanotubes (MWCNTs) embedded in polyvinyl alcohol (PVA) film as a passive saturable absorber.

4.2 Harmonic mode-locked EDFL based on NPR effect in a ring laser cavity with assistance from a 10 km long single-mode fiber

Most of the reports on mode-locked EDFLs were focused on ultrafast fiber lasers that emitted femtosecond and picosecond pulses. There are still lacks of research work on generation of nanosecond pulses. Usually nanosecond pulses emitted from mode-locked fiber lasers are giant-chirped and have large duration and low peak power, which may induce little nonlinear phase accumulation during amplification (Komarov et al., 2006; Zhao et al., 2007). Therefore, a nanosecond pulsed EDFL is preferred as a better alternative seed oscillator than a femtosecond or picosecond pulsed one for chirped pulse amplification (CPA) and average power scaling systems. In this section, generation of nanosecond pulses in EDFL based on NPR technique is demonstrated. We employ a long-cavity ring resonator for producing nanosecond pulses in normal dispersion regime. It is worth noting that although the cavity length is significantly long, the fiber laser still operates at its fundamental repetition rate without pulse breaking. The operation regime of the proposed pulse laser can be tuned from fundamental to 3th order harmonic operating regimes under appropriate polarization orientation and pump power.

The experimental setup of our proposed NPR-based mode-locked EDFL is schematically shown in Fig. 4.1. It has a ring configuration and the total cavity length of more than 10 km. A segment of 3.5 m erbium doped fiber (EDF) with an erbium

concentration of 2000 ppm, cut-off wavelength of 910 nm, a pump absorption coefficient of 24 dB/m at 980 nm and a dispersion coefficient of -21.64 ps/nm·km at 1550 nm was employed as the gain fiber. The rest of the ring was made of standard single mode fiber (SMF), whose GVD parameter was 17 ps/(nm km). . The EDF was pumped by a commercial 980 nm laser diode (LD) through a wavelength division multiplexer (WDM). A polarization dependent isolator (PDI) was spliced in the cavity to ensure unidirectional operation of the laser and at the same time to generate linear light polarization. A polarization controller (van Saarloos & Hohenberg) was employed to adjust polarization of light by fine-tuning the linear cavity birefringence. A 10 km spool of SMF constitutes the long cavity and also serves to increase the nonlinearity and dispersion. A 5% of the circulating light is taken out of the cavity via a 95/5 coupler and then split into two outputs by a 3 dB coupler for optical spectral and temporal analysis. The optical spectrum analyser (OSA, Yokogawa, AQ6370B) is used for the spectral analysis of the proposed EDFL with a spectral resolution of 0.02 nm whereas the oscilloscope is used to observe the output pulse train of the EDFL pulse emission via a 1 GHz bandwidth photo-detector. The cavity is operating in a large negative dispersion region due to the long SMF.

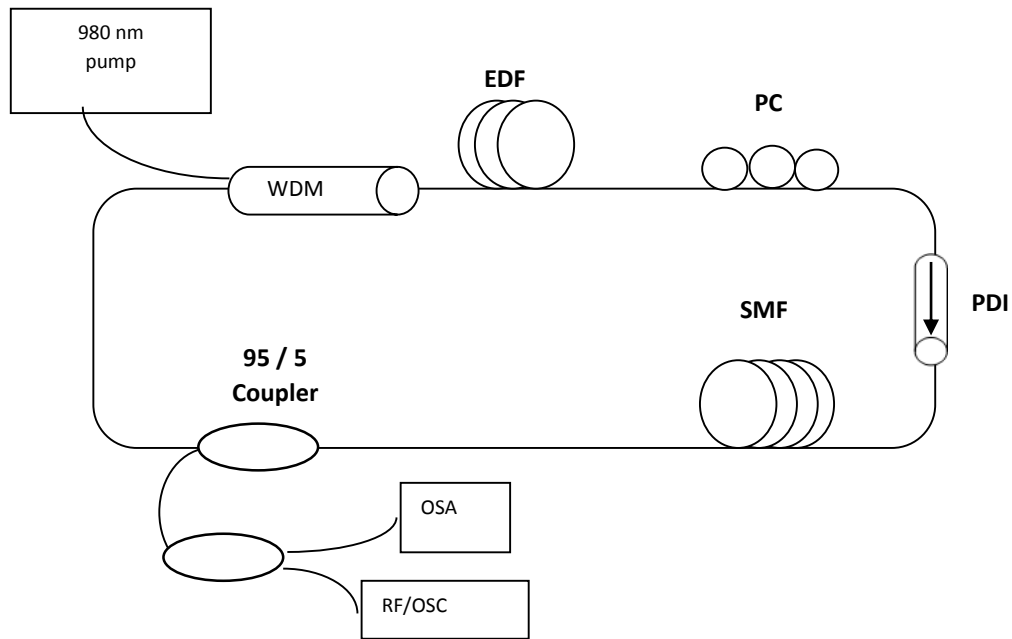
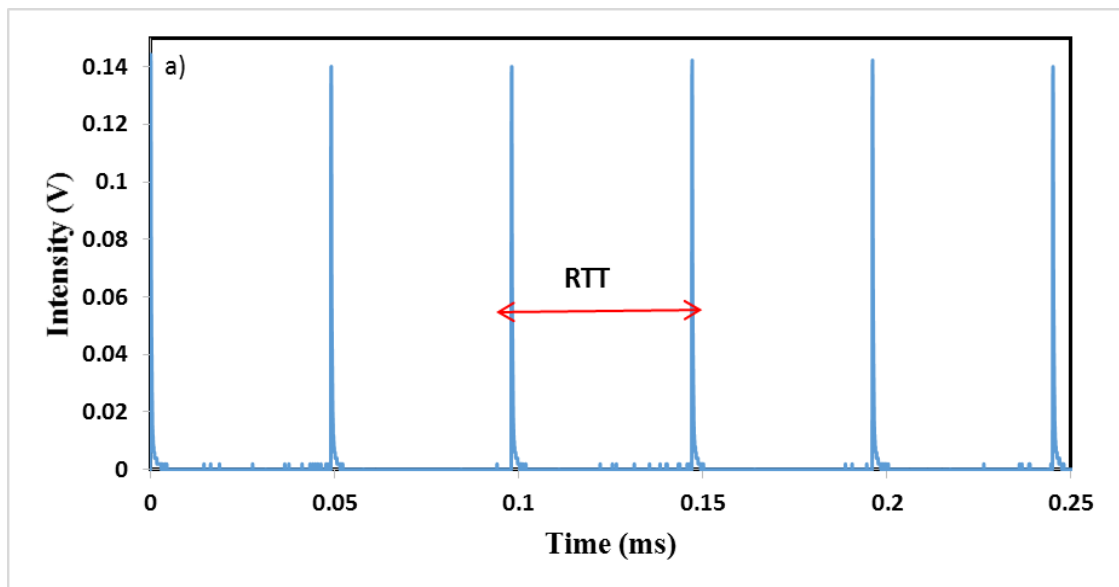


Figure 4. 1: Experimental setup of the proposed EDFL for generating harmonic nanosecond pulses.

The harmonic pulse is generated based on NPR effect in the ring cavity (Becker et al., 1972). The polarization state evolves nonlinearly during the propagation of the pulse inside the EDF and SMF due to SPM and cross phase modulation (XPM) effects in the ring cavity. The state of polarization is non-uniform across the pulse because of the intensity dependence of the nonlinear phase shift. The PC is adjusted so that it forces the polarization to be linear in the central part of the pulse. The polarizing isolator lets the central intense part of the pulse pass but blocks (absorbs) the low-intensity pulse wings. The net result is that the pulse is slightly shortened after one round trip inside the ring cavity, an effect identical to that produced by a fast SA. In other words, the PDI, working together with the birefringence fibers generates an intensity dependent loss mechanism in the cavity that contributes to pulse generation in the cavity.

By carefully adjustment of the PC orientation, pulse emission operating in fundamental repetition rate of 20 kHz could be observed at pumping power threshold of 36 mW as shown in Fig. 4.2(a). To obtain a stable pulse train of laser emission, it is

necessary to have a sufficient nonlinear gain in the cavity. Thus, 10 km SMF provides a nonlinear gain, which is required to obtain a stable pulse train via nonlinear polarisation rotation process. A harmonic pulse can also be formed in round trip time (RTT), where the harmonic's order can be tuned by increasing the pump power as shown in Figs. 4.2(a) to (c). The harmonic's order can be tuned by increasing the pump power. As the pump power is increased to from 36 mW to 158 mW and 282 mW, the repetition rates are shifted to 40 kHz and 60 kHz, which corresponds to 2nd and 3rd harmonics, respectively. The 2nd and 3rd harmonics pulses are shown in Figs. 4.2(b) and (c), respectively



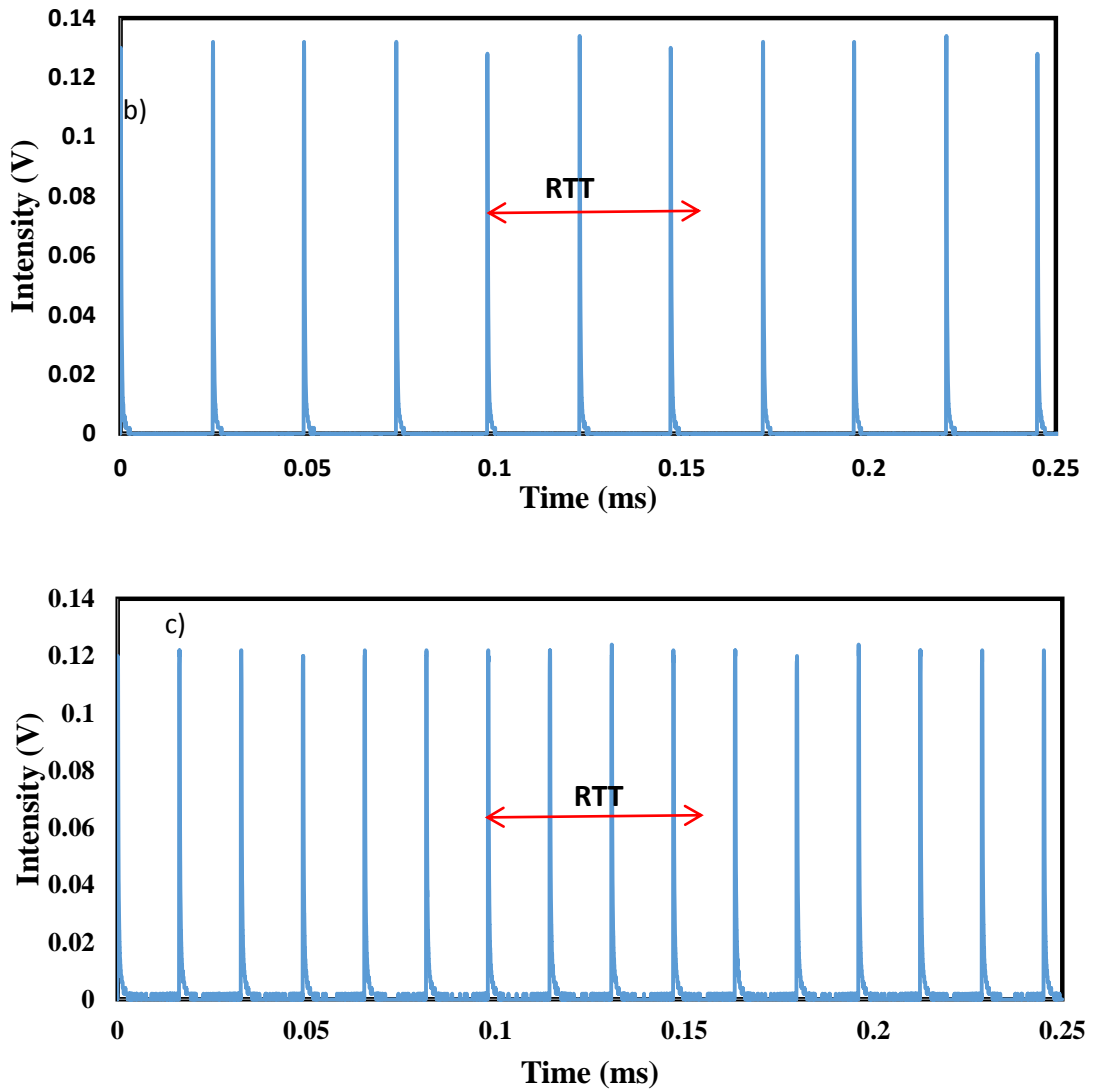


Figure 4. 2: Typical pulse train at different pump powers, which produces a different orders of harmonic (a) fundamental (b) 2nd (c) 3rd

As shown in Fig. 4.2, fundamental repetition rate is observed at 36 mW, whereas 2nd order and 3rd harmonics are obtained at higher pump powers of 158 mW and 282 mW respectively. However, there is no higher harmonic pulses as the pump power is further increased up to 340 mW. This may be caused by the pump power limitation which constrained the pulse from further breaking after the 3th order harmonic. Noted that in high pump power, the pulse trains are able to shift to lower harmonic order by properly adjusting the PC. Higher light intensity may induce a difference in the intensity dependant

phase due to the long and short trajectories in the cavity. With the proper adjustment of PC, the phase variation between the long and short trajectories can be suppressed and achieved plateau harmonic. The output power increases from 0.9 mW to 3.6 mW as the harmonic order is changed from fundamental to 3th order.

Fig. 4.3 shows the radio frequency (RF) spectrum for fundamental of harmonic pulse (at pump power of 36 mW), which reveals the repetition rate of 20 kHz respectively. The signal to noise ratio (SNR) obtained from the intensity ratio of the fundamental peak to the pedestal extinction is estimated to be approximately 50 dB, which indicates the stability of the laser. It is also observed that the pulse energy decreases with the increment of pump power. Harmonic pulses exhibit pulse energy in the nano-Joule range due to the long cavity length used in the laser setup. By increasing the pump power from 36 mW to 282 mW, the pulse energy reduces drastically in a range of 60 to 45 nJ. This is due to the occurrence of pulse breaking phenomena where a single pulse breaks into many pulses; three pulses in this experiment (Liu, 2010). After a single pulse is formed and traverses in the cavity, it encounters high nonlinear effects and dispersion, introduced by the long SMF. A single pulse will break into many pulses where overtaking of different parts of a pulse will lead to optical wave breaking. It can be concluded that a laser should remain single pulse operation in order to realize higher pulse energy.

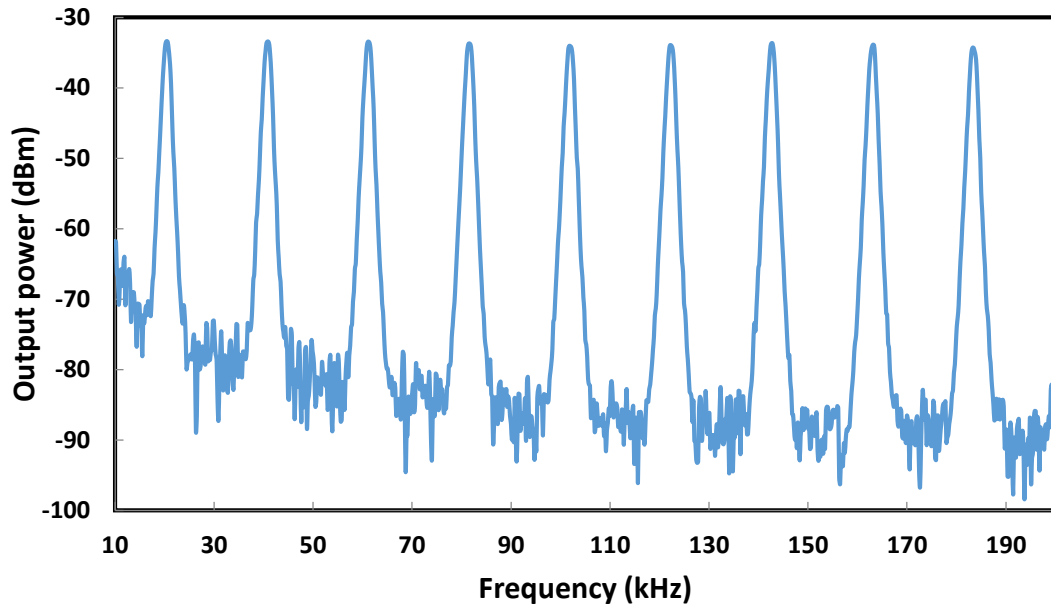


Figure 4. 3: RF spectrum of the generated fundamental harmonic pulse

Fig. 4.4 shows the output spectra of the EDFL at different harmonic orders. By careful adjustment of the PC, the laser produces nanosecond pulses operating in the fundamental, 2nd and 3rd harmonic regimes at pump powers of 36 mW, 158 mW and 282 mW, respectively. The laser operates at 1567 nm and the bandwidth increases with the increase of pulse repetition rate in higher order harmonic. If there is no perturbation introduced to the laser, harmonic pulse EDFL can last several hours under normal laboratory condition.

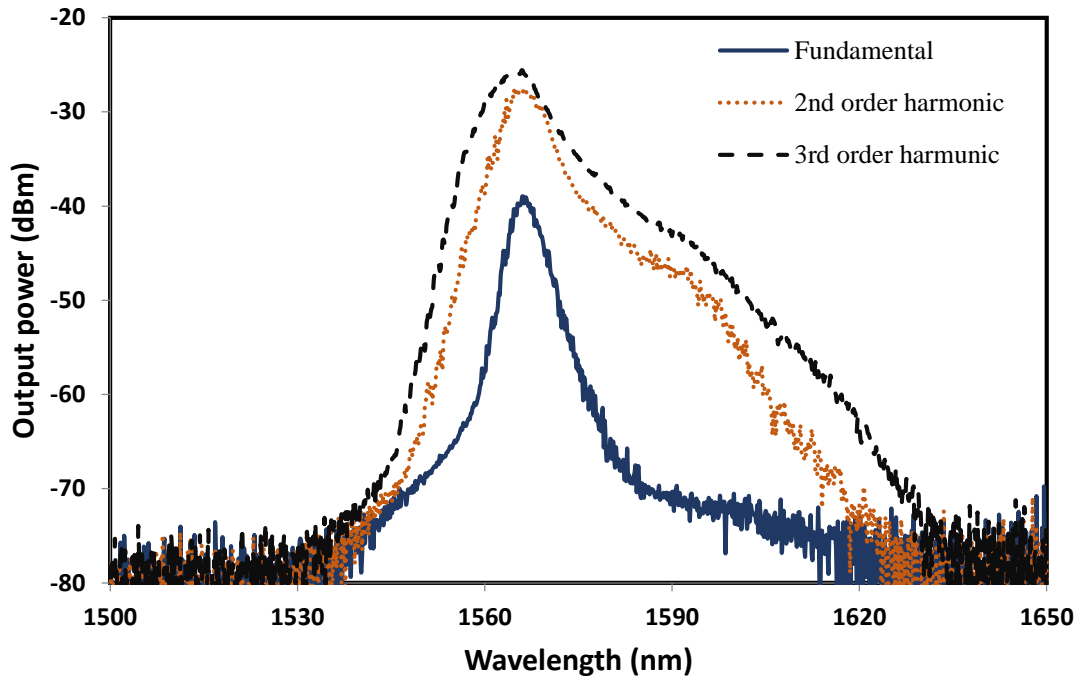


Figure 4. 4: Output spectra of the nanosecond pulses at different order of harmonics.

4.3 Generation of nanosecond pulse with a HNLF

In the previous chapter, highly nonlinear fiber (HNLF) was used to demonstrate nanosecond pulses generation in Brillouin fiber laser (BFL). In this section, nanosecond optical pulse generation is demonstrated in EDFL by using a 100 m long HNLF based on NPR technique. The HNLF plays an important role to induce Kerr effect in the cavity, which allows the polarization rotation occur in the cavity. Compare to BFL, NPR exhibits filtering effect to produce better SNR for nanosecond mode-locked. Fig. 4.5 shows the experimental setup of the proposed EDFL, which is modified version of the previous setup of Fig. 4.1 by replacing the SMF with a HNLF. The HNLF is 100 m long with an effective area of $12.3 \mu\text{m}^2$, dispersion coefficient of 0.15 ps/nm.km at 1550 nm, attenuation of 0.73 dB/km at 1550 nm and nonlinearity coefficient of $10.8 \text{ W}^{-1}\text{km}^{-1}$. The estimated net GVD is 0.88 ps^2 , which in turn increases the energy of the random pulse that emerges from the background noise as light propagates in the cavity. A PDI is used to form a unidirectional cavity and acted as a polarizer to allow only high intensity light

to propagate through. PC is used to tune the polarization in the cavity to achieve phase locked in the cavity. The output of the laser is tapped out of the cavity through a 95/5 coupler while keeping 95% of the light oscillating in the ring cavity. The OSA and oscilloscope are used to inspect the spectrum and the temporal characteristic of the EDFL. The total cavity length of the ring resonator is measured to be around 106 m.

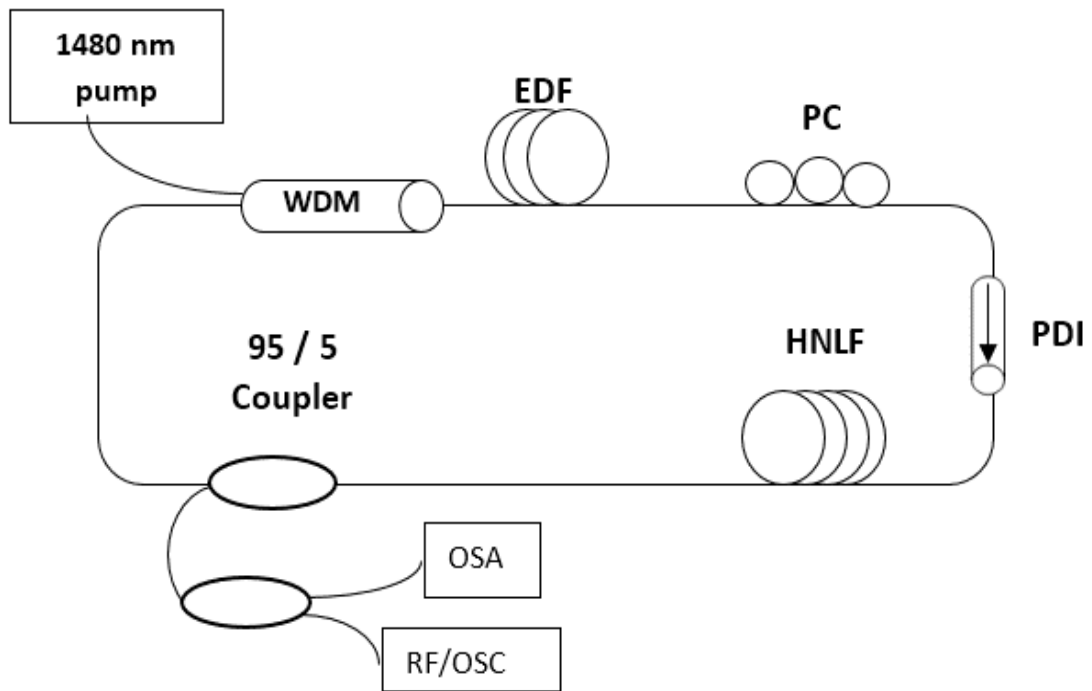


Figure 4. 5: Configuration of the passively mode-locked EDFL with a HNLF

In the experiment, the CW operation of the laser is achieved when the pump power is increased to about 45 mW. By appropriately adjusting PC and pump power, we found that it is easier to achieve nanosecond mode-locked pulses. Fig.4.6 shows the output spectrum of nanosecond mode locked EDFL. As observed in Fig 4.6, the laser operates at around 1567.2 nm with 3-dB bandwidths of 1.62 nm. Besides, a significant spectrum broadening is observed due to SPM effect. It shows a soliton-like spectrum with small Kelly sidebands, which confirms the attainment of the anomalous dispersion. Fig. 4.7 shows a typical oscilloscope trace of the nanosecond pulse trains at pump power of 145 mW. It is observed that the mode-locked laser produces a nanosecond pulse train with a

constant repetition rate of 1.56 MHz throughout the tuning range from 45 mW to 145 mW. This confirmed the mode-locking operation in the cavity. Additionally, with the total cavity length of 140 m, this further identify the laser is operate in fundamental mode. The output power is 2.21 mW at maximum pump power of 145 mW. Taking the average output power divided by pulse repetition rate, the maximum pulse energy is calculated as 1.4 nJ with pulse width of 297 ns. This is considerable high mode-locked pulse energy compare to neither typical picosecond nor femtosecond mode-locked.

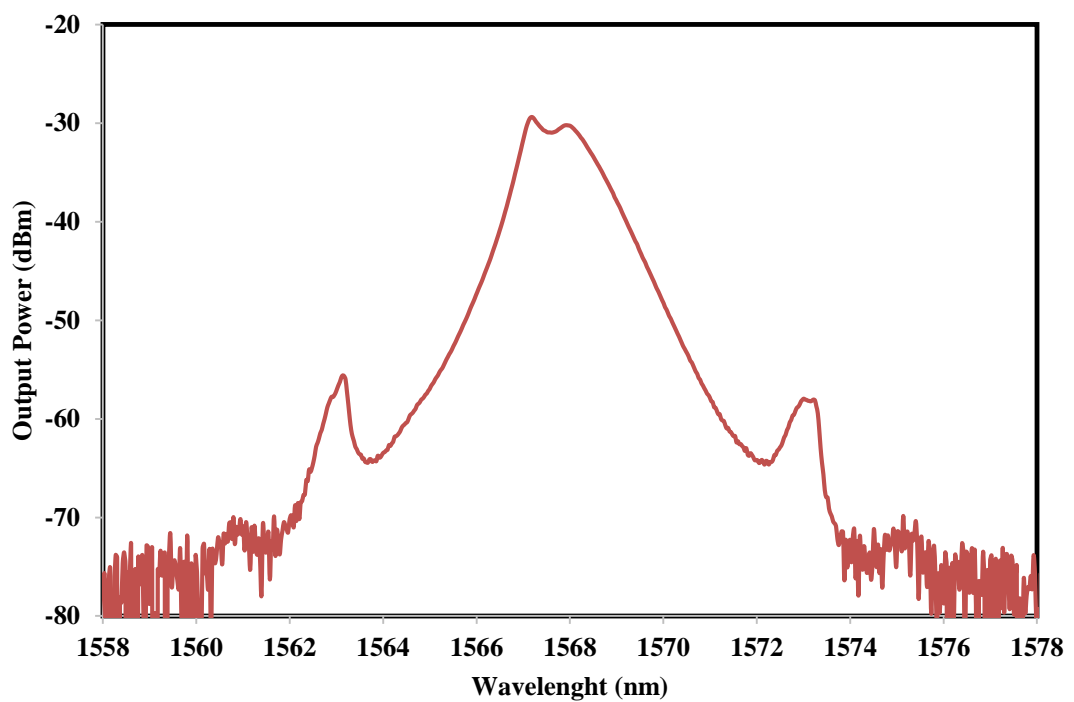


Figure 4. 6: Typical output spectrum of the nanosecond pulse laser

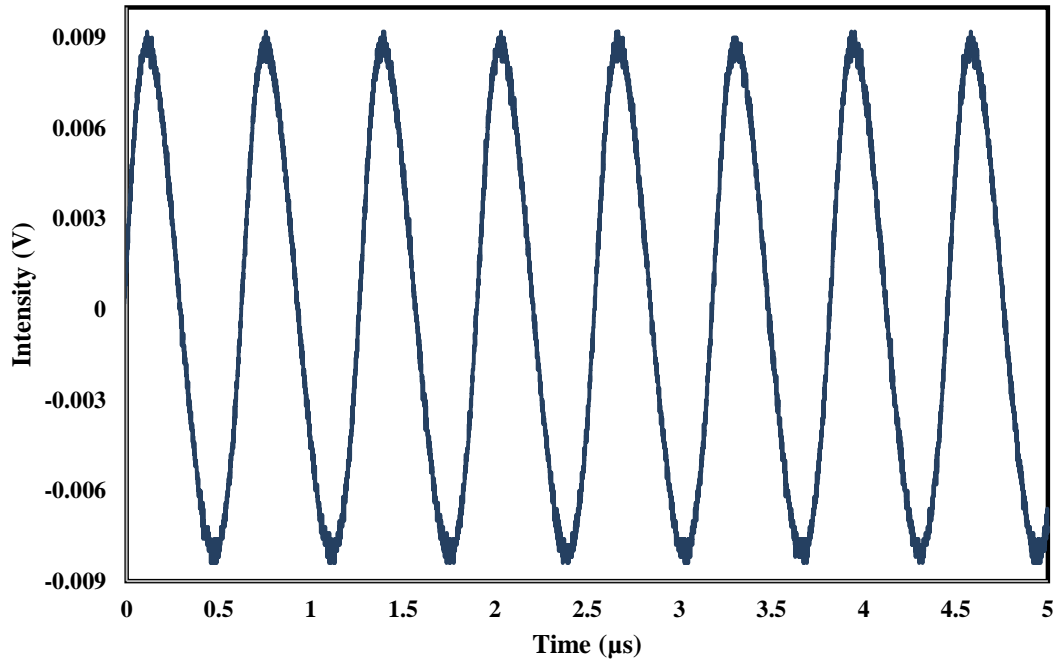


Figure 4. 7: Typical pulse train of the nanosecond mode-locked EDFL

To further identify the mode-locking operation in a single pulse state, the single-pulse temporal profile is also measured as shown in Fig 4.8. The pulse duration (FWHM) was measured to be 297 ns and no bunched pulses were observed in the pulse internal structure. This indicates that the nanosecond pulse obtained is a clean and stable single pulse. In addition, the time-bandwidth product (TBP) of the generated nanosecond pulse is calculated to be 0.401. The deviation from the TBP value of 0.315 expected for transform-limited Sech^2 soliton pulses indicates that the output pulses are heavily chirped. The stability of the nanosecond mode-locked is further studied with radio frequency (RF) spectrum as shown in Fig 4.9. The stability of the nanosecond mode-locked is considerable good as the SNR is more than 50 dB. Besides, the repetition frequency of 1.55 MHz is well tallied with the cavity's fundamental mode. It is believed that the proposed nanosecond pulsed laser with compact all-fiber configuration, high pulse energy and excellent stability can contribute to various applications in optical communication, material processing and biomedicine technology.

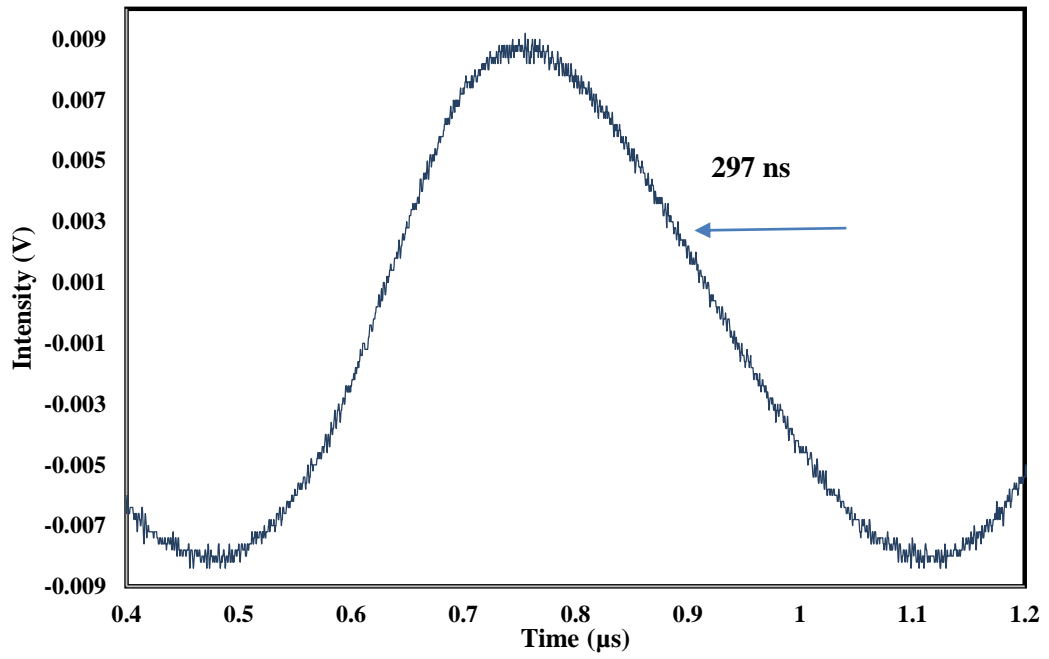


Figure 4. 8: Single pulse envelope

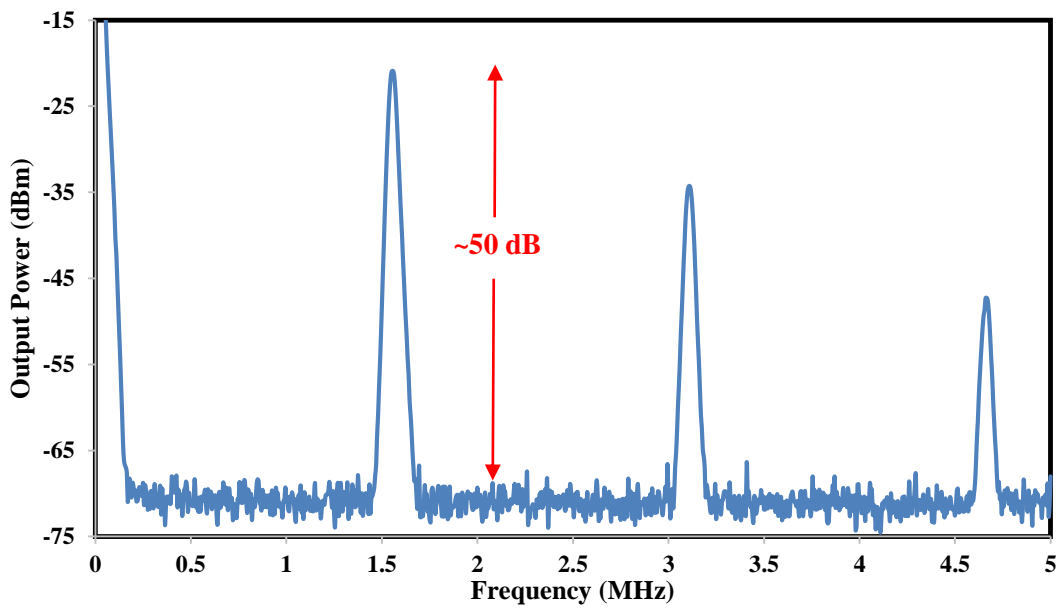


Figure 4. 9: RF spectrum of the nanosecond mode-locking pulse showing a SNR of around 50 dB.

4.4 Q-switched EDFL with HNLF in NOLM cavity

Q-switched pulsed laser systems operating in the eye-safe wavelength region ($\lambda > 1.4 \mu\text{m}$) are promising for applications such as light detection and ranging (lidar)(Reutebuch et al., 2005), differential absorption lidar, optical communication, sensor and instrumentations (Harun et al., 2012; Laroche et al., 2006) Fiber lasers are particularly attractive for such applications due to the fact that the beam quality can be independent of output power and they can be robustly engineered. There is an increasing interest in Q-switched EDFLs, which can be generated by using either active or passive techniques. Compared with the actively Q-switched ones, passively Q switched EDFLs have attracted much attention for their advantages of compactness, low cost, flexibility and simplicity of design. Signac interferometer, such as nonlinear optical loop mirror (NOLM), has been widely used to generate pulsed laser(Duling et al., 1994). NOLM with an imbalance coupler or two different kinds of fiber with imbalanced dispersion (Boscolo et al., 2008) which can operate as a nonlinear power switching device due to the self-phase modulation (SPM) can be used as saturable absorber for pulsed laser.

In this section, a Q-switched EDFL operating in 1561.5 nm band is demonstrated based on NOLM cavity. The laser cavity is based on the figure-of-eight structure. The short range NOLM consisting of a symmetrical coupler and a piece highly nonlinear fiber (HNLF) is used in the laser to generate the intensity dependent transmission so that it functions as a saturable absorber. The proposed laser is capable to generate a Q-switching pulse train with a repetition rate can be controlled within 7.6 kHz to around 22.1 kHz.

4.4.1 Configuration of the proposed NOLM cavity

The experimental setup of the proposed all-fiber passively Q-switched EDFL is shown in Fig. 4.10. The setup is based on our figure-of-eight laser system, where the ring resonator consists of a 3.5 m long EDF as the gain medium, WDM, PDI, 100 m long HNLf, PC and 3 dB couplers. The length and characteristics of EDF and HNLf used are similar with the previous lasers in the earlier sections. The EDF was pumped by a 1480 nm laser diode via the WDM. A PDI was used in the cavity to force the unidirectional operation of the ring, and an in-line PC was inserted in the cavity to adjust the linear birefringence of the cavity. A 2 x 2 3 dB fiber coupler was used to form a figure-of-eight structure with a piece of HNLf is inserted in the new loop to introduce asymmetric nonlinear phase shift between clockwise propagating light and counterclockwise propagating light in the NOLM. The output of the laser is collected from the cavity via a 3dB coupler which retains half of the light in the ring cavity to oscillate.

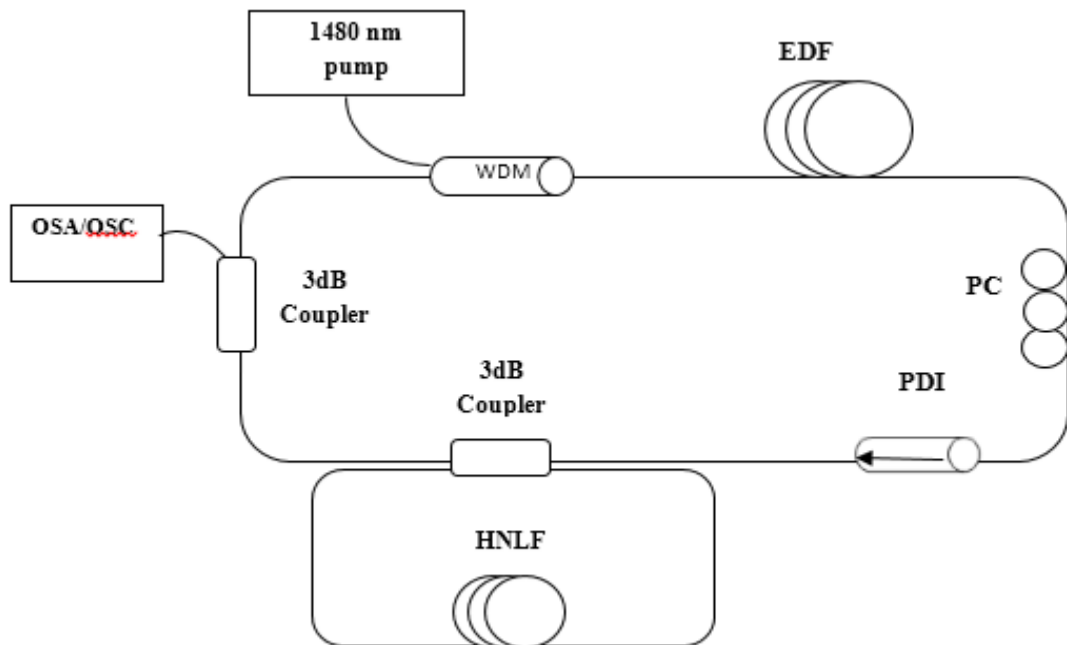
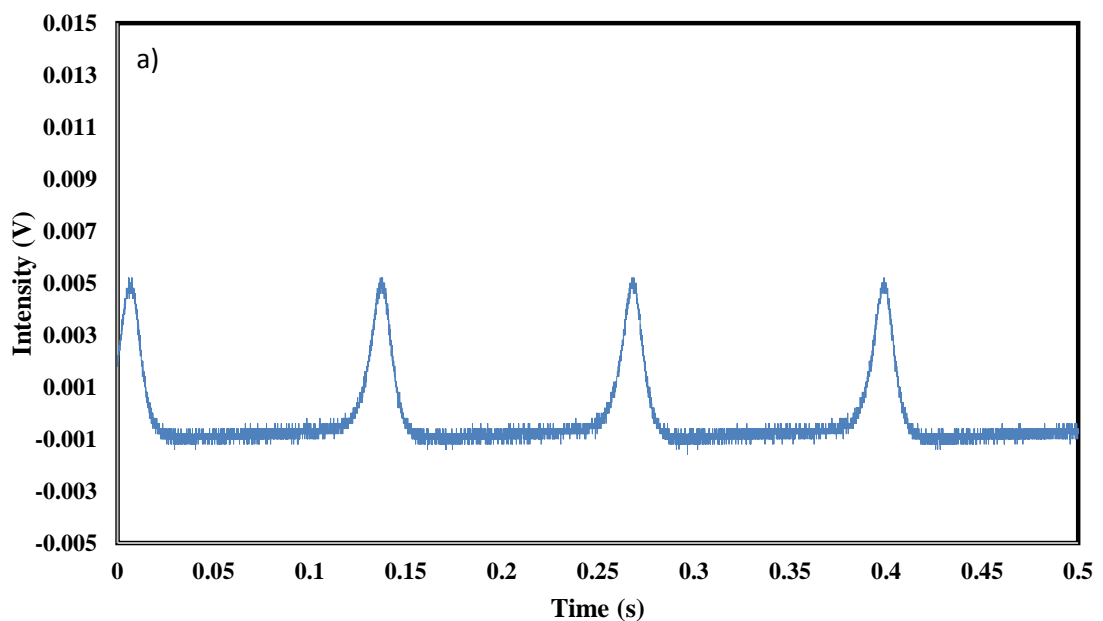


Figure 4. 10: Schematic configuration of the proposed Q-switched EDFL

4.4.2 Q-switching performance

By carefully adjustment of the PC orientation and increase the 1480nm pump over the threshold pump power of 37 mW, Q-switching operation is achieved in the laser. Fig. 4.11 shows the typical pulse train of the laser at three different pump powers. The formation of Q-switching pulse is due to the NOLM structure in the cavity, which functions as an artificial saturable absorber. At first the laser cavity is in high loss and lots of inverted population is accumulated in the upper level of erbium-ion. When the cavity is saturated, the cavity loss rapidly reduces and allows efficient extraction of the stored energy by the laser pulse. The time interval between pulses reduces while the pulse amplitude increases as the pump power increases from 37 to 125 mW, as shown in Fig. 4.11. Unlike the mode-locked fiber laser wherein the repetition rate is dependent on cavity length, the repetition rate of the Q-switched fiber laser increases with pump power.



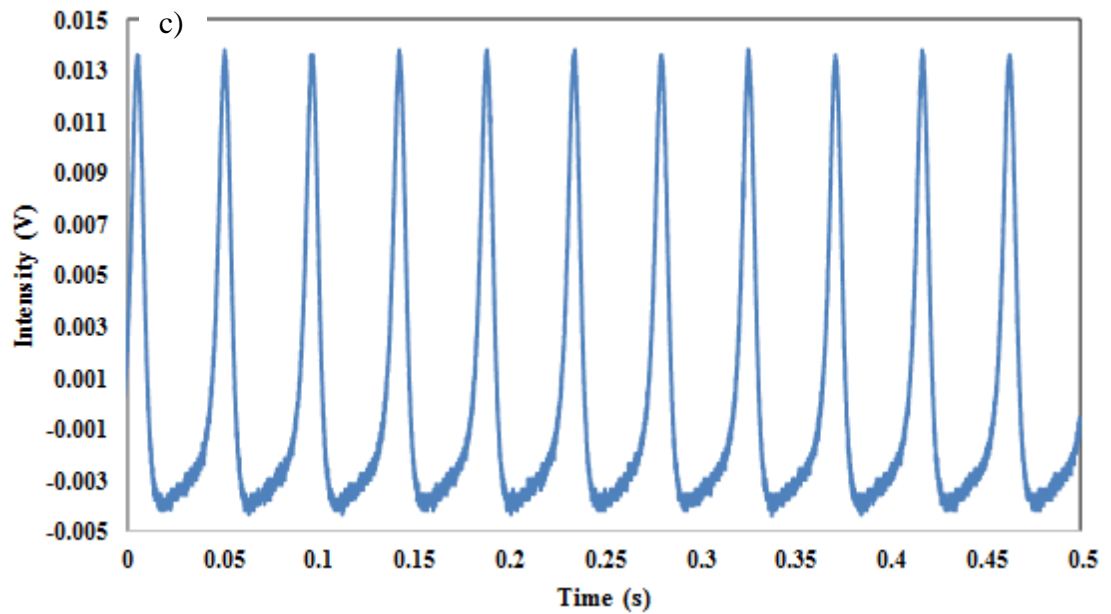
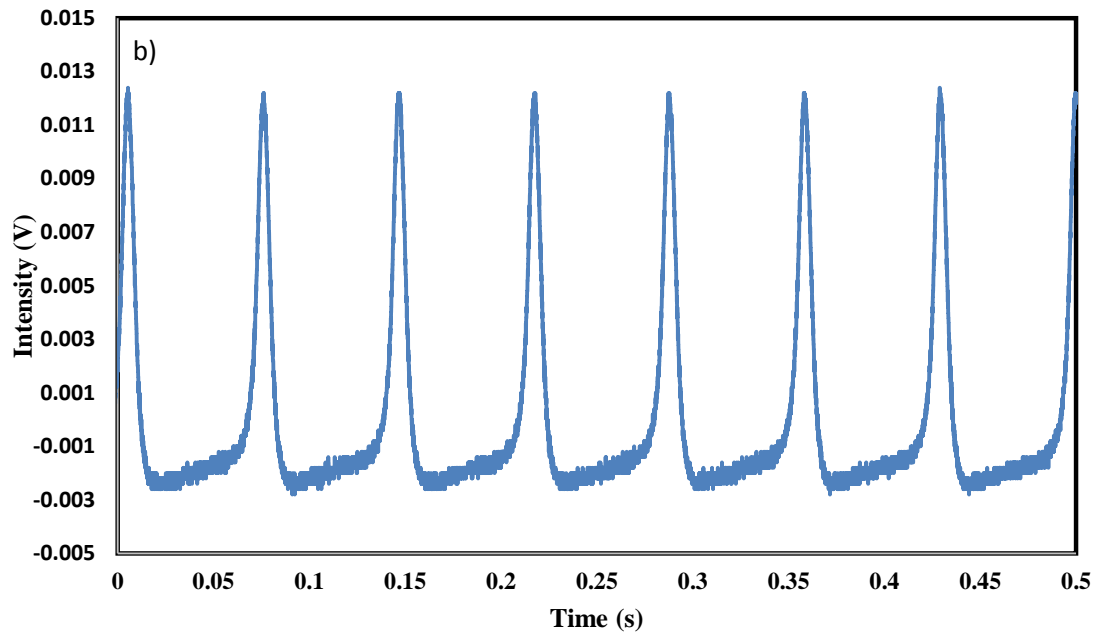


Figure 4. 11: Q-switched pulse emission of the proposed EDFL at different pump power

Fig. 4.12 shows the output spectrum of the Q-switched EDFL when the pump power is fixed at 125 mW. The laser operates at central wavelength of 1561.5 nm with a 3 dB bandwidth of 2.5 nm. A significant spectrum broadening is also observed due to SPM effect. Fig. 4.13 shows how repetition rate and pulse width are related to the pump power. The dependence of the pulse repetition rate can be seen to increase almost linearly with the pump power, whereas pulse width decreases almost linearly with the pump

power. This agrees well with the passive Q-switching theory. The pulse repetition rate of the Q-switched EDFL can be widely tuned from 7.6 to 22.11 kHz by varying the pump power from 37 to 125 mW. On the other hand, the pulse width reduces from 9 to 5.7 μs as the pump power increases from 37 to 125 mW. Fig. 4.14 shows how the average output power and pulse energy of the all fiber passively Q-switched EDFL are related with the pump power. As shown in the figure, average output power almost linearly increases from 5 μW to 18 μW as the pump power increases from 37 to 125 mW while the pulse energy increases from 0.6 to 8.2 nJ at the same pump power range.

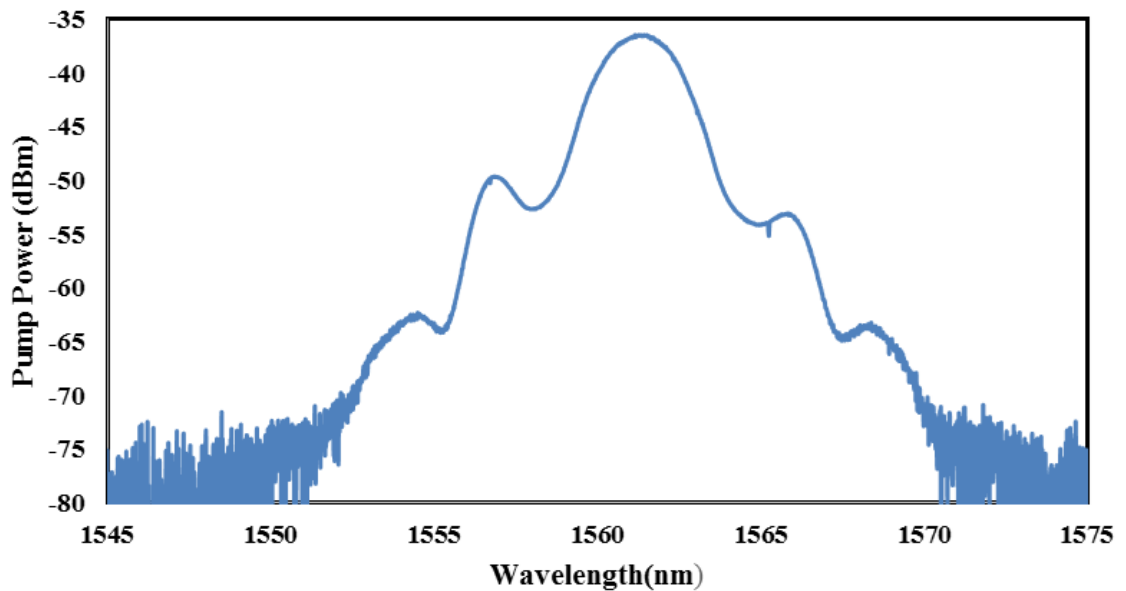


Figure 4. 12: Output spectrum of the NOLM based Q-switched EDFL.

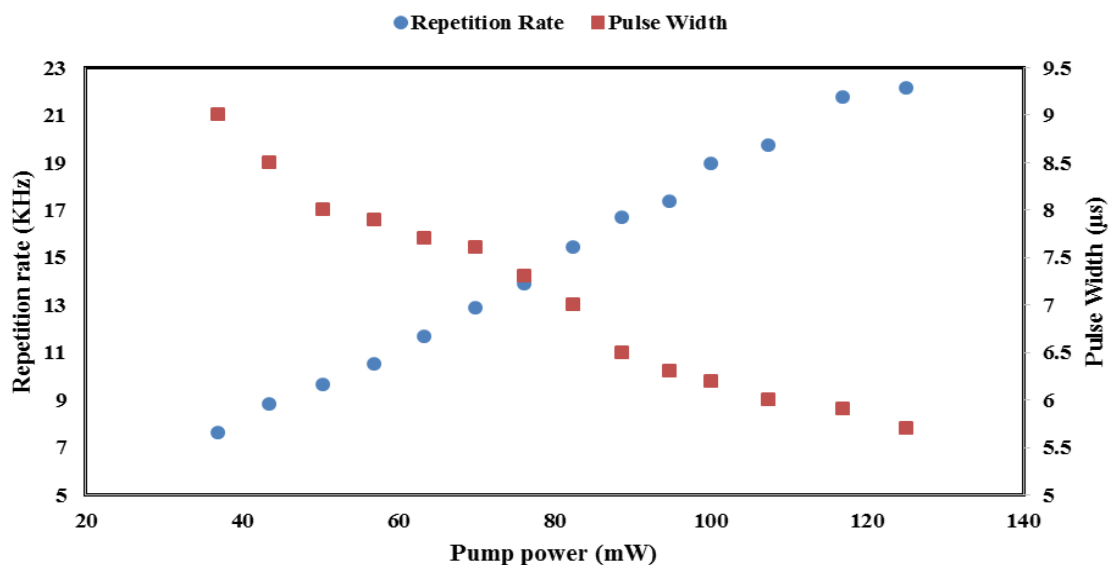


Figure 4. 13: The change of repetition rate and pulse width against pump power.

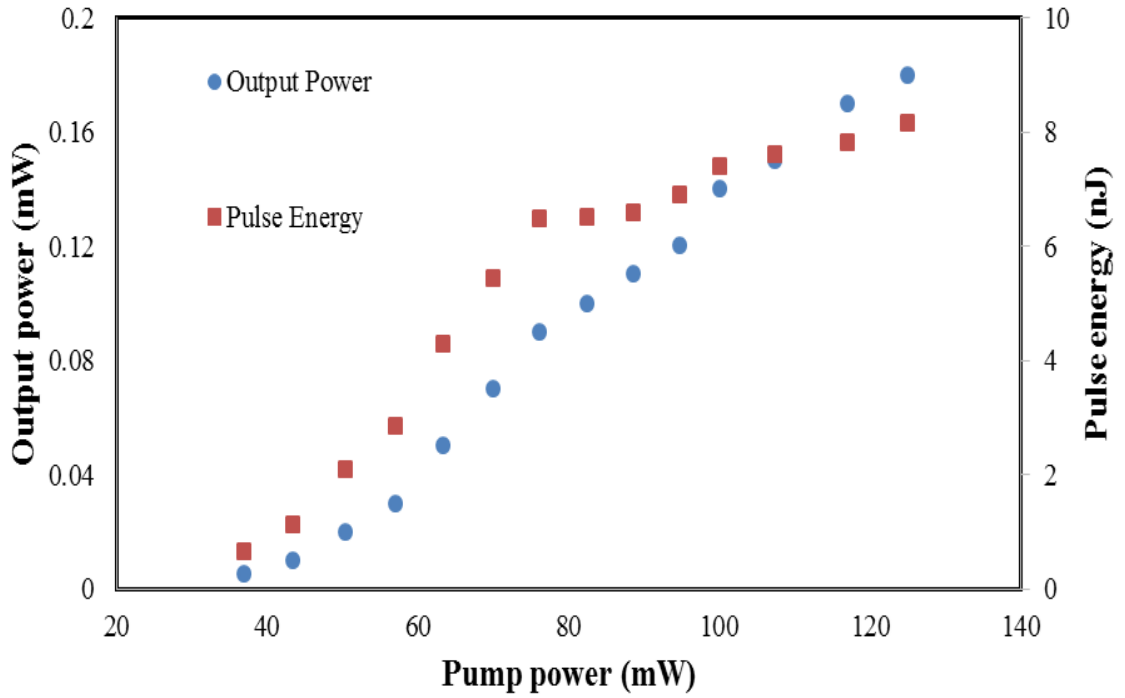


Figure 4. 14: Average output power and pulse energy of the laser against pump power

4.5 Q-switched Brillouin fiber laser with MWCNT SA

Q-switched fibre lasers are mainly used for generating high energy pulses at relatively low repetition rates. They can be constructed by various passive techniques such as NPR and NOLM techniques. They have also been intensively investigated using different kinds of saturable absorbers (SAs) such as transition metal-doped crystals and semiconductor saturable absorber mirrors (Huang et al., 2009; Pan et al., 2007). However, these SAs are complex and expensive to fabricate. Furthermore, they are incompatible with many optical fibres which limits widespread application.

In the past few years, single-walled carbon nanotubes (SWCNTs) have been discovered to have promising potential for SA applications because of their intrinsic saturable absorption properties, ultrafast recovery time and wide absorption wavelength bandwidth (Harun et al., 2012; Hasan et al., 2009). Recently, new, multi-walled carbon nanotubes (MWCNTs) (Iijima, 1991; Su et al., 2012) have also attracted much attention

because they possess many advantages in non-linear optics. The growth of the MWCNT material does not need complicated techniques or special growing conditions so that its production yield is high for each growth. Therefore, the production cost of MWCNT material is about 50%–20% of that of SWCNT material (L. Zhang et al., 2011). In addition, MWCNT material has good thermal characteristics, which is of great importance for high power ultrafast laser development. Compared with SWCNTs, the MWCNTs have higher mechanical strength, better thermal stability as well as the ability to absorb more photons per nanotube because of its higher mass density of the multi-walls. These favourable features are because of the structure of MWCNTs which takes the form of a stack of concentrically rolled graphene sheets. The outer walls can protect the inner walls from damage or oxidation so that the thermal or laser damage threshold of MWCNTs is higher than that of SWCNTs (Banhart, 1999; Ramadurai et al., 2008). However, there are reported that the MWCNTs has a high saturation intensity and thus it was considered a not good SA for mode-locking operation as this would require high irradiation intensity to reach absorption saturation (Elim et al., 2004; Lim et al., 2006). Therefore to date, there are only a few reported works on application of MWCNTs material as a SA. For instance, Lin et al. (Lin et al., 2013) employ multi-walled MWCNTs based SA for mode locking of a Nd:YVO₄ laser. In another work, Q-switched Nd-YAG laser is demonstrated using the MWCNTs based SA as a Q-switcher (Wong et al., 2007).

On the other hand, many works have also been reported on Brillouin fibre lasers (BFL), which use a non-linear effect in optical fibre to generate a narrow linewidth and high coherence laser (Jusoh et al., 2013; Shirazi et al., 2008). The applications of such a laser include optical gyroscope, microwave frequency generation, high-rate amplitude modulation, interferometric position sensors and laser radar. In the previous chapter, the temporal characteristics of BFL was investigated and demonstrated for realizing a pulse laser. We have successfully demonstrated a Q-switched and mode-locked BFL by

manipulating the cavity of the laser. A Q-switched EDFL is also demonstrated in the previous section based on NOLM effect. In this section, a Q-switched BFL using a passive SA made of MWCNTs embedded in a polyvinyl alcohol (PVA) film is demonstrated for the first time. It exploits the stimulated Brillouin scattering (SBS) effect from the interaction between intense pump light and acoustic waves in a 5 km long dispersion shifted fibre (DSF) to generate a non-linear laser shifted by 0.08 nm from the pump wavelength. The SA is constructed by sandwiching a MWCNTs-PVA film between two fiber connectors. The laser delivers Q-switched pulses with a repetition rate of 30.21 kHz and pulse width of 1.11 μ s at the pump power of 6 dBm.

4.5.1 SA preparation and experimental setup

The MWCNTs material used for the fabrication of the absorber in this experiment was dispersed in water with assistance of surfactant. The diameter of the MWCNTs used was about 10–20 nm and their length was around 1 to 2 μ m. The surfactant solution was prepared by dissolving 4 g of sodium dodecyl sulphate (SDS) in 400 ml deionized water. Then 250 mg of MWCNT was added to the solution and the homogenous dispersion of MWCNTs was achieved after the mixed solution was sonicated for 60 minutes at 50 W. The solution was then centrifuged at 1000 rpm to remove large particles of undispersed MWCNTs to obtain a stable dispersed suspension. Next, PVA solution was prepared by dissolving 1 g of PVA in 120 ml of deionized water. Afterward, the dispersed MWCNTs suspension was poured into the PVA solution at four to one ratio to obtain MWCNTs-PVA composite. The MWCNTs-PVA composite was made homogeneous by sonification process for more than one hour. It was then casted onto a glass petri dish and left to dry at room temperature for about one week to produce thin film with thickness around 50 μ m. The SA is fabricated by cutting a small part of the prepared film and sandwiching it

between two FC/PC fiber connectors, after depositing index-matching gel onto the fiber ends. The insertion loss of the SA was measured to be around 3 dB at 1550 nm.

The experimental set-up of the proposed BFL is illustrated in Fig. 4.15 which consists of a Brillouin pump (BP), a 3-port optical circulator, a 5 km DSF, a 80:20 coupler and a MWCNTs-PVA SA. The BP is an external tunable laser source (TLS) with a maximum power of 6 dBm at 1550 nm wavelength. The BP is launched into the DSF from port 1 to port 2 of the optical circulator to generate the backward propagating Stokes via the SBS process. The Stokes oscillates inside the ring cavity to initiate laser at a wavelength which is downshifted by 0.08 nm from the BP wavelength. The MWCNTs-PVA SA is used to generate a Q-switching pulse train. The output of the laser is collected from the cavity via a 80:20 coupler which retains 80% of the light in the ring cavity to oscillate. The OSA is used for the spectral analysis of the BFL's wavelength with a spectral resolution of 0.02 nm. The temporal characteristic of the laser is measured by a photo-detector and an oscilloscope.

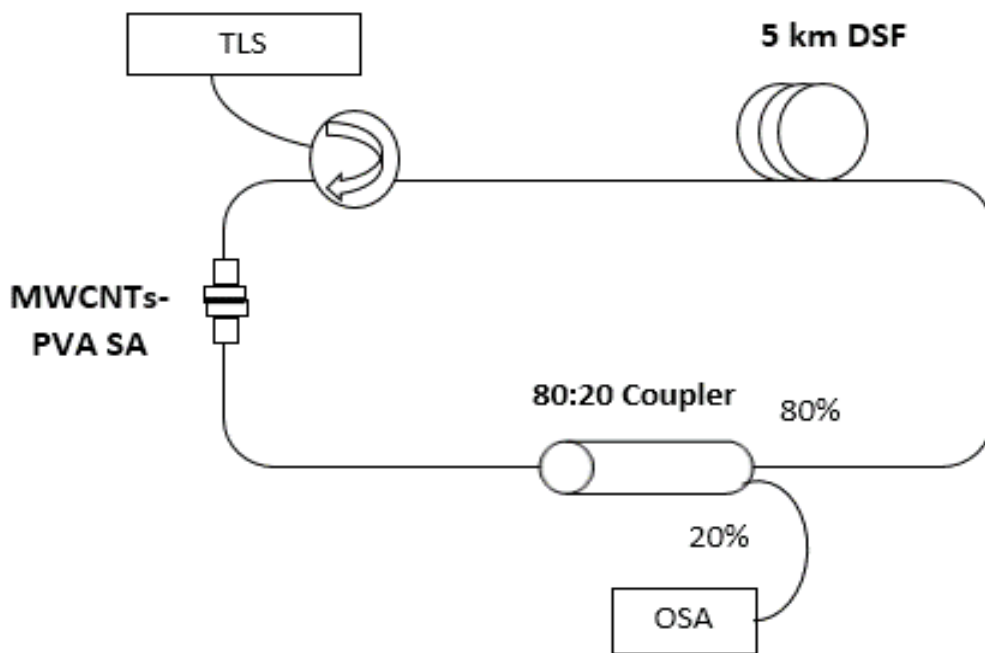


Figure 4. 15: Schematic configuration of the proposed-switched BFL

4.5.2 Characteristics of SA

In order to check the existence of the MWCNTs in the film, we use the Field Emission Scanning Electron Microscope (FESEM) and Raman spectrometer to check the image and its material characteristic, respectively. Fig. 4.16 illustrates the FESEM image of the film at magnification of 35,000 times which indicates the MWCNTs are randomly embedded in the polymer composite. Fig. 4.17 shows the Raman spectrum, which is dominated by two peaks; the G band at 1593 cm^{-1} , which corresponds to tangential C-C stretching vibrations in the nanotube wall plane and the D-band at 1356 cm^{-1} , which originates from a double resonance process and is due to the presence of amorphous disordered carbon. In the SWCNT, there is a series of bands appearing at the frequency region of around 200 cm^{-1} known as Radial Breathing Mode or RBM bands. The RBM bands correspond to the expansion and contraction of the tubes. The RBM modes are not presented in the MWCNT because the outer tubes restrict the breathing mode. The G' band is also observed at 2720 cm^{-1} due to two-phonon scattering phenomena. In addition, another intense peak at 2915 cm^{-1} is also obtained due to the existence of PVA polymer. We also use the UV-Vis/NIR spectrophotometer to check the transmission spectrum of the film at 1550 nm wavelength region. The initial transmission at 1550 nm is measured to be around 46 % as shown in Fig. 4.18. The dependence of the linear transmission of the MWCNTs-PVA film on the signal power is also investigated as shown in Fig. 4.19. In the experiment, the input signal wavelength is fixed at 1550 nm. The curve indicates that the film has the saturable absorption (modulation depth) of around 4% and non saturable absorption of around 45%.

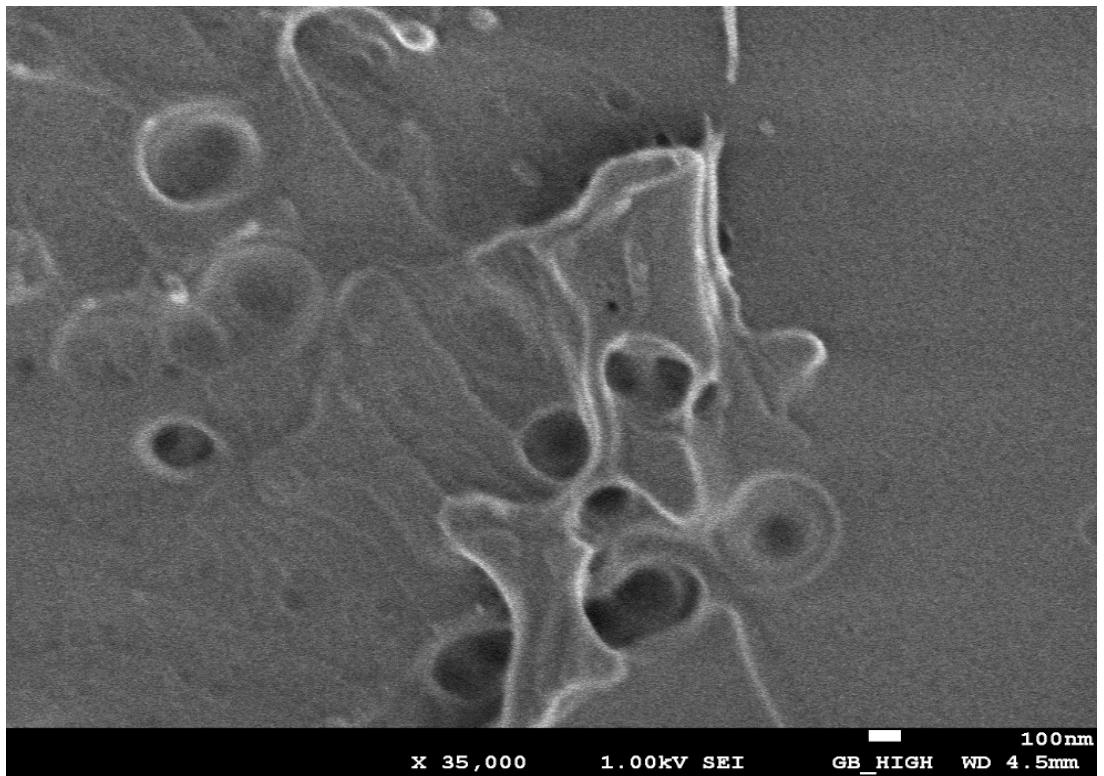


Figure 4. 16: FESEM image of the prepared MWCNTs-PVA film

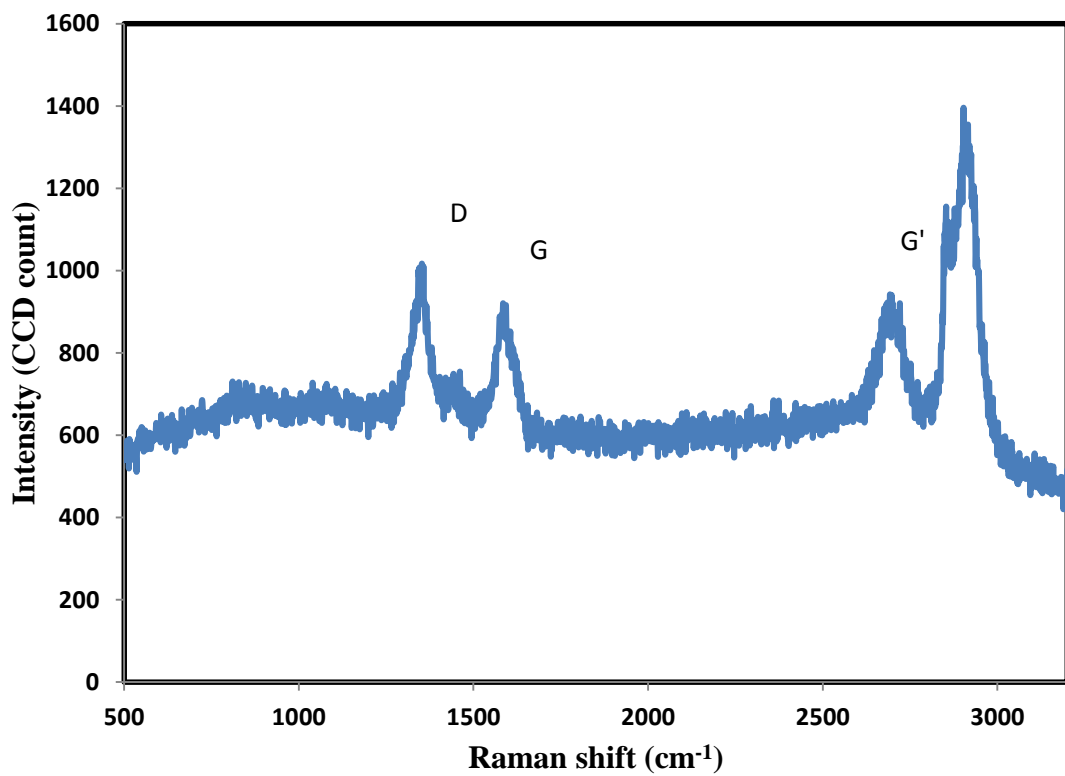


Figure 4. 17: Raman spectrum obtained from the MWCNTs-PVA film

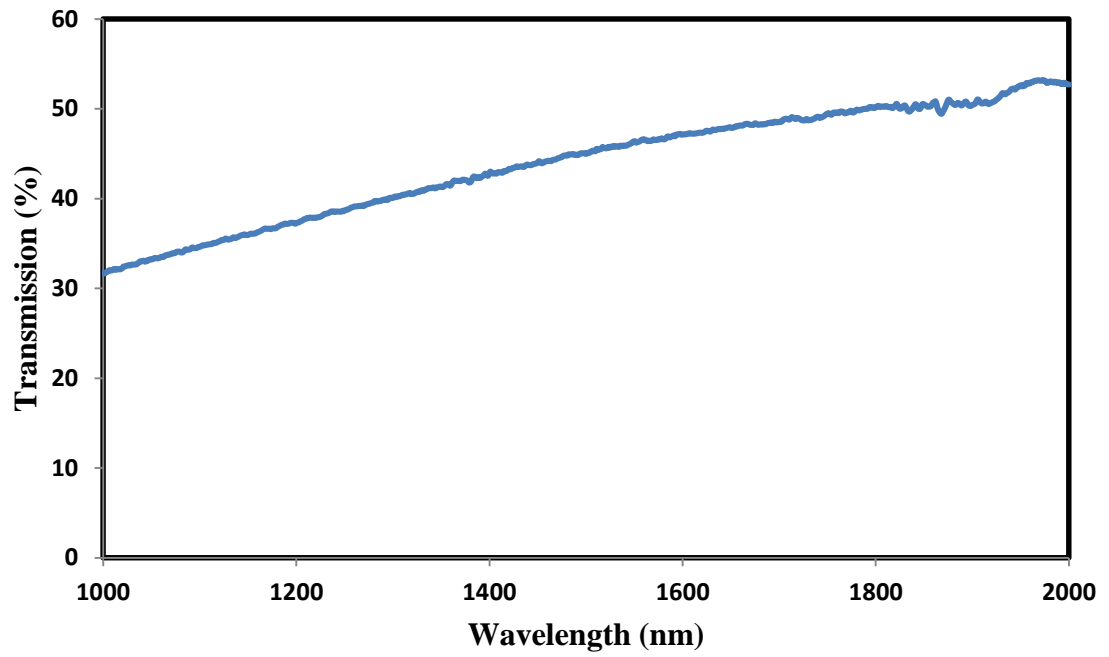


Figure 4. 18: Transmission spectrum of the MWCNTs-PVA film

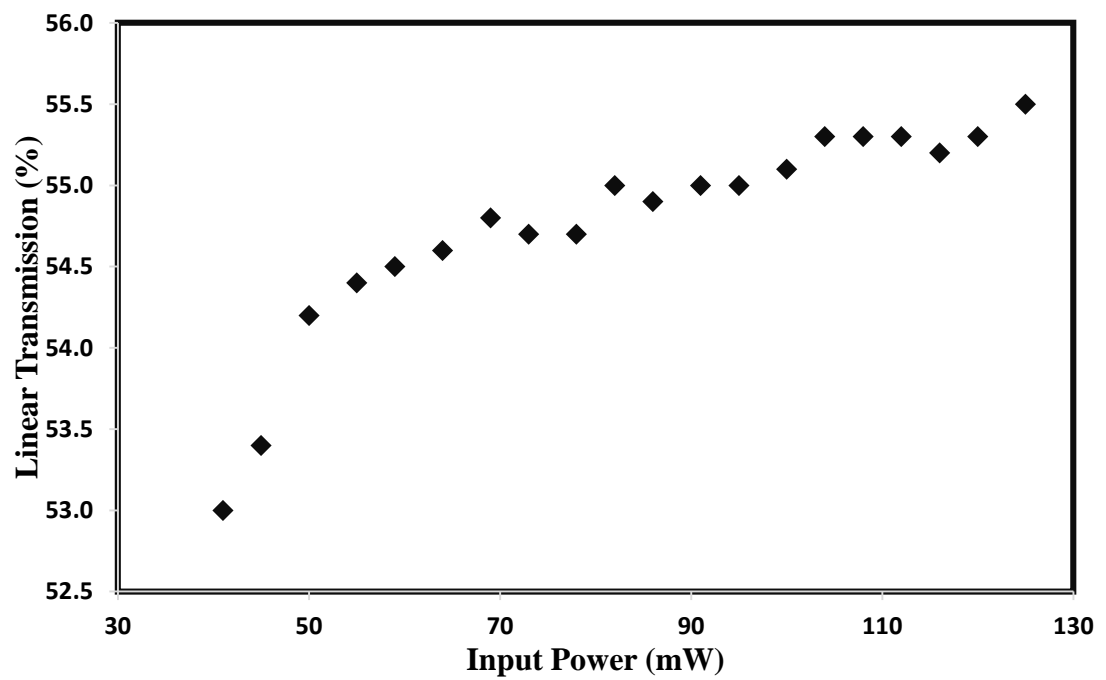


Figure 4. 19: Linear transmission curve of the MWCNTs-PVA film, which shows that the saturable absorption and non saturable absorption of around 4% and 45%, respectively

4.5.3 Performance of the Q-switched BFL

Fig. 4.20 shows the output spectrum of the Q-switched BFL at different pump powers. The Brillouin Stokes operates at a wavelength which is 0.08 nm shifted from the BP wavelength at BP power of 4.5 dBm. By increasing the BP power to 5 dBm, the peak power of the Stokes increases drastically from -49.4 dBm to -15.5 dBm. The peak power linearly increases to -9.8 dBm as the pump power further increases to 6 dBm. As shown in Fig.4.6, anti-Stokes is also obtained at a wavelength, which is 0.08 nm shorter than the BP. The regenerative FWM between co-propagating Rayleigh-backscattered pump and Brillouin Stokes waves can generate an idler wave or anti-Stokes at the wavelength 0.08 nm shorter than the pump. However, the power of the idler should be proportional to the pump power squared times the Stokes power. Another idler is also expected to appear at a wavelength 0.08nm longer than the Stokes wave due to the FWM interaction. Since the anti-Stokes power is almost unchanged with the pump power and another idler cannot be found in Fig. 4.20, we expect the origin of the anti-Stokes component may be spontaneous anti-Stokes Brillouin scattering. The plot of the peak power against the BP power is shown in Fig. 4.21 for both BFLs configured with and without the SA. Without the MWCNTs-PVA SA, the BFL threshold is observed to be around 1 dBm. As the SA is incorporated in the cavity, the cavity loss is increased and the Brillouin laser threshold increases to around 5 dBm. After reaching the threshold, the peak power of the BFL linearly increases with the pump power. The average output power is lower in the Q-switched BFL due to the SA insertion loss.

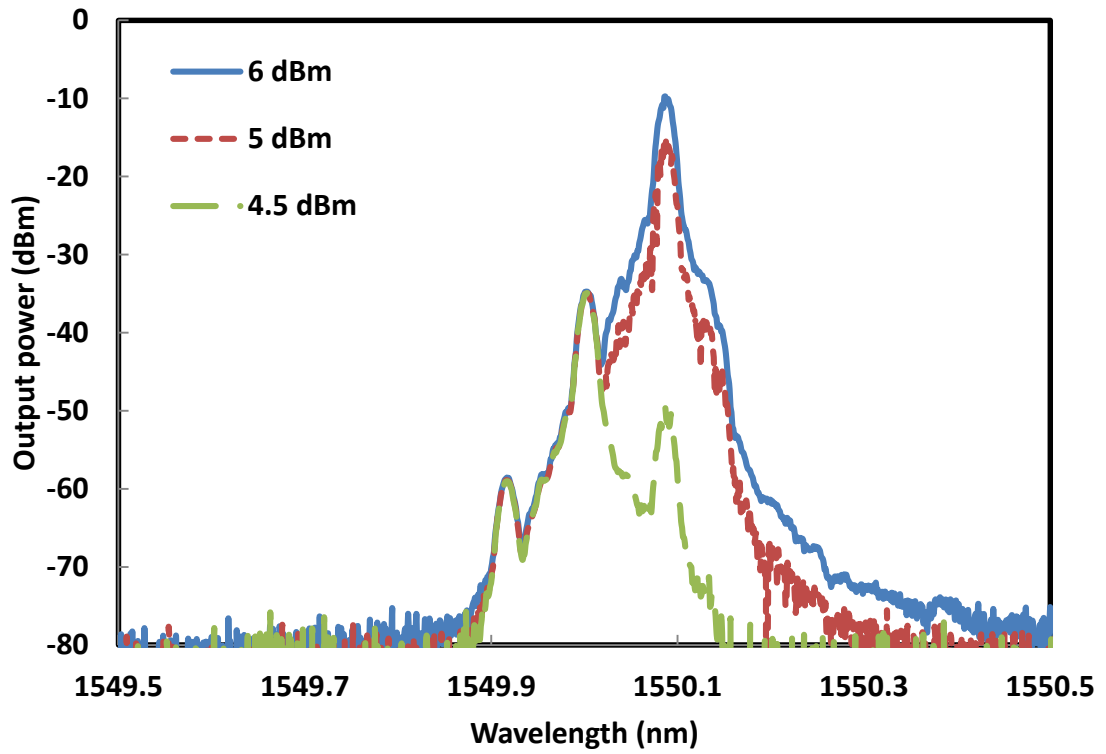


Figure 4. 20: Output spectrum of the proposed Q-switched BFL with MWCNTs-PVA SA

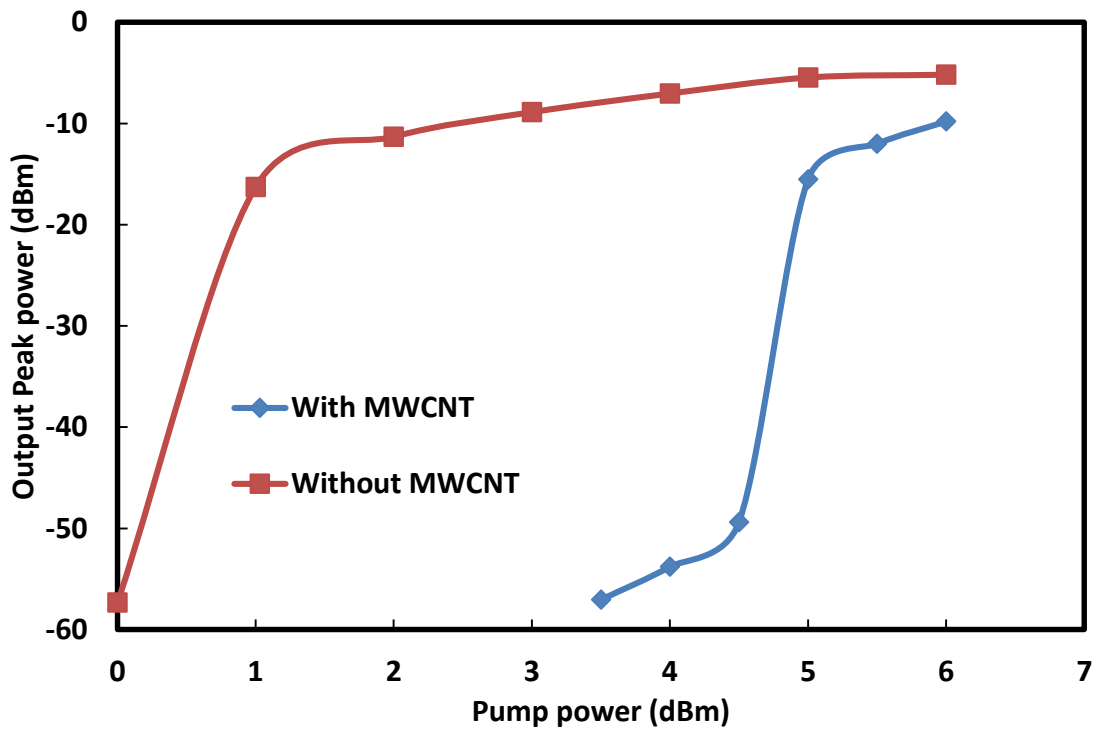


Figure 4. 21: Output peak power of the BFL against the BP power with and without the MWCNTs-PVA SA in the laser cavity.

Fig. 4.22 shows the typical oscilloscope trace of the BFL configured without the SA at two different BP powers of 1 and 5 dBm. At threshold pump power of 1 dBm, a random pulse is obtained due to a nonlinear self-pulsing mechanism based on inherent instability of the BFL. The origin of this instability lies in the relaxation oscillation, a natural trait of fiber laser which occurs around the laser threshold (Fotiadi et al., 1999) that causes a series of avalanche processes. The Stokes power generated by the BP does not approach its steady state value monotonically but exhibits relaxation oscillations with a period of $2T_r$, where $T_r = L/v_g$ is the transit time for a fiber of length L and v_g is the group velocity. In the closed cavity, the relaxation oscillations can be turned into a stable oscillation where both pump and Stokes wave can develop self-induced intensity modulation. Even though the group velocity v_g is nearly the same for the pump and the Stokes wave, their relative speed is $2v_g$ because of their counter-propagating nature. Relaxation oscillations occur as a result of this group velocity mismatch. As the BP power increases the self-pulsing disappears. Therefore, we only observe noise at BP power of 5 dBm.

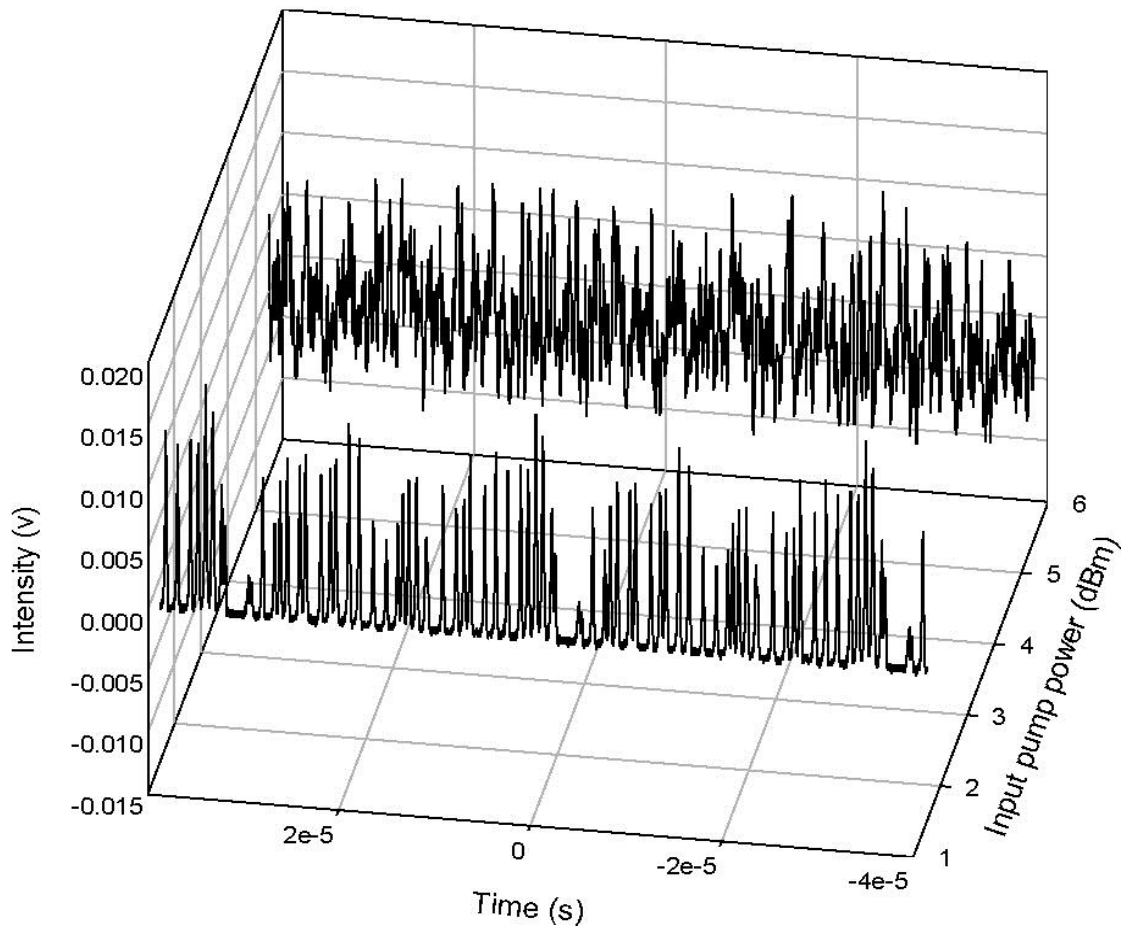


Figure 4. 22: The typical oscilloscope trace from the BFL configured without the SA at two different BP powers; 1.0 and 5.0 dBm.

With the assistance of MWCNTs in the cavity, a stable Q-switched pulse train is self-started at BP power of 5 dBm. Fig. 4.23 shows the pulse train evolution as the BP power increases from 5 to 6 dBm. At the threshold BP power of 5 dBm, the pulse train exhibits peak to peak duration of about $36 \mu\text{s}$, which can be translated to a repetition rate of 27.75 kHz. The corresponding pulse width is measured to be $3.25 \mu\text{s}$. By increasing the BP power, the repetition rate shows an increasing trend to the maximum value of 30.21 kHz at BP power of 6 dBm. On the other hand, the pulse width is inversely proportional to the BP power. The pulse width reduces from 3.25 to $1.11 \mu\text{s}$ as the BP power increases from 5 to 6 dBm. At BP power of 6.0 dBm, the pulse energy is calculated to be about 0.13 nJ. The intensities have slight negative values in the curves shown in Figs.4.8 and 9 due to the un-calibrated oscilloscope.

The output frequency spectrum of the laser is also analyzed with the RF spectrum analyzer (at BP power of 5.5 dBm) as shown in Fig. 4.24. As seen in the figure, the fundamental frequency of the laser is obtained at 29.01 kHz, which corresponds to the repetition rate of the laser. The signal to noise ratio (SNR) obtained is around 50 dB, which confirms the stability of the pulses. These results show that the MWCNTs can be used as a SA to realize a passive Q-switched BFL. The proposed BFL is capable of producing Q-switching pulses with extensive wavelength tenability, which has many potential applications such as for supercontinuum generation, fiber sensors and Brillouin optical amplifier. The laser can perform as a low-cost and easy-built all fiber light source, and can be modified by including an optical feedback in the cavity to produce multi-wavelength output. The Q-switched multi-wavelength laser has potential applications in various fields i.e., temperature or strain fiber sensors(Junqing et al., 2012).

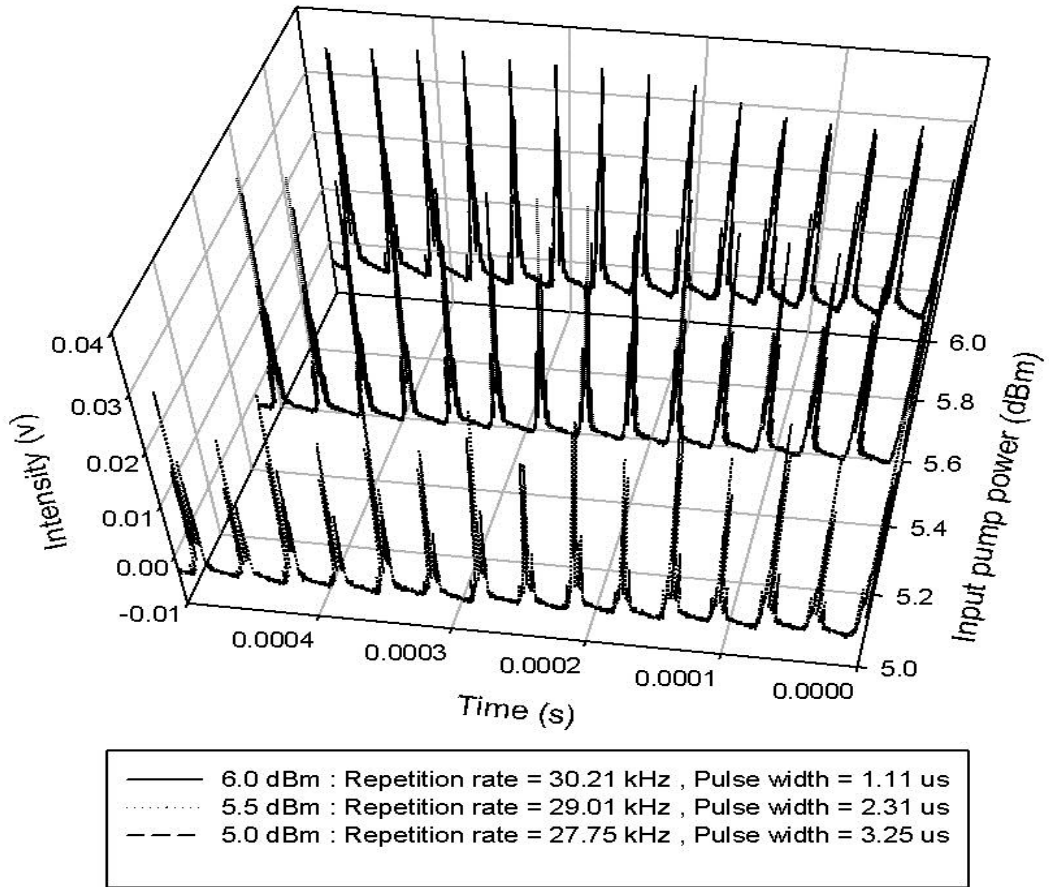


Figure 4. 23: Typical pulse train of the Q-switched BFL at three different BP powers of 5.0, 5.5 and 6.0 dBm

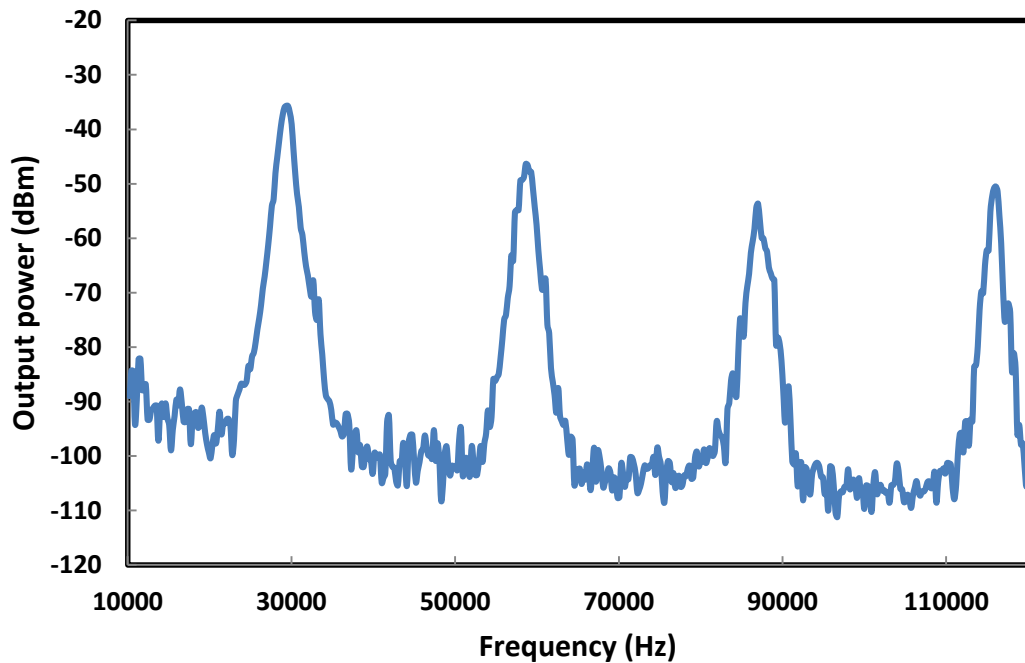


Figure 4. 24: The RF spectrum of the Q-switched BFL at BP power of 5.5 dBm.

4.6 Summary

Several passively mode-locked and Q-switched fiber lasers were successfully demonstrated by means of nonlinear effects such as NPR and SA. A nanosecond harmonic pulse laser source operating with ultra-low repetition rate was demonstrated by inserting a 10 km long SMF in the ring cavity. The SMF plays an important role to induce Kerr effect in the cavity, which allows the polarization rotation occur in the cavity. This allows a mode-locking pulse is generated based on NPR technique. A stable harmonic pulse was obtained at the fundamental repetition rate of 20 kHz at a threshold pump power of 36 mW. The harmonic pulse can be switch from fundamental to 3th order harmonic by increasing the pump power. Then, a nanosecond optical pulse generation was demonstrated in the similar EDFL cavity by replacing the SMF section with a 100 m long HNLF. The laser operated at 1567.2 nm and produced a pulse train with a constant repetition rate of 1.56 MHz and pulse width of 297 ns. The maximum pulse energy of 1.4 nJ was obtained at the maximum pump power of 145 mW. The nanosecond mode-locked was considered stable since the SNR of the RF spectrum was more than 50 dB. To improve the pulse energy, a Q-switched EDFL was also demonstrated based on NOLM cavity. The NOLM was used in the laser cavity to generate the intensity dependent transmission so that it functions as a saturable absorber. The Q-switched laser operated at 1561.5 nm with the pulse repetition rate varied from 7.6 to 22.11 kHz as the pump power is increased from 37 to 125 mW. On the other hand, the lowest pulse width of 5.7 μ s and the maximum pulse energy of 8.2 nJ were obtained at the maximum pump power of 125 mW. Finally, a Q-switched BFL was successfully demonstrated using MWCNTs embedded in PVA film as a SA. The SA was obtained by sandwiching the developed MWCNTs–PVA film between two FC/PC fiber connectors after depositing index matching gel onto the fiber ends. The proposed Q-switched BFL incorporated a 5 km long DSF in a ring cavity structure to generate Stokes shifted by 0.08 nm from the

Brillouin pump wavelength. The BFL starts to generate a Q-switching pulse train at threshold pump power of 5 dBm. As the BP power is varied from 5.0 to 6.0 dBm, the repetition rate of the Q-switched BFL exhibits an increasing trend from 27.75 to 30.21 kHz, whereas the pulse width exhibits a decreasing trend from 3.25 μ s to 1.11 μ s. The maximum pulse energy of 0.13 nJ is obtained at maximum BP power of 6.0 dBm.

CHAPTER 5

SUPERCONTINUUM GENERATION

5.1 Introduction

Supercontinuum (SC) generation describes extreme spectral broadening induced by the interaction of a high peak power sub picosecond pulse laser with a nonlinear optical fiber. It has been a hot topic due to its many applications in a variety of areas such as optical coherent tomography (Humbert et al., 2006), sensing (Kaminski et al., 2008) and optical communication (Morioka et al., 1996). Investigations have been carried out to understand the phenomenon as well as to find its applications. Specialty optical fibers such as photonic crystal fibers (PCFs) and highly nonlinear fiber (HNLF) possess high nonlinearity with managed dispersion profile, and thus are suitable for generating SC light (Nicholson et al., 2003). The SC can be generated using picosecond to nanosecond pulses, or even a continuous wave pump where spectral broadening is initiated in the so-called “long pulse” regime (Dudley et al., 2002; Genty et al., 2009). Research has now shifted to producing SC using a more robust and cheaper mode-locked laser through some innovative design as well as to seeking new understanding of the SC process with picosecond or nanosecond pulse lasers.

In the previous chapter, several passively mode-locked and Q-switched fiber lasers were demonstrated based on nonlinear effects inside the ring laser cavity. These lasers have been tried to be implemented in the experiment to generate SC, but the result is not promising. In this chapter, new mode-locked fiber lasers are proposed and demonstrated for a SC generation. A mode-locked EDFL with dark pulse output is also proposed and demonstrated for realizing a simple optical fiber-based supercontinuum source.

5.2 SC generation by a continuous wave mode-locked and Q-switched mode-locked fiber lasers

Supercontinuum generation is the formation of an ultrabroad spectral broadening induced by the coupling of a high peak power sub picosecond pulse laser with a nonlinear optical fiber of adequate length (Chernikov et al., 1997). The supercontinuum spectrum is determined by the sequence of events in the supercontinuum generation, and is dependent on both the pump pulse and the fiber characteristics namely the pump pulse wavelength, power, and pulse duration. The dominant nonlinear effects occurring in the generation of an SC includes self-phase modulation, stimulated Raman scattering and soliton effects. Since supercontinuum was first discovered in 1970 by Alfano (R. Alfano et al., 1970), many works have been performed to understand the phenomenon as well as its implementation in practical devices where it has found applications in areas of semiconductor, biology, chemistry, optical coherent tomography, sensing and optical communication, femtosecond carrier-envelope phase stabilization, ultrafast pulse compression, time and frequency metrology, and atmospheric science (R. R. Alfano, 1989; Hartl et al., 2001; Kaminski et al., 2008). These included the study of primary events in photosynthesis, nonradiative processes in photoexcited chemicals, excitation of optical phonons, surgery and frequency clocks (Keller, 2003).

Mode-locking operation can be classified into two categories, which are continuous wave mode-locked (CWML) and Q-switched mode-locked (QML) (Svelto, 2010). For CWML, the ultra-short pulses can be generated for each round trip time in the laser cavity, which typically produces megahertz (MHz) pulse repetition rate (Svelto, 2010). Meanwhile, QML possesses Q-switching modulation pulse repetition rate in kilohertz (kHz) range (Yang et al., 2007). Therefore, the QML pulses may be attractive

in precise fabrication of microstructures and nonlinear frequency conversion (Neev et al., 1996).

In this section, SC generation in HNLF is investigated using QML and CWML as the pump source (Kneis et al, 2015). These pulses are formed under nonlinear polarization rotation (NPR) effect in an Erbium-doped fiber laser (EDFL) cavity. The SC generation is investigated in 100 m long highly nonlinear fiber (HNLF) with a zero dispersion wavelength of around 1550 nm and nonlinear coefficient of $11.5 \text{ W}^{-1}\text{km}^{-1}$.

5.2.1 Experimental arrangement

The experimental setup for investigating the SC generation using a QML EDFL as a pump is shown in Fig. 5.1. The mode-locked laser resonator consists of a 3.5 m long EDF as the linear gain medium, wavelength division multiplexer (WDM), polarization-dependent isolator (PDI) and polarization controller (van Saarloos & Hohenberg). The EDF has a cutoff wavelength of 945 nm, core diameter of 4 μm and numerical aperture of 0.23. Since the core diameter of the fiber is small, the fiber nonlinearity is expected to be reasonably high in this EDF compared to the standard EDF with core diameter of around 8 μm . The absorption of the EDF is 11.9 and 17.5 dB/m at 979 and 1531 nm, respectively. A 1480 nm laser diode is used to pump the EDF via the WDM. A PDI and PC are incorporated in the laser cavity to ensure unidirectional propagation of the oscillating laser and to enable nonlinear polarization rotation (NPR) process in the ring cavity, respectively. The output of the laser is tapped out from the cavity via 5/95 fiber coupler while allowing 95% of the light to oscillate in the cavity. The 5% output from the ring resonator is then amplified by an Erbium-doped fiber amplifier (EDFA) before it is launched into 100 m long HNLF which acts as nonlinear gain medium for SC generation. The maximum average output power after the EDFA is about 18.0 dBm.

The SC generation performance is also investigated with the CWML EDFL, which was obtained by incorporating a 200 m long single-mode fiber (SMF) in the cavity and then adjusting a PC. The dispersion parameter of the SMF is 17 ps/nm km.

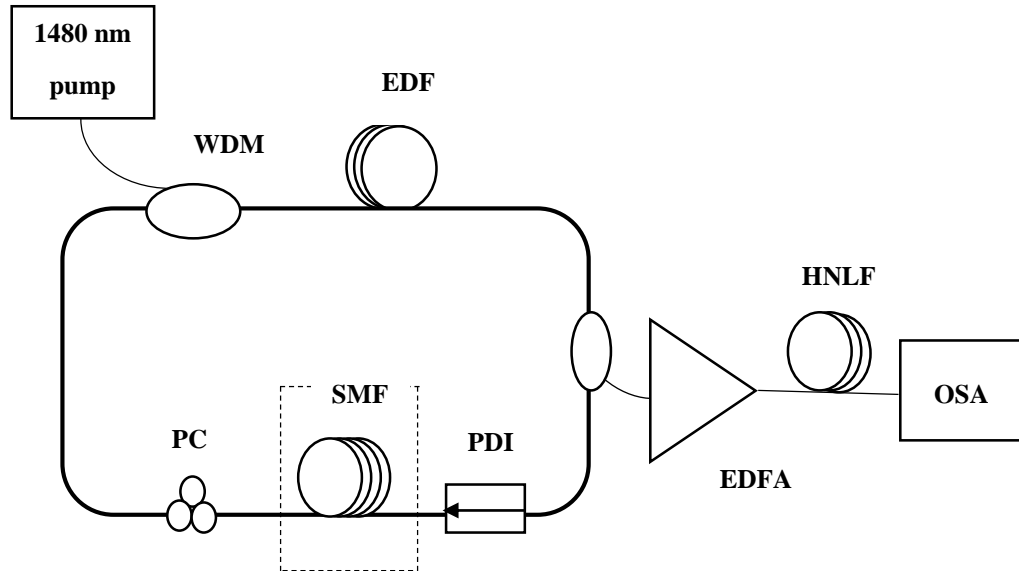


Figure 5. 1: Schematic diagram of experimental setup used for generating SC with QML EDFL. 200 m long SMF is incorporated in the ring EDFL's cavity to change the pulse train output from QML to CWML.

5.2.2 Performance of QML and CWML EDFLs

At first, QML pulse train is successfully formed under NPR effect in the ring EDFL's cavity at threshold pump power of 45 mW by proper adjusting of the intra-cavity PC. A typical output in the QML range is sustained until the maximum pump power of 145 mW. Fig. 5.2 shows the output spectrum, operating at center wavelength about 1560.5 nm, measured before EDFA at pump power of 145 mW. Spectral broadening due to self-phase modulation (SPM) effect in the cavity can be clearly observed. The temporal characteristic of the QML laser is shown in Fig. 5.3. Fig. 5.3(a) shows a typical pulse train of the laser at 145 mW pump power with a Q-switching repetition rate of 49 kHz and pulse width of 3.53 μ s. Fig. 5.3 (b) shows a single envelop of the Q-switched pulse with mode-locking repetition rate of 9.4 MHz and constant pulse width. The pulse energy

is calculated to be around 81 nJ, whilst the maximum average output power is measured as 4 mW at maximum pump power. The QML pulse width is further investigated by using auto-correlator (AC) as shown in Fig. 5.4. The curve fitting of the AC is also shown using Sech² pulse with 100 fs resolution. As shown in Fig. 5.4, the pulse width of the mode-locking pulse train of the laser is estimated to be around 1 ps. Fig. 5.5 shows RF spectrum of the QML pulse at pump power of 145 mW, which indicates a constant pulse repetition rate of 9.4 MHz. The stability of QML pulse is further studied by the RF spectrum analyzer, and the SNR is measured to be around 34 dB at fundamental frequency of 9.4 MHz.

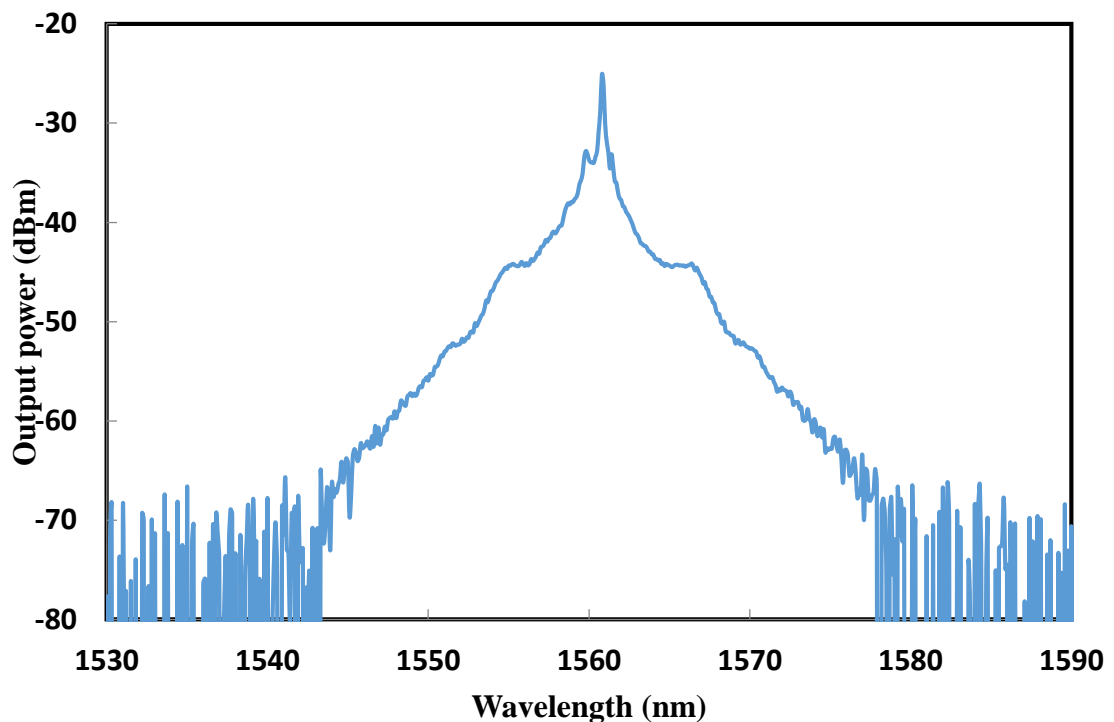


Figure 5. 2: Output spectrum of the QML laser at pump power of 145 mW.

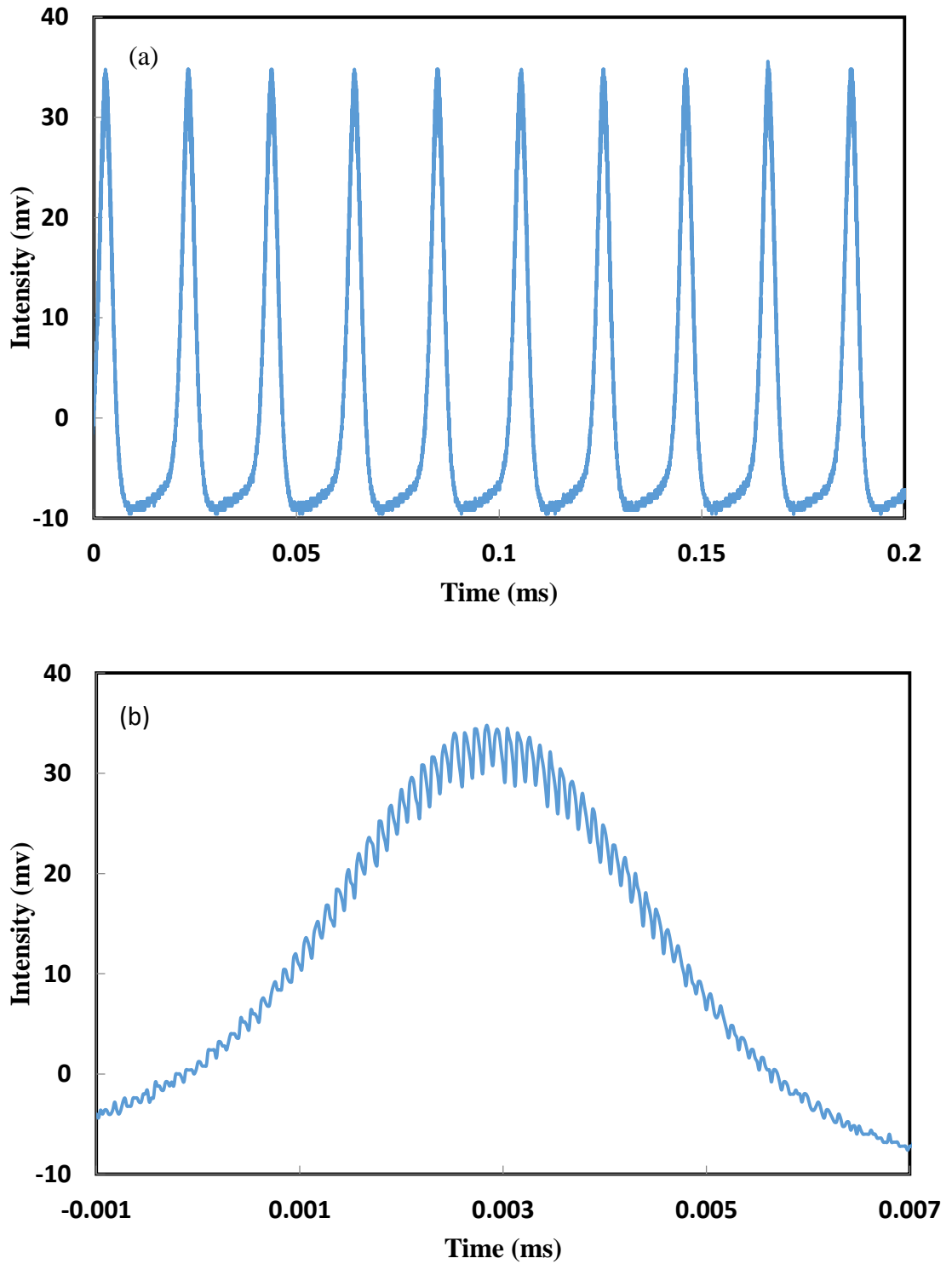


Figure 5. 3: Temporal characteristic of the QML laser (a) Typical pulse train at pump power of 145 mW, showing the Q-switching repetition rate of 49 kHz (b) A single pulse envelop with mode-locking repetition rate of 9.4 MHz.

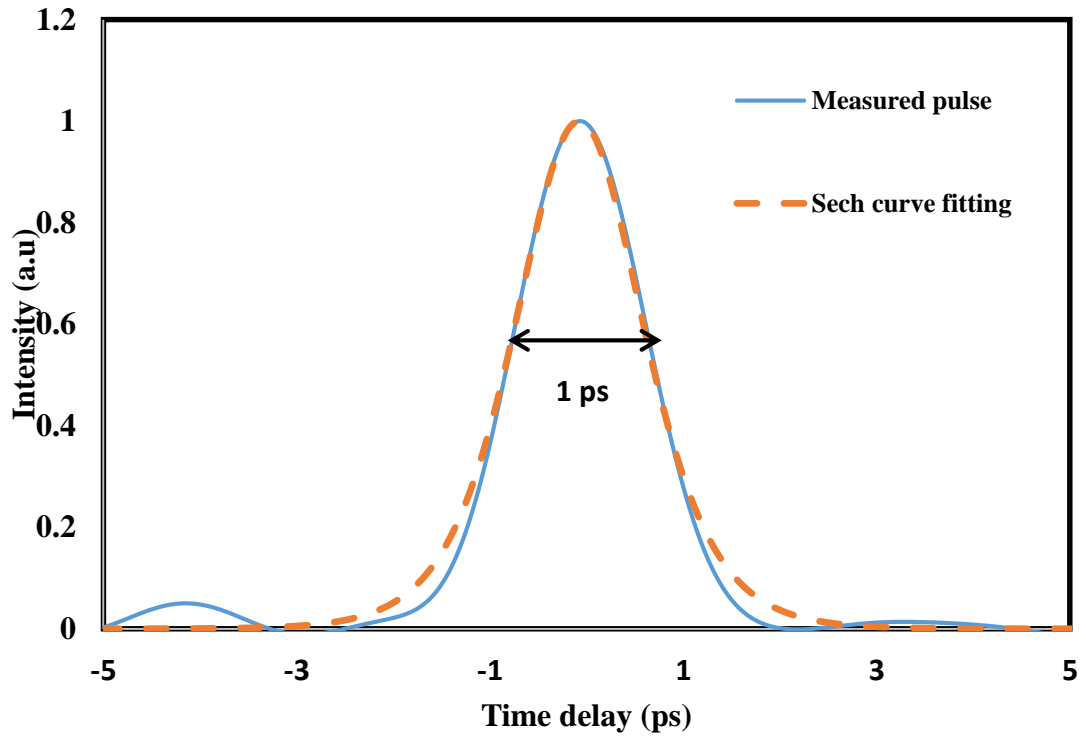


Figure 5. 4: Autocorrelation trace of the QML output pulse

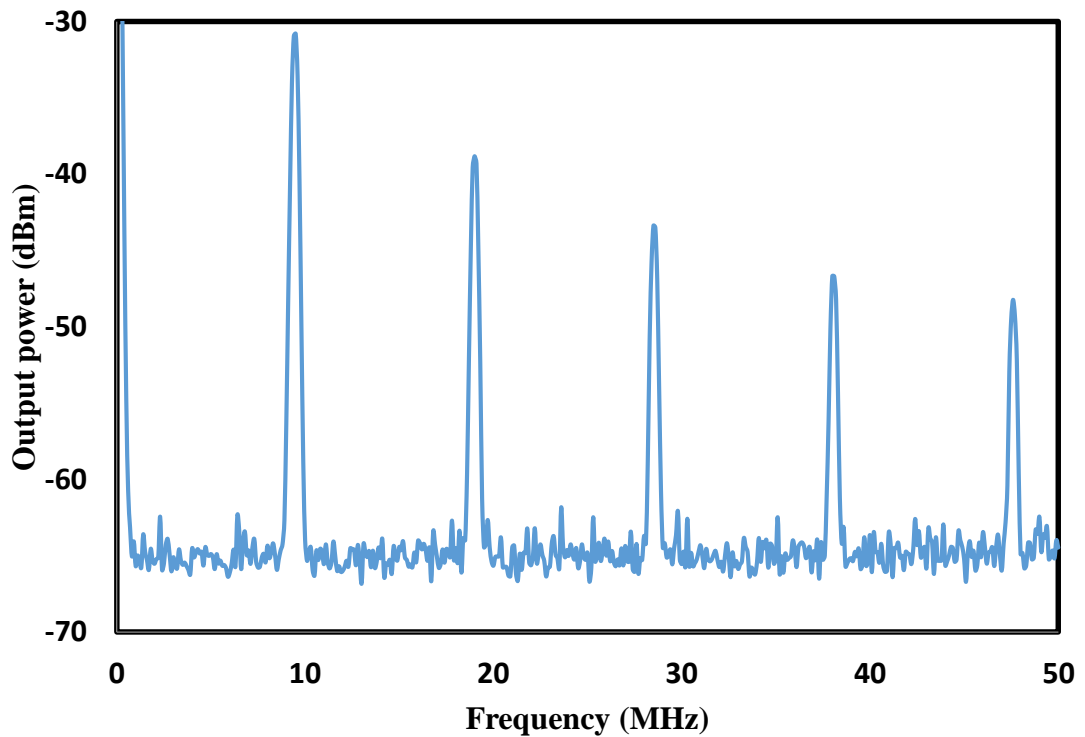


Figure 5. 5: RF spectrum of the QML pulse at pump power of 145 mW.

The QML pulse can be switched to the CWML pulse by adding a 200 m long SMF in the ring cavity of Fig. 5.1 and adjusting the PC. Despite of the fact that no

polariser was inserted in the cavity and no other mode-locking technique was adopted, it was observed that the mode locking could still self-start in the laser cavity as the pump power is increased gradually to around 45 mW. It produced a stable stretched pulse because of the large residual polarization dependent loss (PDL) of the cavity component, which acts as an artificial saturable absorption. Fig. 5.6 shows the output spectrum characteristic of the stretched pulse CWML laser when the pump power is fixed at the maximum value of 145 mW. As shown in the figure, the output peak of -35.5 dBm is obtained at the central wavelength of 1565 nm with a 3 dB bandwidth of 23.8 nm. The spectral bandwidth of the laser is broadened due to changes in dispersion characteristics of the cavity.

Fig. 5.7 shows the typical pulse train of the CWML laser, which reveals that the pulses repeat with a repetition rate of 942 kHz. The pulse width of the laser is obtained at around 367 ns. The pulse energy is calculated to be around 2.7 nJ at the maximum pump power of 145 mW. Fig. 5.8 shows the RF spectrum of CWML pulse at maximum pump power of 145 mW. The SNR is measured to be around 55 dB at fundamental frequency of 942 kHz. This indicates the stability of the laser. The output pulse train is then amplified by an EDFA before it is launched into a HNLF for SC generation.

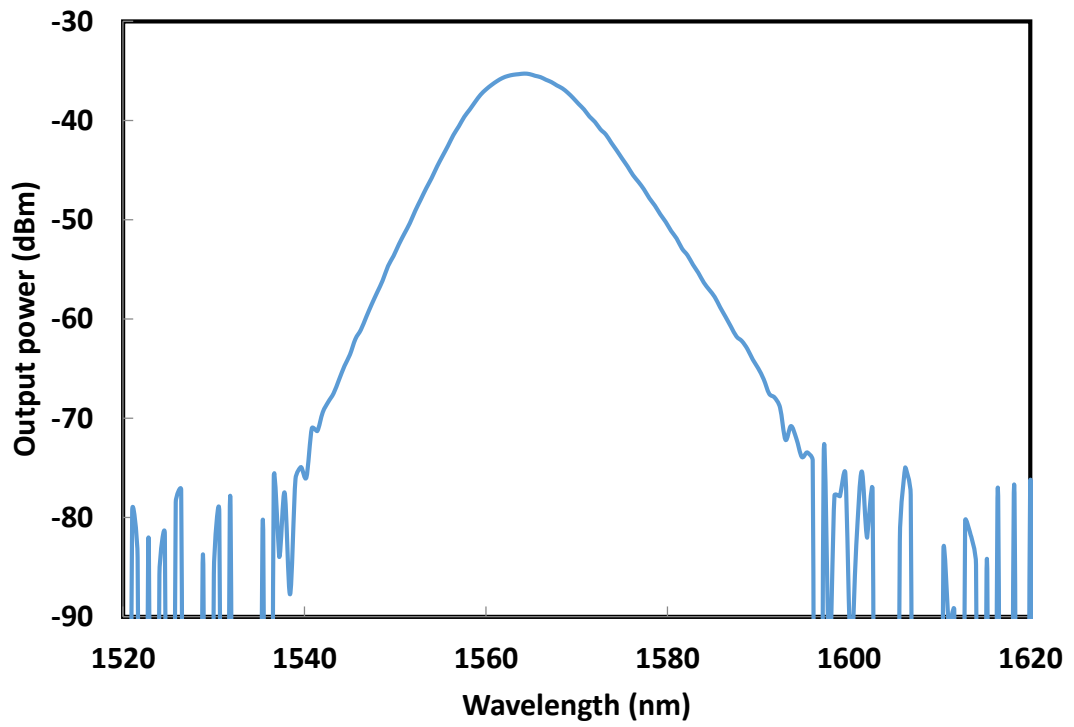


Figure 5. 6: Output spectrum of the CWML pulse laser, which is obtained before being launched into EDFA.

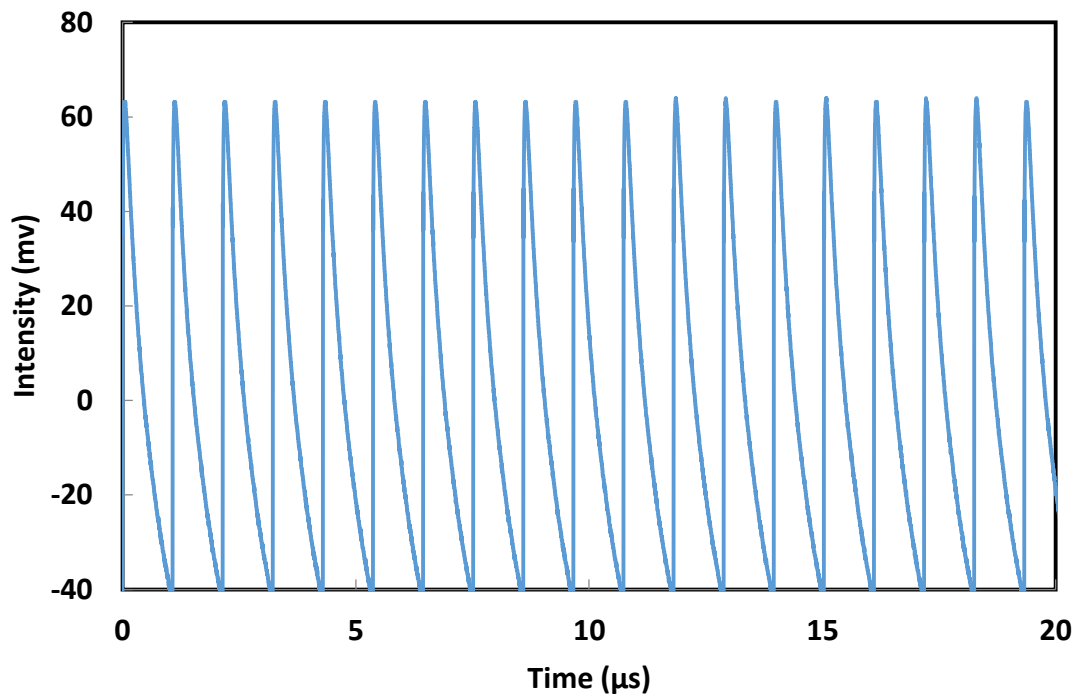


Figure 5. 7: Typical pulse train of the CWML pulse.

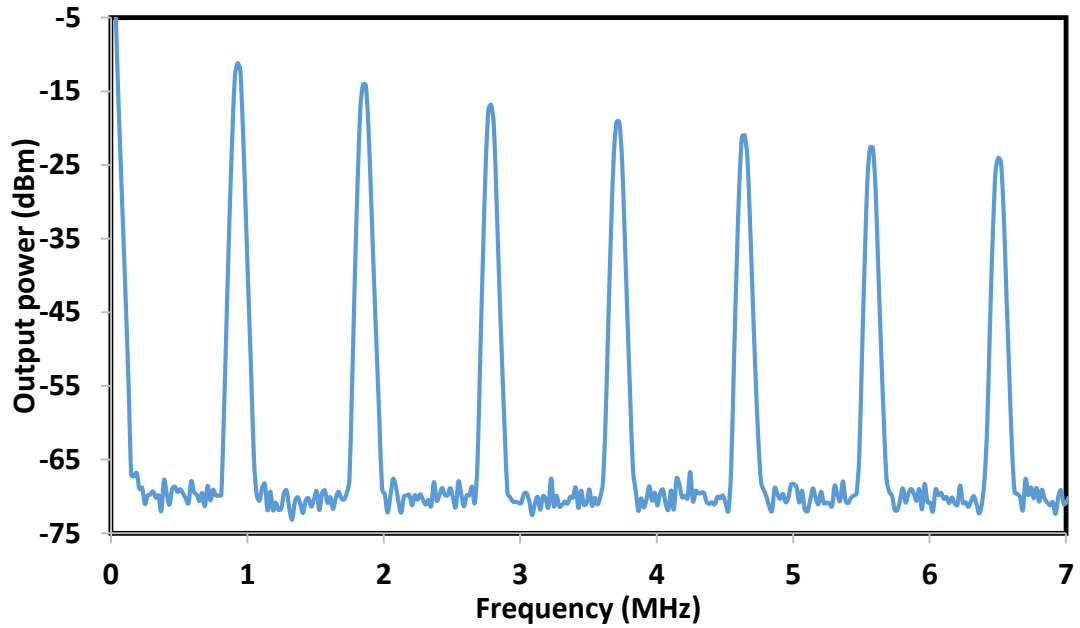


Figure 5. 8: RF spectrum of the CWML pulse at pump power of 145 mW

5.2.3 Performance of the SC generation

Fig. 5.9 shows the attenuated SC spectrum, which was generated by a 100 m long HNLF which is pumped by the amplified QML EDFL. The QML laser operates at 1560.5 nm wavelength with a repetition rate of 49 kHz. In the experiment, the amplified pump power is varied from 11.5 to 18.0 dBm by controlling the pumping power of the EDFA. It worth to note that, there is no supercontinuum light at lower pump power. As shown in Fig. 5.9, the SC light is successfully obtained at pump power of 11.5 dBm with the spectrum starts at wavelength as small as 1410 nm. The SC spectrum broadens and starts at a shorter wavelength as the pump power increases. For instance, at the maximum pump power of 18.0 dBm, the SC spectrum is obtained within 1350 nm to 1950 nm wavelength region. At first, the symmetrical sidebands are generated in the spectrum due to modulation instability and self-phase modulation (SPM). Further propagation of pump light causes multiple sidebands to grow from the phase matched Four Wave Mixing

(FWM) process and the spreading of continuum to larger wavelength side occurs due to the overlap with Raman bandwidth and the Stimulated Raman Scattering (SRS) effect. Higher pump power makes SPM effects dominant over the other nonlinear processes involved in the SC generation, thus leading to a smoother emitted spectrum as shown in Fig. 5.9. The spectral peak at around 1560.5 nm is due to the residual QML EDFL pump.

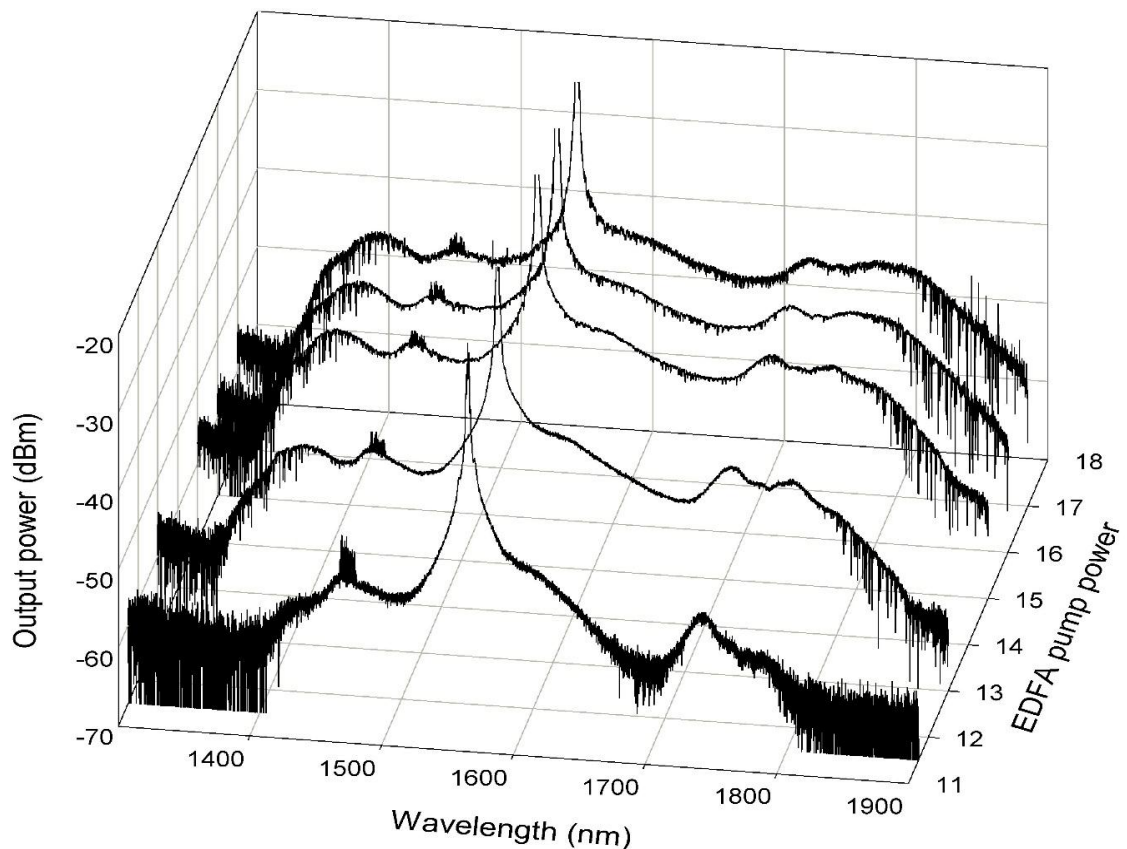


Figure 5. 9: SC spectra from the QML EDFL at various pump power

Fig. 5.10 shows the attenuated SC spectrum obtained as the HNLF is pumped by the CWML EDFL operating at 1565 nm with repetition rate of 942 kHz. The SC generation shows the similar trend with the previous result with QML laser. Fig. 5.11 compares the attenuated SC spectra from a 100 m long HNLF between QML and CWML pulse. As shown in the figure, the CWML pulse generates a slightly broader SC spectrum

compared to the QML pulse. The spectral broadening below 1200 nm region is not examined due to spectral sensitivity of the OSA. The output power intensity is also higher with the CWML pulse even though the pulse energy was higher in the QML pulse before amplification. This proves that the SC generation is more efficient with CWML pulse compared to the conventional QML pulse. This is most probably due to the CWML pulse are less affected by the fiber loss and background noise than the QML pulse (Hönninger et al., 1999).

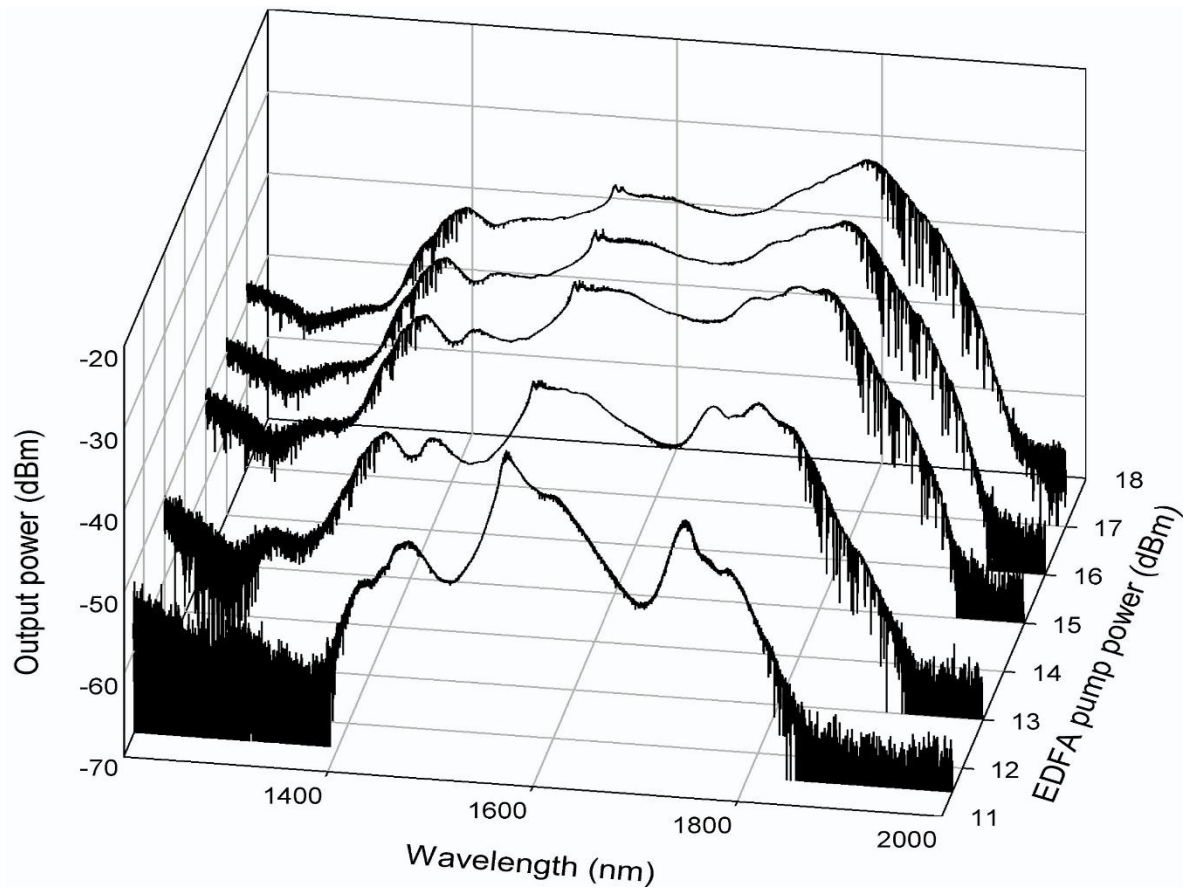


Figure 5. 10: SC spectra from the CWML EDFL at various pump power

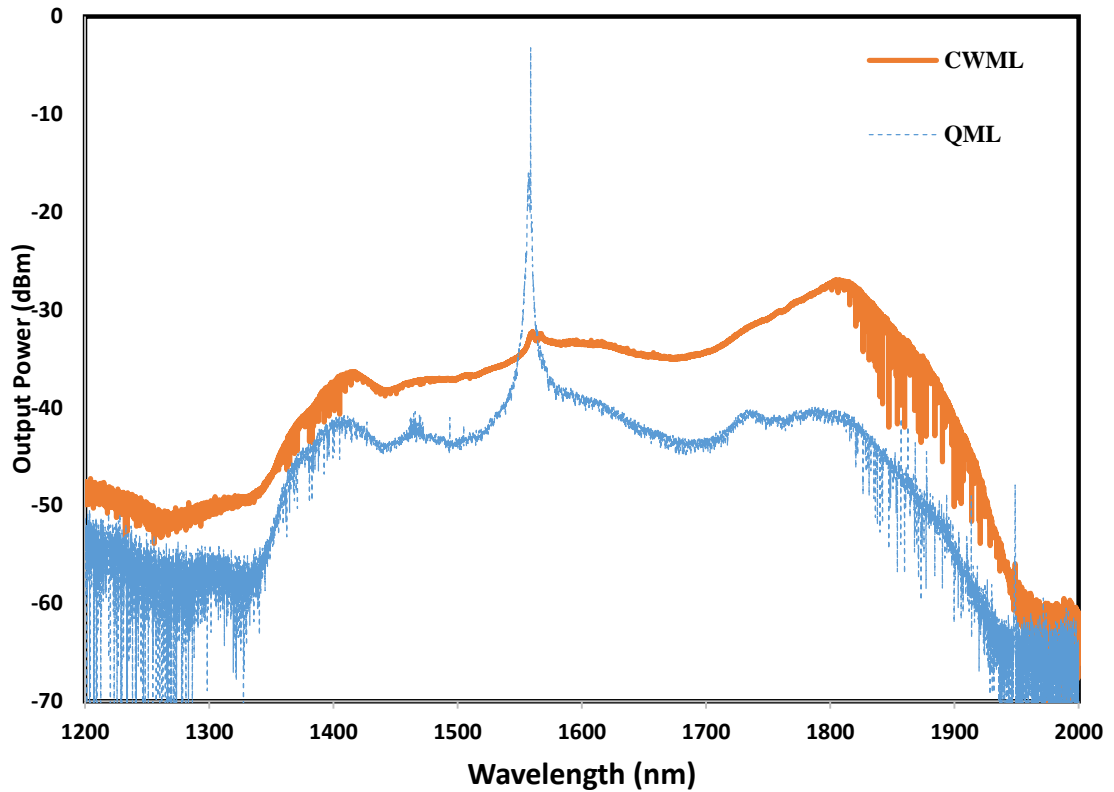


Figure 5. 11: Comparison of SC generation between QML and bright pulse at the maximum pump power of 18.0 dBm

5.3 Enhance SC generation with picosecond dark pulse

Soliton formation is a topic that has attracted an extensive investigation in recent years due to its many potential applications in optical communications, sensors and instrumentations. To date, most of the reported works on soliton mode-locked lasers are operating under the bright pulse regime (Tiu et al., 2014). Besides bright pulses, there are also other types of mode-locking pulses, the so-called dark solitons that are also solutions of the nonlinear Schrödinger equation (NLSE) (Zakharov & Shabat, 1973) and the complex Ginzburg-Landau equation (CGLE) (van Saarloos & Hohenberg, 1992; Zakharov & Shabat, 1973). Here, dark pulses are referred to as a train of intensity dips in a continuous wave (CW) background of the laser emission to date, most of the SC generations were reported using a bright soliton pulses.

In this section, we investigate a SC generation in various gain medium using dark soliton pulses. These pulses are formed under NPR effect in the EDFL cavity. The SC generation is investigated in three samples of gain medium; 50 m long photonic crystal fiber (PCF), 100 m long highly nonlinear fiber (HNLF) and 20 km long standard single-mode fiber (SMF) with a zero dispersion wavelength of around 1550 nm and nonlinear coefficients of $11 \text{ W}^{-1}\text{km}^{-1}$, $11.5 \text{ W}^{-1}\text{km}^{-1}$ and $1.3 \text{ W}^{-1}\text{km}^{-1}$ respectively.

5.3.1 Experimental arrangement

The experimental setup for the SC generation from a dark pulse soliton mode-locked EDFL is shown in Fig. 5.12. The mode-locked laser resonator consists of a 3.5 m long EDF as the linear gain medium, wavelength division multiplexer (WDM), polarization-dependent isolator (PDI), polarization controller (van Saarloos & Hohenberg). The EDF used has an Erbium ion concentration of 2000 ppm, core diameter of $4 \mu\text{m}$, mode field diameter of $6 \mu\text{m}$ and NA of 0.24. A 1480 nm laser diode is used to pump the EDF via the WDM. A PDI and PC are incorporated in the laser cavity to ensure unidirectional propagation of the oscillating laser and to act as a polarizer to enable NPR process in the ring cavity. The output of the laser is tapped out from the cavity via 5/95 fiber coupler while allowing 95% of the light to oscillate in the cavity. The 5% output from the ring resonator is then amplified by an EDFA before it is launched into a piece of nonlinear gain medium for SC generation. In this experiment, the performance of the SC generation is investigated for three different nonlinear gain media; 50 m long PCF, 100 m long HNLF and 20 km long SMF. The nonlinearity coefficient of the PCF, HNLF and SMF are $11 \text{ W}^{-1}\text{km}^{-1}$, $11.5 \text{ W}^{-1}\text{km}^{-1}$ and $1.3 \text{ W}^{-1}\text{km}^{-1}$ respectively.

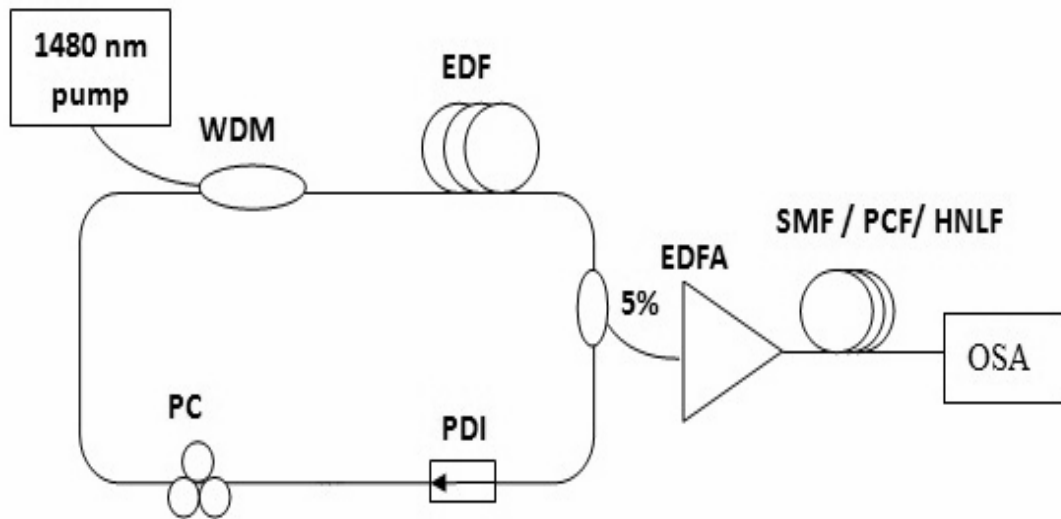


Figure 5. 12: Experimental setup to investigate the SC generation with a dark pulse

5.3.2 Performance of the dark pulse and SC generations

A nonlinear Schrödinger equation (NLSE) type dark soliton (Weiner et al., 1988) is formed under NPR effect in the laser cavity at threshold pump power of 45 mW by proper adjusting of the intra-cavity PC. It is observed that the dark pulse train operation is sustained until the maximum pump power of 145 mW. Fig. 5.13 shows the typical pulse train of the dark pulse generated by the proposed laser cavity, which is measured before EDFA at pump power of 145 mW. Formation of dark pulse is represented as a narrow intensity dip in the strong CW laser emission background as shown in the figure. CW noise is observed at the flat positive peaks, whereas the negative peaks are referring to the dip intensity. The generation of dark pulse is due to the change of linear refractive index coefficient in the normal dispersion cavity.

Fig. 5.14 shows the output spectrum of the mode-locked EDFL, which exhibits single peak profile. This shows that the generated pulse is a NLSE type of dark pulse. As shown in Fig. 5.14, the output spectrum operates at a center wavelength of about 1570 nm. The spectral broadening is also observed, which is due to SPM effect in the laser

cavity. The dark pulse width is further studied by using auto-correlator (AC) as shown in Fig. 5.15. We use a sech^2 pulse trend with 100 fs resolution to curve fit the AC result. The AC curve shows a pulse width of 0.82 ps. However, conventional AC can only measure the positive pulse width. Hence, by taking the ratio of negative width over positive width to multiply with the curve fitting result, the dark pulse width is estimated to be around 0.5 ps. It is observed that the output laser power and pulse energy are directly proportional with the pump power within the pump power region from 45 to 145 mW. The maximum average output power is measured as 2.9 mW at maximum pump power of 145 mW. With a constant pulse repetition rate of 8.06 MHz and constant pulse width of 0.5 ps throughout the tuning range, the pulse energy is calculated to be around 360 pJ at maximum pump power of 145 mW. The stability of dark pulse is further studied by RF spectrum analyzer. As shown in Fig. 5.16, the SNR is measured to be around 45 dB at fundamental frequency of 8.06 MHz.

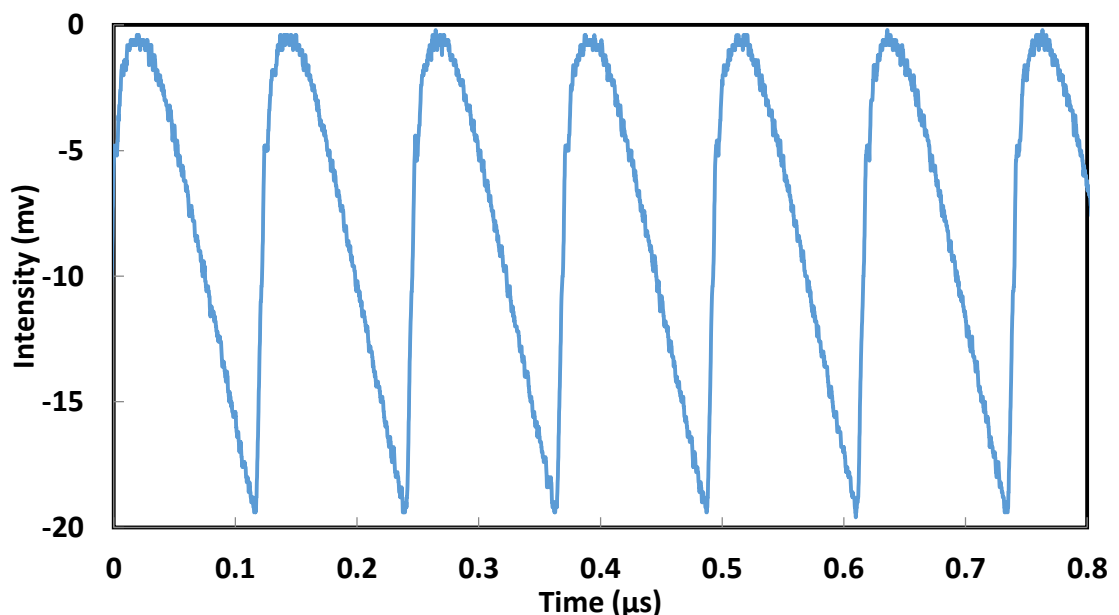


Figure 5. 13: Typical dark pulse train obtained from the mode-locked EDFL

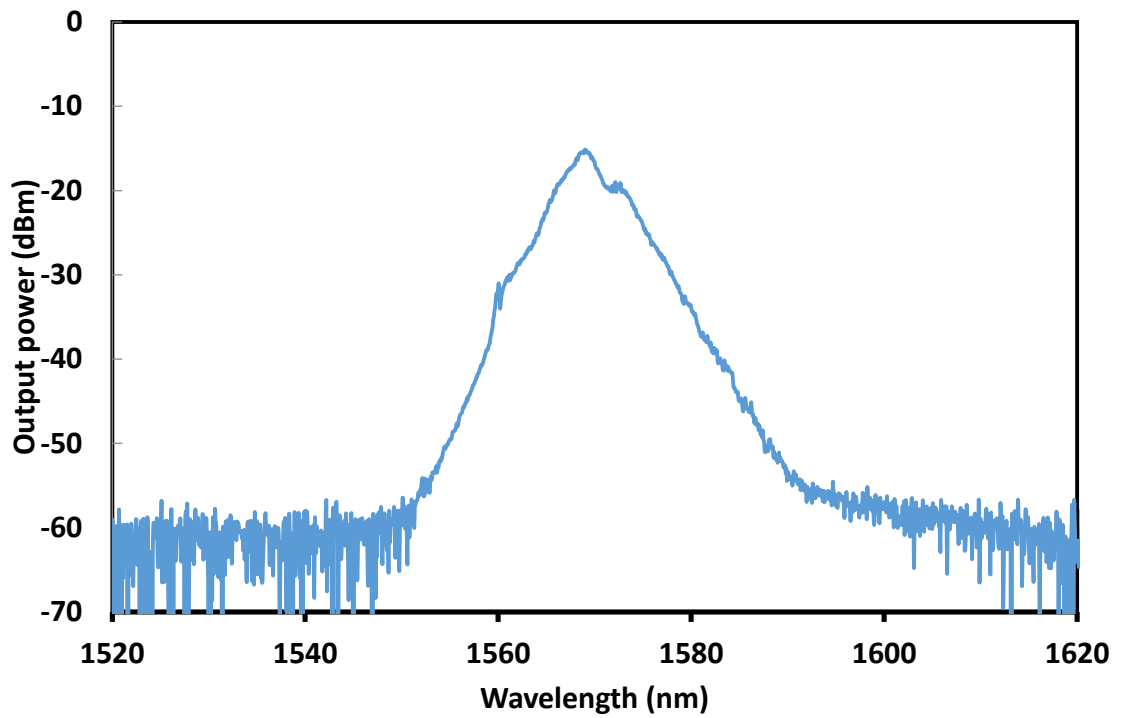


Figure 5. 14: Output spectrum from the mode-locked EDFL at pump power of 145 mW.

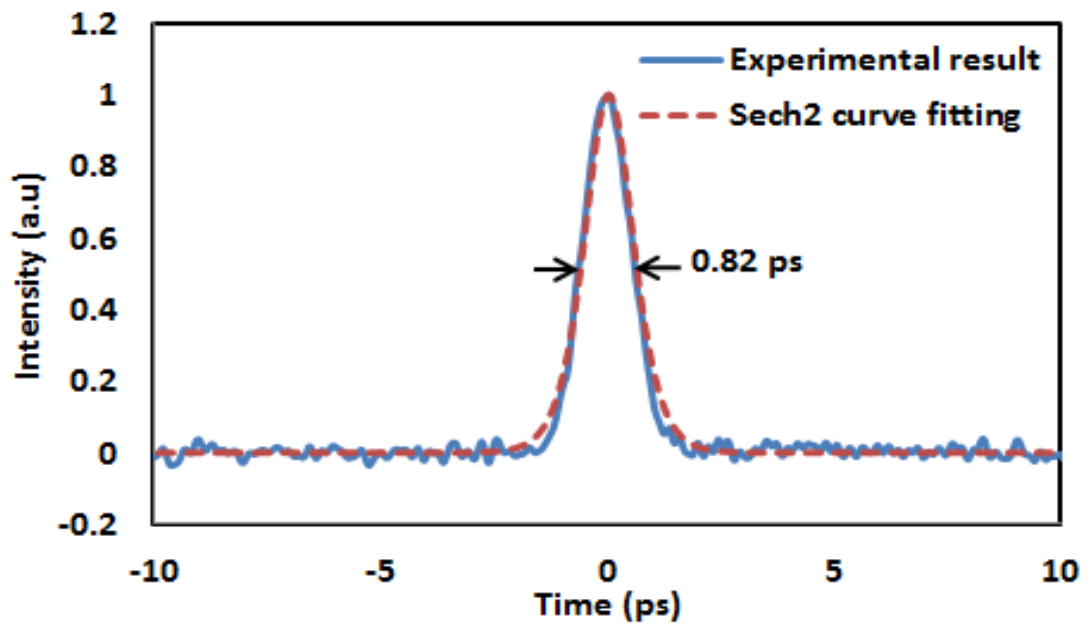


Figure 5. 15: AC Sech2 pulse curve fitting with resolution of 100 fs.

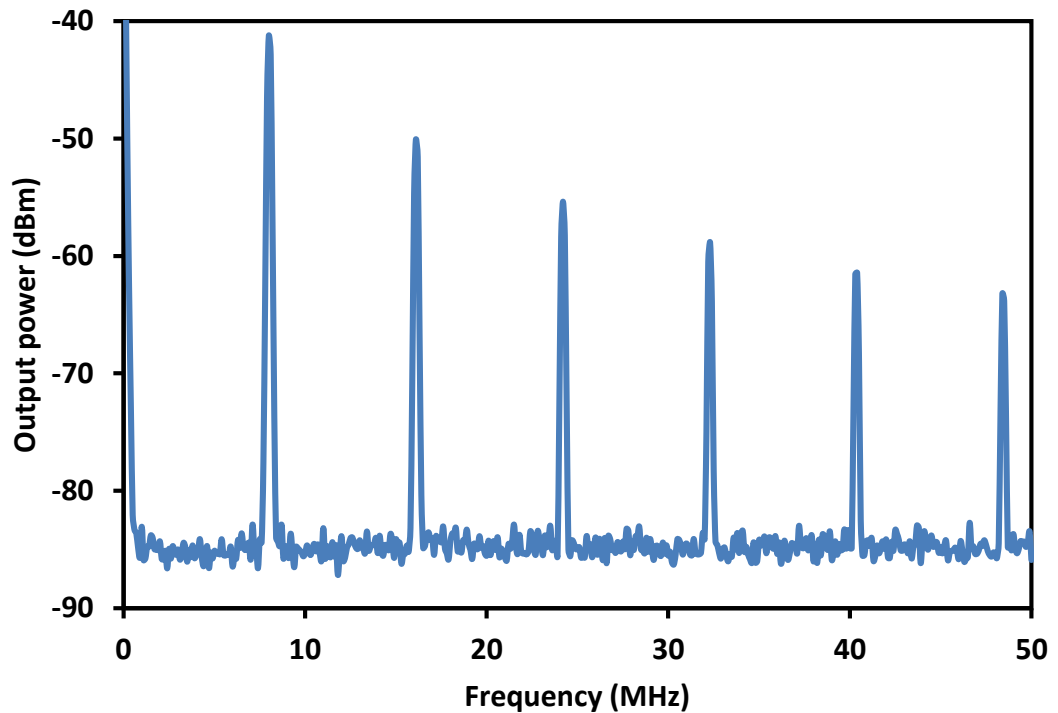


Figure 5. 16: RF spectrum of the dark pulse soliton at pump power of 145 mW.

Fig. 5.17 shows the attenuated SC spectra at 3 different nonlinear media using an amplified 1570 nm nanosecond dark pulse laser as a pump. In the experiment, the output power from the EDFA is constantly maintained at 18 dBm. The spectral broadening below 1200 nm region is not examined due to spectral sensitivity of the OSA. It is observed that the SC spectrum wavelength spans from 1200 nm to 1810 nm, 1200 nm to 1920 nm and 1480 nm to 1740 nm with the use of PCF, HNLF and SMF respectively, as the nonlinear gain medium. This wavelength range is obtained by considering -30 dBm power level of Fig. 5 as a SC operation output power threshold. This is due to, most of the optical devices, in general, have a sensitivity lower than -30 dBm. The SC bandwidth is smallest in SMF since it exhibits the lowest nonlinearity. The bandwidth is increased from 181 nm to 222 nm as the gain medium is changed to 50 m long PCF, which has a higher nonlinearity of about $11 \text{ W}^{-1}\text{km}^{-1}$. As HNLF exhibits almost similar nonlinearity with PCF, the SC bandwidth can be almost doubled to around 466 nm by using 100 m

long HNLF (double the length of PCF) as the gain medium. The spectral peak at around 1570 nm is the residual mode locked EDFL pump.

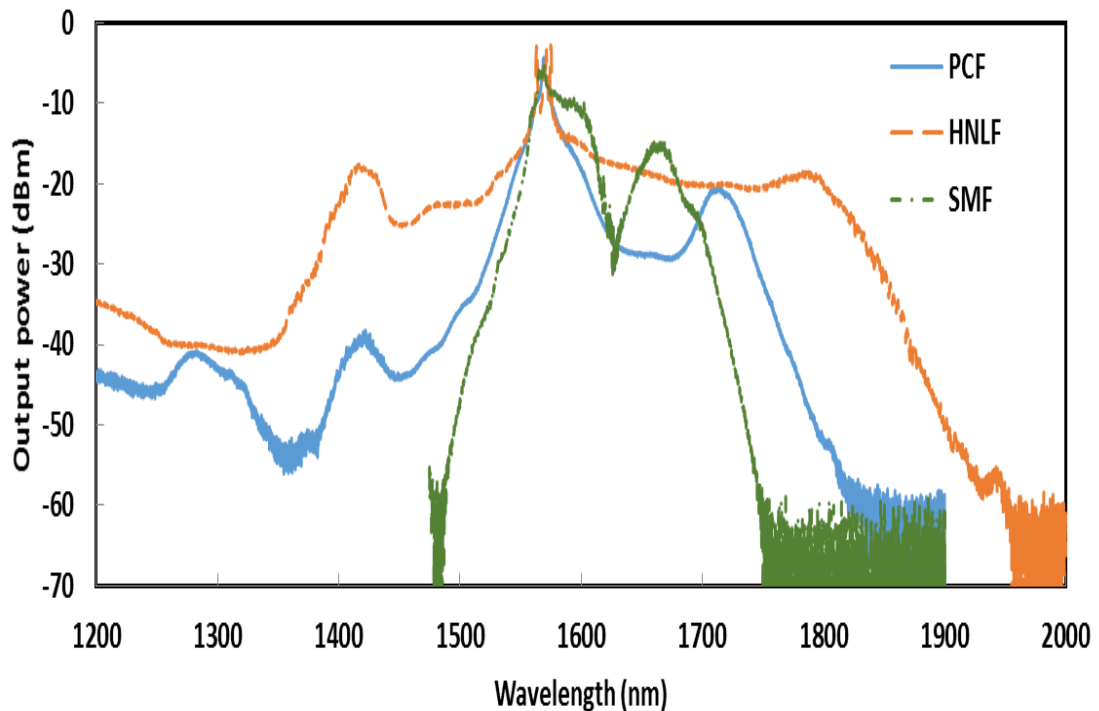


Figure 5. 17: Supercontinuum spectra at three different gain media using the amplified dark pulse soliton.

5.4 Summary

SC generation has been successfully demonstrated in all three NPR-based pulse EDFLs. At first, the performance of SC generation in QML and CWML EDFLs, which was amplified by an EDFA as pump source was investigated and demonstrated. The QML EDF laser generates a pulse train operating at 1560.5 nm which is amplified up to 18 dBm of average power by the EDFA to produce SC ranging from about 1350 nm to 1900 nm. On the other hand, SC generated by CWML was operating at 1565 nm with slightly better performances in term of output power and bandwidth. A SC generation based on dark pulse was also demonstrated in three different fiber spools in a passively mode locked EDFL. The mode locked EDF laser generates a dark pulse train operating at 1570 nm

with a repetition rate of 8.06 MHz and a pulse width of 0.55 ps. It is amplified up to 18 dBm of average power by the EDFA to produce SC ranging from 1200 nm to 1810 nm, 1200 nm to 1920 nm and 1480 nm to 1740 nm with the use of 50 m long PCF, 100 m long HNLFF and 20 km long PCF.

CHAPTER 6

CONCLUSION AND FUTURE WORK

6.1 Conclusion

Nonlinear effects are harmful and unwanted in Dense Wavelength Division Multiplexing (DWDM) system as they cause distortion and degradation to the carried information. Regardless of this drawback, nonlinear effects can be utilized for many applications such as optical amplification, laser and optical switching. Among the significant applications of nonlinear effects are in pulsed laser and super-continuum (SC) generations. Pulsed laser has been widely used in industry for micromachining such as cutting, drilling and welding while in medical, pulsed laser is employed for surgery. For communication purposes, pulsed laser with narrow pulse width is the key enabler for high speed communication in Optical Time Division Multiplexing (OTDM). On the other hand, SC light source is very useful for different applications such as spectroscopy, frequency metrology, device characterization and medical science.

The generation of pulsed laser can be categorized into two techniques; the active and passive techniques. This thesis aimed to propose and demonstrate both Q-switched and mode-locked pulse lasers using passive techniques based on nonlinear effects. The nonlinear effects were also employed to generate SC light source. In this work, various techniques such as self-pulsing with stimulated Brillouin scattering (SBS), and nonlinear polarization rotation (NPR) techniques were used to generate laser pulses.

In chapter 3, SBS effect in optical fiber was investigated for pulse generation. At first, we investigated SBS effect in a standard single mode fiber (SMF) and microfiber structures such as non-adiabatic microfiber and inline Mach-Zhender interferometer (IMZI). Both non-adiabatic microfibre and IMZI were fabricated from a standard silica fibre using a flame brushing technique to produce mode interference. It was observed that

the Stokes wavelength is up-shifted by 0.088 nm (10 GHz) from the BP wavelength while the anti-Stokes wavelength is downshifted by the same spacing. It was found that the IMZI can produce higher spontaneous Brillouin scattering Stokes and anti-Stokes powers due to its stronger multimode interference effect compared to the non-adiabatic microfiber. However, both microfiber structures cannot produce the SBS and laser in a ring configuration due to the limitation of our facilities such as high BP power source. Therefore, a 10 km long SMF was used in this study to demonstrate Brillouin fiber laser (BFL) and pulse generation.

The threshold BP powers for the ring BFL were obtained at 1.2, 1.5, 2.2 dBm for the laser cavity configured with 10/90, 20/80, and 50/50 output coupler, respectively. The maximum laser's peak power of -3.12 dBm is obtained for the BFL configured with 50/50 coupler. The temporal characteristic of proposed BFL with 10/90 output coupler was also investigated. At a threshold pump power of 1.2 dBm, the pulse width and repetition frequency of the laser are obtained at 440 μ s and 2 kHz, respectively. As the pump power increases, the pulse width becomes shorter while the repetition rate increases. This Q-switching or pulsing behavior is due to the relaxation oscillation, a natural trait of fiber laser, which occurs around the laser threshold as the SBS grows. In another work, a single wavelength Brillouin Erbium fiber laser (BEFL) was successfully demonstrated by using only a 3-m-long Erbium-doped fiber (EDF) as both linear and nonlinear gains mediums. The BEFL is obtained at a wavelength of the 1561.5nm region with a peak power of -5dBm and an SMSR of more than 5 dB with the BP and 1480nm pump powers of 5dBm and 34mW, respectively. The BEFL also shows a self-pulsing characteristic with repetition rates of 66.7 kHz as the 1480nm pump power is set within 13–20mW. However, the amplitude of the pulse is significantly lower than the conventional BFL, which has a longer cavity length.

At the end of Chapter 3, the BFL with a mode-locking characteristic was demonstrated using a 100m-long highly nonlinear fiber (HNLF) as a Brillouin gain medium in conjunction with relaxation oscillation technique. The BFL generates a self-starting pulse train with a repetition rates of 1.76 MHz at BP power of 10.9 Bm. The pulse width of the laser is maintained at around 270 ns. These results are useful for applications in distributed medical surgery, temperature and strain sensing as well as the line width measurement of narrow line width laser and so on.

Chapter 4 presented and demonstrated several passively mode-locked and Q-switched fiber lasers based on nonlinear effects inside the ring laser cavity. At first, the nonlinear polarization rotation (NPR) based mode-locked EDFL with three switchable operation states was proposed and demonstrated by incorporating a 10 km long SMF and in the ring cavity. The SMF plays an important role to induce Kerr effect in the cavity, which allows the polarization rotation occur in the cavity. We have successfully obtained a nanosecond harmonic pulse train operating with ultra-low repetition rate with the proposed laser cavity. A stable harmonic pulse was obtained at the fundamental repetition rate of 20 kHz at a threshold pump power of 36 mW. The harmonic pulse can be switch from fundamental to 3th order harmonic by increasing the pump power.

Then, a nanosecond optical pulse operating in fundamental mode was successfully generated in the similar EDFL cavity by replacing the SMF section with a 100 m long HNLF. The laser operated at 1567.2 nm and produced a pulse train with a constant repetition rate of 1.56 MHz and pulse width of 297 ns. The maximum pulse energy of 1.4 nJ was obtained at the maximum pump power of 145 mW. The nanosecond mode-locked was considered stable since the SNR of the RF spectrum was more than 50 dB.

To improve the pulse energy, a Q-switched EDFL was proposed and demonstrated based on nonlinear optical loop mirror (NOLM) cavity. The NOLM was

used in the laser cavity to generate the intensity dependent transmission so that it functions as a saturable absorber (SA). The proposed Q-switched laser operated at 1561.5 nm with the pulse repetition rate varied from 7.6 to 22.11 kHz as the pump power is increased from 37 to 125 mW. On the other hand, the lowest pulse width of 5.7 μ s and the maximum pulse energy of 8.2 nJ were obtained at the maximum pump power of 125 mW. A Q-switched BFL was also demonstrated using multi-walled carbon nanotubes (MWCNTs) embedded in polyvinyl alcohol (PVA) film as a passive SA. In the proposed BFL, a 5 km long dispersion shifted fiber (DSF) was used as a Brillouin gain medium. The SA was obtained by sandwiching the MWCNT–PVA film between two FC/PC fibre connectors. The self-starting Q-switching pulse train was successfully generated as the BP reaches a threshold pump power of 5.0 dBm. As the BP power is increased from 5.0 to 6.0 dBm, the repetition rate of the Q-switched BFL increases from 27.75 to 30.21 kHz, whereas the pulse width decreases from 3.25 μ s to 1.11 μ s. The maximum pulse energy of 0.13 nJ is obtained at BP power of 6 dBm.

These lasers have been tried to be implemented in the experiment to generate SC, but the result is not promising. Therefore, three new mode-locked fiber lasers were proposed and demonstrated in Chapter 5 for a SC generation. Mode-locking operation can be classified into two categories, which are continuous wave mode-locked (CWML) and Q-switched mode-locked (QML). For CWML, the ultra-short pulses can be generated for each round trip time in the laser cavity which typically produces megahertz (MHz) pulse repetition rate. Meanwhile, QML possesses Q-switching modulation pulse repetition rate in kilohertz (kHz) range. At first, SC generation in HNLF is investigated using QML and CWML as the pump source. These pulses are formed under NPR effect in an EDFL cavity. The SC generation is investigated in 100 m long HNLF with a zero dispersion wavelength of around 1550 nm and nonlinear coefficient of 11.5 W⁻¹km⁻¹.

The proposed QML EDFL generated a pulse train operating at 1560.5 nm. At 145 mW pump power, the laser produced Q-switching repetition rate of 49 kHz with pulse width of 3.53 μ s. In a single envelop of the Q-switched pulse, there were mode-locking pulse train with a repetition rate of 9.4 MHz and 1 ps pulse width. The pulse energy was calculated to be around 81 nJ. The QML laser was then amplified up to 18 dBm of average power by the EDFA to produce SC ranging from about 1350 nm to 1900 nm. The CWML operating at 1565 nm was realized in the same laser cavity by incorporating a 200 m long SMF. The laser produced a pulse train with 942 kHz repetition rate, 367 ns pulse width 2.7 nJ pulse energy at the maximum pump power of 145 mW. The output pulse train is then amplified by an EDFA before it is launched into a HNLF for SC generation. It is found that SC light generated by CWML was slightly better in term of output power and bandwidth. This is most probably due to the CWML pulses are less affected by the fiber loss and background noise than the QML pulse.

To date, most of the reported works on soliton mode-locked lasers are operating under the bright pulse regime. Besides bright pulses, there are also other types of mode-locking pulses, the so-called dark solitons that are also solutions of the nonlinear Schrödinger equation (NLSE) and the complex Ginzburg-Landau equation (CGLE). To date, most of the SC generations were reported using a bright soliton pulses. In the final section of Chapter 5, A SC generation based on dark pulse was demonstrated in three different fiber spools in a passively mode locked EDFL. Here, dark pulses are referred to as a train of intensity dips in a continuous wave (CW) background of the laser emission. The mode locked EDF laser generates a dark pulse train operating at 1570 nm with a repetition rate of 8.06 MHz and a pulse width of 0.55 ps. It is amplified up to 18 dBm of average power by the EDFA to produce SC ranging from 1200 nm to 1810 nm, 1200 nm to 1920 nm and 1480 nm to 1740 nm with the use of 50 m long PCF, 100 m long HNLF and 20 km long PCF.

In conclusion, we have successfully demonstrated various practical pulsed fiber lasers and SC light sources by utilizing various nonlinear effects in optical fibers. The SC light source is of great interest for different applications such as spectroscopy, frequency metrology, device characterization and medical science

6.2 Future Outlooks

In this thesis, many works have been carried out on both pulsed laser and SC generation. However, there are still many works that can be further explored and investigated in the future. For instance, pulse width of BFL can be further reduced by replacing the long fibers with a shorter nonlinear medium like microfibers. Besides, SBS self-pulsing with semiconductor optical amplifier (SOA) is another prospect that can be investigated in the future. Pulse width of NPR based EDFL can also be made narrower, near transform limit by optimizing the net dispersion in the cavity. With the advancement of ultra-fast laser system, the cavity length can be reduced to several meters to allow hundreds of Mega-Hertz and also Giga-Hertz repetition rate for applications in high capacity telecommunication systems and photonic switching devices. NPR based pulsed laser can also be extended to other regions such as 1 μm and 2 μm .

NPR based Q-switched and mode-locked fiber lasers can be further studied to allow tunable operation. New saturable absorbers such as graphene can also be explored for ultra-short pulse fiber laser generation. Another related field of interest is to construct SC light source by using pulsed BFL as well as NPR based EDFL. This light source can then be sliced into many wavelengths for DWDM applications. Future directions can also include engaging high power laser diode to produce high pulse energy by scaling up the energy to micro-Joule and generate supercontinuum in shorter nonlinear medium. With this, it is hoped that this work will contribute to the further development of ultra-fast optics.

REFERENCES

- Abedin, K. S. (2005). Observation of strong stimulated Brillouin scattering in single-mode As₂Se₃ chalcogenide fiber. *Optics Express*, 13(25), 10266-10271.
- Abeeluck, A. K., Headley, C., & Jørgensen, C. G. (2004). High-power supercontinuum generation in highly nonlinear, dispersion-shifted fibers by use of a continuous-wave Raman fiber laser. *Optics letters*, 29(18), 2163-2165.
- Agrawal, G. (2001). *Applications of nonlinear fiber optics*: Academic press.
- Agrawal, G. P. (1997). *Fiber-optic communication systems* (Vol. 1).
- Agrawal, G. P. (2007). *Nonlinear fiber optics*: Academic press.
- Agrawal, G. P., & Olsson, N. A. (1989). Self-phase modulation and spectral broadening of optical pulses in semiconductor laser amplifiers. *Quantum Electronics, IEEE Journal of*, 25(11), 2297-2306.
- Ahmad, H., Muhammad, F., Zulkifli, M., & Harun, S. (2013). Graphene-Based Mode-Locked Spectrum-Tunable Fiber Laser Using Mach–Zehnder Filter. *Photonics Journal, IEEE*, 5(5), 1501709-1501709.
- Ahmad, H., Shahi, S., & Harun, S. (2010). Bismuth-based erbium-doped fiber as a gain medium for L-band amplification and Brillouin fiber laser. *Laser physics*, 20(3), 716-719.
- Alfano, R., & Shapiro, S. (1970). Observation of self-phase modulation and small-scale filaments in crystals and glasses. *Physical Review Letters*, 24(11), 592.
- Alfano, R. R. (1989). The supercontinuum laser source.
- Asobe, M., Ohara, T., Yokohama, I., & Kaino, T. (1996). Low power all-optical switching in a nonlinear optical loop mirror using chalcogenide glass fibre. *Electronics Letters*, 32(15), 1396-1397.
- Banhart, F. (1999). Irradiation effects in carbon nanostructures. *Reports on progress in physics*, 62(8), 1181.
- Becker, M., Kuizenga, D. J., & Siegman, A. (1972). Harmonic mode locking of the Nd:YAG laser. *Quantum Electronics, IEEE Journal of*, 8(8), 687-693. doi: 10.1109/JQE.1972.1077271

- Bernini, R., Minardo, A., & Zeni, L. (2002, 2002). *A reconstruction technique for stimulated Brillouin scattering fiber-optic sensors for simultaneous measurement of temperature and strain*. Paper presented at the Sensors, 2002. Proceedings of IEEE.
- Beugnot, J. C., Ahmad, R., Rochette, M., Laude, V., Maillotte, H., & Sylvestre, T. (2013). *Stimulated Brillouin scattering in chalcogenide-PMMA hybrid microwires*. Paper presented at the Workshop on Specialty Optical Fibers and their Applications.
- Bloembergen, N. (1996). *Nonlinear optics*: World Scientific.
- Boscolo, S., Turitsyn, S. K., & Blow, K. J. (2008). Nonlinear loop mirror-based all-optical signal processing in fiber-optic communications. *Optical Fiber Technology*, 14(4), 299-316.
- Boyd, R. W. (2003). *Nonlinear optics*: Academic press.
- Buck, J. A. (2004). *Fundamentals of optical fibers*: John Wiley & Sons.
- Chernikov, S., Zhu, Y., Taylor, J., & Gapontsev, V. (1997). Supercontinuum self-Q-switched ytterbium fiber laser. *Optics letters*, 22(5), 298-300.
- Chraplyvy, A. R. (1990). Limitations on lightwave communications imposed by optical-fiber nonlinearities. *Journal of Lightwave Technology*, 8(10), 1548-1557.
- Cordeiro, C. M. B., Wadsworth, W. J., Birks, T. A., & Russell, P. S. J. (2005). Engineering the dispersion of tapered fibers for supercontinuum generation with a 1064 nm pump laser. *Optics letters*, 30(15), 1980-1982. doi: 10.1364/OL.30.001980
- Cotter, D. (1983). Stimulated Brillouin scattering in monomode optical fiber. *Journal of Optical Communications*, 4(1), 10-19.
- Dainese, P., Russell, P. S. J., Joly, N., Knight, J. C., Wiederhecker, G. S., Fragnito, H. L., . . . Khelif, A. (2006). Stimulated Brillouin scattering from multi-GHz-guided acoustic phonons in nanostructured photonic crystal fibres. *Nat Phys*, 2(6), 388-392. doi: http://www.nature.com/nphys/journal/v2/n6/supinfo/nphys315_S1.html
- Dainese, P., Russell, P. S. J., Wiederhecker, G. S., Joly, N., Fragnito, H. L., Laude, V., & Khelif, A. (2006). Raman-like light scattering from acoustic phonons in photonic crystal fiber. *Optics Express*, 14(9), 4141-4150. doi: 10.1364/OE.14.004141

- Degnan, J. J. (1995). Optimization of passively Q-switched lasers. *Quantum Electronics, IEEE Journal of*, 31(11), 1890-1901.
- Delgado-Pinar, M., Zalvidea, D., Diez, A., Perez-Millan, P., & Andres, M. (2006). Q-switching of an all-fiber laser by acousto-optic modulation of a fiber Bragg grating. *Optics Express*, 14(3), 1106-1112.
- Dennis, M. L., & Duling III, I. N. (1994). Experimental study of sideband generation in femtosecond fiber lasers. *Quantum Electronics, IEEE Journal of*, 30(6), 1469-1477.
- Desurvire, E. (2002). *Erbium-doped fiber amplifiers: principles and applications*: Wiley-Interscience.
- Dinu, M., Quochi, F., & Garcia, H. (2003). Third-order nonlinearities in silicon at telecom wavelengths. *Applied Physics Letters*, 82(18), 2954-2956.
- Dong, B., Hao, J., Hu, J., & Liaw, C.-y. (2011). Short linear-cavity Q-switched fiber laser with a compact short carbon nanotube based saturable absorber. *Optical Fiber Technology*, 17(2), 105-107.
- Dudley, J. M., Provino, L., Grossard, N., Maillotte, H., Windeler, R. S., Eggleton, B. J., & Coen, S. (2002). Supercontinuum generation in air-silica microstructured fibers with nanosecond and femtosecond pulse pumping. *JOSA B*, 19(4), 765-771.
- Duling, I., Chen, C., Wai, P., & Menyuk, C. (1994). Operation of a nonlinear loop mirror in a laser cavity. *IEEE journal of quantum electronics*, 30(1), 194-199.
- Duling III, I. N. (2006). *Compact sources of ultrashort pulses* (Vol. 18): Cambridge University Press.
- El-Sherif, A. F., & King, T. A. (2003). High-energy, high-brightness Q-switched Tm 3+-doped fiber laser using an electro-optic modulator. *Optics Communications*, 218(4), 337-344.
- Elim, H., Ji, W., Ma, G., Lim, K., Sow, C., & Huan, C. (2004). Ultrafast absorptive and refractive nonlinearities in multiwalled carbon nanotube films. *Applied Physics Letters*, 85(10), 1799-1801.
- Englender, J., Beregi, J. P., Fayoux, D., Astier, R., Perennec, J., Antonetti, A., & Lecarpentier, Y. (1992). Stretched nanosecond pulses of a Q-switched Nd-YAG laser: Transmission through optical fibres and in vitro effects on human calcified tissues. *Lasers in Medical Science*, 7(1-4), 467-476. doi: 10.1007/BF02594090

- Feng, X., Tam, H.-y., & Wai, P. (2006). Stable and uniform multiwavelength erbium-doped fiber laser using nonlinear polarization rotation. *Optics Express*, *14*(18), 8205-8210.
- Fotiadi, A. A., Ikiades, A., Vainos, N. A., Deparis, O., & Kiyan, R. V. (1999). *Q-switching dynamics in SBS/Er fiber laser with low-power pump*. Paper presented at the Photonics East'99.
- Genty, G., & Dudley, J. M. (2009). Route to coherent supercontinuum generation in the long pulse regime. *Quantum Electronics, IEEE Journal of*, *45*(11), 1331-1335.
- Geusic, J., Marcos, H., & Van Uitert, L. (1964). Laser oscillations in Nd-doped yttrium aluminum, yttrium gallium and gadolinium garnets. *Applied Physics Letters*, *4*(10), 182-184.
- Ghatak, A., & Thyagarajan, K. (1998). *An introduction to fiber optics*: Cambridge university press.
- Gupta, K. K., Onodera, N., Abedin, K. S., & Hyodo, M. (2002). Pulse repetition frequency multiplication via intracavity optical filtering in AM mode-locked fiber ring lasers. *Photonics Technology Letters, IEEE*, *14*(3), 284-286.
- Hargrove, L., Fork, R., & Pollack, M. (1964). Locking of He-Ne laser modes induced by synchronous intracavity modulation. *Applied Physics Letters*, *5*(1), 4-5.
- Hartl, I., Li, X., Chudoba, C., Ghanta, R., Ko, T., Fujimoto, J., . . . Windeler, R. (2001). Ultrahigh-resolution optical coherence tomography using continuum generation in an air-silica microstructure optical fiber. *Optics letters*, *26*(9), 608-610.
- Harun, S., Ismail, M., Ahmad, F., Ismail, M., Nor, R., Zulkepely, N., & Ahmad, H. (2012). A Q-switched erbium-doped fiber laser with a carbon nanotube based saturable absorber. *Chinese Physics Letters*, *29*(11), 114202.
- Harun, S., Shahi, S., & Ahmad, H. (2010). Brillouin fiber laser with a 49 cm long Bismuth-based erbium-doped fiber. *Laser Physics Letters*, *7*(1), 60-62.
- Hasan, T., Sun, Z., Wang, F., Bonaccorso, F., Tan, P. H., Rozhin, A. G., & Ferrari, A. C. (2009). Nanotube-polymer composites for ultrafast photonics. *Advanced Materials*, *21*(38-39), 3874-3899.
- Haus, H. A. (2000). Mode-locking of lasers. *IEEE Journal of Selected Topics in Quantum Electronics*, *6*(6), 1173-1185.

- Hellwarth, R. (1961). *Control of fluorescent pulsations*. Paper presented at the Advances in quantum electronics.
- Hirao, K., & Miura, K. (1998). Writing waveguides and gratings in silica and related materials by a femtosecond laser. *Journal of non-crystalline solids*, 239(1), 91-95.
- Hönninger, C., Paschotta, R., Morier-Genoud, F., Moser, M., & Keller, U. (1999). Q-switching stability limits of continuous-wave passive mode locking. *JOSA B*, 16(1), 46-56.
- Huang, J., Huang, W., Zhuang, W., Su, K., Chen, Y., & Huang, K. (2009). High-pulse-energy, passively Q-switched Yb-doped fiber laser with AlGaInAs quantum wells as a saturable absorber. *Optics letters*, 34(15), 2360-2362.
- Huang, J., Zhuang, W., Huang, W., Su, K., Huang, K., & Chen, Y. (2011). Hybrid Q-switched Yb-doped fiber laser. *Optics Express*, 19(10), 9364-9370.
- Humbert, G., Wadsworth, W., Leon-Saval, S., Knight, J., Birks, T., St J Russell, P., . . . Breuer, E. (2006). Supercontinuum generation system for optical coherence tomography based on tapered photonic crystal fibre. *Optics Express*, 14(4), 1596-1603.
- Iijima, S. (1991). Helical microtubules of graphitic carbon. *nature*, 354(6348), 56-58.
- Jackson, J. D., & Jackson, J. D. (1962). *Classical electrodynamics* (Vol. 3): Wiley New York etc.
- Jasim, A., Harun, S., Lim, K., Rahman, B., & Ahmad, H. (2012). Microfibre Mach-Zehnder interferometer and its application as a current sensor. *Optoelectronics, IET*, 6(6), 298-302.
- Javan, A., Bennett Jr, W., & Herriott, D. (2013). Population Inversion and Continuous Optical Maser Oscillation in a Gas Discharge. *Essentials of Lasers: The Commonwealth and International Library: Selected Readings in Physics*, 167.
- Jonsson, F. (2003). Lecture Notes on.
- Junqing, Z., Peiguang, Y., Shuangchen, R., Yongqin, Y., Geguo, D., Gelin, Z., . . . Jie, L. (2012). Multi-wavelength graphene-based Q-switched erbium-doped fiber laser. *Optical Engineering*, 51(7), 074201-074201-074201-074204.

- Jusoh, Z., Shahabuddin, N., Ali, N., Ahmad, H., & Harun, S. (2013). Nanosecond Pulse Generation Using the Stimulated Brillouin Scattering Effect in a Photonic Crystal Fiber. *Chinese Physics Letters*, 30(11), 114204.
- Kaminski, C., Watt, R., Elder, A., Frank, J., & Hult, J. (2008). Supercontinuum radiation for applications in chemical sensing and microscopy. *Applied Physics B*, 92(3), 367-378.
- Kang, M. S., Brenn, A., Wiederhecker, G. S., & Russell, P. S. J. (2008). Optical excitation and characterization of gigahertz acoustic resonances in optical fiber tapers. *Applied Physics Letters*, 93(13), 131110.
- Kawamura, K., Ogawa, T., Sarukura, N., Hirano, M., & Hosono, H. (2000). Fabrication of surface relief gratings on transparent dielectric materials by two-beam holographic method using infrared femtosecond laser pulses. *Applied Physics B*, 71(1), 119-121.
- Keller, U. (2003). Recent developments in compact ultrafast lasers. *nature*, 424(6950), 831-838.
- Kennedy, J. T., Hart, R. A., Laughman, L., Fontanella, J., Demaria, A. J., Newman, L. A., & Henschke, R. (2004). Q-switched cavity dumped CO₂ laser for material processing: Google Patents.
- Kivshar, Y. S., Emplit, P., Hamaide, J.-P., & Haelterman, M. (1994). Gordon–Haus effect on dark solitons. *Optics letters*, 19(1), 19-21.
- Kneis, C., Donelan, B., Berrou, A., Manek-Hönninger, I., Cadier, B., Robin, T., ... & Kieleck, C. (2015). 4.5 W mid-infrared supercontinuum generation in a ZBLAN fiber pumped by a Q-switched mode-locked Tm³⁺-doped fiber laser. *SPIE LASE* (pp. 93420B-93420B). International Society for Optics and Photonics.
- Komarov, A., Leblond, H., & Sanchez, F. (2006). Passive harmonic mode-locking in a fiber laser with nonlinear polarization rotation. *Optics Communications*, 267(1), 162-169. doi: <http://dx.doi.org/10.1016/j.optcom.2006.06.012>
- Lacroix, S., Gonthier, F., Black, R. J., & Bures, J. (1988). Tapered-fiber interferometric wavelength response: the achromatic fringe. *Optics letters*, 13(5), 395-397. doi: 10.1364/OL.13.000395
- Lamminpää, A. (2003). Measurement of nonlinearity of optical fiber. *Helsinki university of technology, Master thesis, 17th of July*.

- Laroche, M., Gilles, H., Girard, S., Passilly, N., & Aït-Ameur, K. (2006). Nanosecond pulse generation in a passively Q-switched Yb-doped fiber laser by Cr 4+: YAG saturable absorber. *Photonics Technology Letters, IEEE*, 18(6), 764-766.
- Lee, J., Koo, J., Debnath, P., Song, Y.-W., & Lee, J. H. (2013). A Q-switched, mode-locked fiber laser using a graphene oxide-based polarization sensitive saturable absorber. *Laser Physics Letters*, 10(3), 035103.
- Lim, S., Elim, H., Gao, X., Wee, A., Ji, W., Lee, J., & Lin, J. (2006). Electronic and optical properties of nitrogen-doped multiwalled carbon nanotubes. *Physical Review B*, 73(4), 045402.
- Lin, X. C., Zhang, L., Tsang, Y. H., Wang, Y. G., Yu, H. J., Yan, S. L., . . . Hou, W. (2013). Multi-walled carbon nanotube as a saturable absorber for a passively mode-locked Nd: YVO₄ laser. *Laser Physics Letters*, 10(5), 055805.
- Liu, X. (2010). Mechanism of high-energy pulse generation without wave breaking in mode-locked fiber lasers. *Physical Review A*, 82(5), 053808.
- Luo, Z., Luo, A., Xu, W., Song, C., Gao, Y., & Chen, W. (2009). Sideband controllable soliton all-fiber ring laser passively mode-locked by nonlinear polarization rotation. *Laser Physics Letters*, 6(8), 582.
- Luo, Z., Zhou, M., Weng, J., Huang, G., Xu, H., Ye, C., & Cai, Z. (2010). Graphene-based passively Q-switched dual-wavelength erbium-doped fiber laser. *Optics letters*, 35(21), 3709-3711.
- Maiman, T. H. (1960). Stimulated optical radiation in ruby.
- McGrath, A. J., Munch, J., Smith, G., & Veitch, P. (1998). Injection-seeded, single-frequency, Q-switched erbium: glass laser for remote sensing. *Applied Optics*, 37(24), 5706-5709.
- Mears, R., Reekie, L., Poole, S., & Payne, D. (1986). Low-threshold tunable CW and Q-switched fibre laser operating at 1.55 μm . *Electronics Letters*, 22(3), 159-160.
- Mikulla, B., Leng, L., Sears, S., Collings, B., Arend, M., & Bergman, K. (1999). Broad-band high-repetition-rate source for spectrally sliced WDM. *IEEE Photonics Technology Letters*, 11(4), 418-420.
- Mills, D. (1991). *Nonlinear optics*: Springer Berlin etc.

- Milonni, P. W., & Eberly, J. H. (2010). Laser physics. from <http://www.books24x7.com/marc.asp?bookid=43238>
- Mocker, H. W., & Collins, R. (1965). Mode competition and self-locking effects in aq-switched ruby laser. *Applied Physics Letters*, 7(10), 270-273.
- Morioka, T., Takara, H., Kawanishi, S., Kamatani, O., Takiguchi, K., Uchiyama, K., . . . Kanamori, T. (1996). 1 Tbit/s (100 Gbit/s× 10 channel) OTDM/WDM transmission using a single supercontinuum WDM source. *Electronics Letters*, 32(10), 906-907.
- Muhammad, M. Z., Jasim, A. A., Ahmad, H., Arof, H., & Harun, S. W. (2013). Non-adiabatic silica microfiber for strain and temperature sensors. *Sensors and Actuators A: Physical*, 192(0), 130-132. doi: <http://dx.doi.org/10.1016/j.sna.2012.12.036>
- Nakazawa, M., Kubota, H., Sahara, A., & Tamura, K. (1998). Time-domain ABCD matrix formalism for laser mode-locking and optical pulse transmission. *Quantum Electronics, IEEE Journal of*, 34(7), 1075-1081.
- Neev, J., Da Silva, L. B., Feit, M. D., Perry, M. D., Rubenchik, A. M., & Stuart, B. C. (1996). Ultrashort pulse lasers for hard tissue ablation. *Selected Topics in Quantum Electronics, IEEE Journal of*, 2(4), 790-800.
- Nelson, L., Jones, D., Tamura, K., Haus, H., & Ippen, E. (1997). Ultrashort-pulse fiber ring lasers. *Applied Physics B: Lasers and Optics*, 65(2), 277-294.
- Nicholson, J., Abeeluck, A., Headley, C., Yan, M., & Jørgensen, C. (2003). Pulsed and continuous-wave supercontinuum generation in highly nonlinear, dispersion-shifted fibers. *Applied Physics B*, 77(2-3), 211-218.
- Nikles, M., Thévenaz, L., & Robert, P. A. (1997). Brillouin gain spectrum characterization in single-mode optical fibers. *Lightwave Technology, Journal of*, 15(10), 1842-1851.
- Nikles, M., Thévenaz, L., & Robert, P. A. (1996). Simple distributed fiber sensor based on Brillouin gain spectrum analysis. *Optics letters*, 21(10), 758-760.
- Nodop, D., Limpert, J., Hohmuth, R., Richter, W., Guina, M., & Tünnermann, A. (2007). High-pulse-energy passively Q-switched quasi-monolithic microchip lasers operating in the sub-100-ps pulse regime. *Optics letters*, 32(15), 2115-2117.
- Palais, J. C. (1988). *Fiber optic communications*: Prentice Hall Englewood Cliffs.

- Pan, L., Utkin, I., & Fedosejevs, R. (2007). Passively Q-switched ytterbium-doped double-clad fiber laser with a Cr 4+: YAG saturable absorber. *Photonics Technology Letters, IEEE*, 19(24), 1979-1981.
- Poole, S., Payne, D. N., & Fermann, M. E. (1985). Fabrication of low-loss optical fibres containing rare-earth ions. *Electronics Letters*, 21(17), 737-738.
- Popa, D., Sun, Z., Hasan, T., Torrisi, F., Wang, F., & Ferrari, A. (2010). Graphene Q-switched, tunable fiber laser. *arXiv preprint arXiv:1011.0115*.
- Ramadurai, K., Cromer, C. L., Lewis, L. A., Hurst, K. E., Dillon, A. C., Mahajan, R. L., & Lehman, J. H. (2008). High-performance carbon nanotube coatings for high-power laser radiometry. *Journal of Applied Physics*, 103(1), 013103.
- Reutebuch, S. E., Andersen, H.-E., & McGaughey, R. J. (2005). Light detection and ranging (LIDAR): an emerging tool for multiple resource inventory. *Journal of Forestry*, 103(6), 286-292.
- Ruffin, A. B. (2004). *Stimulated Brillouin scattering: an overview of measurements, system impairments, and applications*. Paper presented at the Technical Digest: Symposium on Optical Fiber Measurements.
- Russell, P. S. J. (2006). Photonic-Crystal Fibers. *Lightwave Technology, Journal of*, 24(12), 4729-4749. doi: 10.1109/JLT.2006.885258
- Shahabuddin, N., Awang, N., Ahmad, H., Arof, H., Dimyati, K., Yusoff, Z., & Harun, S. (2012). Supercontinuum generation using a passive mode-locked stretched-pulse bismuth-based erbium-doped fiber laser. *Optics & Laser Technology*, 44(4), 741-743.
- Shank, C., & Ippen, E. (1974). Subpicosecond kilowatt pulses from a mode-locked cw dye laser. *Applied Physics Letters*, 24(8), 373-375.
- Shee, Y., Mahdi, M., Al-Mansoori, M., Ismail, A., Hambali, N., Zamzuri, A., . . . Yaakob, S. (2009). Threshold reduction of stimulated Brillouin scattering in photonic crystal fiber. *Laser physics*, 19(12), 2194-2196.
- Shi, K. (2007). *Supercontinuum imaging and spectroscopy*: ProQuest.
- Shibata, N., Azuma, Y., Horiguchi, T., & Tateda, M. (1988). Identification of longitudinal acoustic modes guided in the core region of a single-mode optical fiber by Brillouin gain spectra measurements. *Optics letters*, 13(7), 595-597.

- Shirazi, M., Harun, S., Biglary, M., & Ahmad, H. (2008). Linear cavity Brillouin fiber laser with improved characteristics. *Optics letters*, 33(8), 770-772.
- Siegman, A. E. (1986). Lasers University Science Books. *Mill Valley, CA*, 37.
- Smith, R. G. (1972). Optical power handling capacity of low loss optical fibers as determined by stimulated Raman and Brillouin scattering. *Applied Optics*, 11(11), 2489-2494.
- Snitzer, E. (1961). Optical maser action of Nd³⁺ in a barium crown glass. *Physical Review Letters*, 7(12), 444.
- Sobon, G., Sotor, J., Jagiello, J., Kozinski, R., Librant, K., Zdrojek, M., . . . Abramski, K. M. (2012). Linearly polarized, Q-switched Er-doped fiber laser based on reduced graphene oxide saturable absorber. *Applied Physics Letters*, 101(24), 241106.
- Sotor, J., Sobon, G., Krzempek, K., & Abramski, K. M. (2012). Fundamental and harmonic mode-locking in erbium-doped fiber laser based on graphene saturable absorber. *Optics communications*, 285(13), 3174-3178.
- Spühler, G., Paschotta, R., Fluck, R., Braun, B., Moser, M., Zhang, G., . . . Keller, U. (1999). Experimentally confirmed design guidelines for passively Q-switched microchip lasers using semiconductor saturable absorbers. *JOSA B*, 16(3), 376-388.
- Su, L., Wang, Y., Liu, J., Zheng, L., Su, L., & Xu, J. (2012). Double-wall carbon nanotube absorber for passively mode-locked Yb³⁺: Sc₂SiO₅ laser. *Laser Physics Letters*, 9(2), 120-125.
- Svelto, O. (2010). Properties of laser beams *Principles of Lasers* (pp. 475-504): Springer.
- Tiu, Z. C., Tan, S. J., Ahmad, H., & Harun, S. W. (2014). Dark pulse emission in nonlinear polarization rotation-based multiwavelength mode-locked erbium-doped fiber laser. *Chinese Optics Letters*, 12(11), 113202.
- van Saarloos, W., & Hohenberg, P. (1992). Fronts, pulses, sources and sinks in generalized complex Ginzburg-Landau equations. *Physica D: Nonlinear Phenomena*, 56(4), 303-367.
- Weiner, A., Heritage, J., Hawkins, R., Thurston, R., Kirschner, E., Leaird, D., & Tomlinson, W. (1988). Experimental observation of the fundamental dark soliton in optical fibers. *Physical Review Letters*, 61(21), 2445.

- Wong, T.-H., Gupta, M. C., & Hernandez-Garcia, C. (2007). Nanosecond laser pulse-induced electron emission from multiwall carbon nanotube film. *Nanotechnology*, *18*(13), 135705.
- Wood, T. C., & Elson, D. S. (2012). A tunable supercontinuum laser using a digital micromirror device. *Measurement Science and Technology*, *23*(10), 105204.
- Woodward, R., Kelleher, E., Popov, S., & Taylor, J. (2014). Stimulated Brillouin scattering of visible light in small-core photonic crystal fibers. *Optics letters*, *39*(8), 2330-2333.
- Wu, X., Tang, D., Zhang, H., & Zhao, L. (2009). Dissipative soliton resonance in an all-normal-dispersion erbium-doped fiber laser. *Optics Express*, *17*(7), 5580-5584.
- Xu, C., Liu, X., & Wei, X. (2004). Differential phase-shift keying for high spectral efficiency optical transmissions. *Selected Topics in Quantum Electronics, IEEE Journal of*, *10*(2), 281-293.
- Yang, K., Zhao, S., Li, G., Li, M., Li, D., Wang, J., & An, J. (2007). Diode-pumped passively Q-switched mode-locked c-cut Nd: GdVO₄ laser with a GaAs coupler. *Optical Materials*, *29*(9), 1153-1158.
- Yoshizawa, N., & Imai, T. (1993). Stimulated Brillouin scattering suppression by means of applying strain distribution to fiber with cabling. *Lightwave Technology, Journal of*, *11*(10), 1518-1522.
- Zajac, A., Skorczakowski, M., Swiderski, J., & Nyga, P. (2004). Electrooptically Q-switched mid-infrared Er: YAG laser for medical applications. *Optics Express*, *12*(21), 5125-5130.
- Zakharov, V., & Shabat, A. (1973). Interaction between solitons in a stable medium. *Sov. Phys. JETP*, *37*(5), 823-828.
- Zhang, H., Tang, D., Zhao, L., & Wu, X. (2009). Dark pulse emission of a fiber laser. *Physical Review A*, *80*(4), 045803.
- Zhang, L., Wang, Y., Yu, H., Sun, L., Hou, W., Lin, X., & Li, J. (2011). Passive mode-locked Nd: YVO₄ laser using a multi-walled carbon nanotube saturable absorber. *Laser physics*, *21*(8), 1382-1386.
- Zhao, L. M., Tang, D. Y., Cheng, T. H., & Lu, C. (2007). Nanosecond square pulse generation in fiber lasers with normal dispersion. *Optics Communications*, *272*(2), 431-434. doi: <http://dx.doi.org/10.1016/j.optcom.2006.11.035>

Zhou, W., Bai, X., Wang, E., & Xie, S. (2009). Synthesis, Structure, and Properties of Single-Walled Carbon Nanotubes. *Advanced Materials*, 21(45), 4565-4583.

LIST OF PUBLICATIONS

- Zarei, A.**, Jasim, A. A., Harun, S. W., & Ahmad, H. (2014). Investigation of spontaneous Brillouin scattering generation based on non-adiabatic microfibres. *Laser Physics Letters*, *11*(12), 125105.
- Zarei, A.**, Rosdin, R. Z. R. R., Ali, N. M., Ahmad, H., & Harun, S. W. (2014). Brillouin Lasing with a Reduced Self-Pulsing Characteristic Using a Short-Length Erbium-Doped Fiber as the Nonlinear Gain Medium. *Chinese Physics Letters*, *31*(5), 054202.
- Tiu, Z. C., Tan, S. J., **Zarei, A.**, Ahmad, H., & Harun, S. W. (2014). Nonlinear Polarization Rotation-Based Mode-Locked Erbium-Doped Fiber Laser with Three Switchable Operation States. *Chinese Physics Letters*, *31*(9), 094206.
- Tiu, Z. C., Ahmad, F., Tan, S. J., **Zarei, A.**, Ahmad, H., & Harun, S. W. (2014). Multi-wavelength Q-switched Erbium-doped fiber laser with photonic crystal fiber and multi-walled carbon nanotubes. *Journal of Modern Optics*, *61*(14), 1133-1139.
- Tiu, Z. C., **Zarei, A.**, Tan, S. J., Ahmad, H., & Harun, S. W. (2014). Q-Switching Pulse Generation with Thulium-Doped Fiber Saturable Absorber. *Chinese Physics Letters*, *31*(12), 124203.
- Zarei, A.**, Tiu, Z. C., Ahmad, F., Ahmad, H., & Harun, S. W. (2015). Q-switched Brillouin fibre laser with multi-wall carbon nanotube saturable absorber. *IET Optoelectronics*, *9*(2), 96-100.
- Zian, C. T., **Arman. Z.**, Sin, J. T., Harith, A., & Sulaiman, W. H. (2015). Harmonic Dark Pulse Emission in Erbium-Doped Fiber Laser. *Chinese Physics Letters*, *32*(3), 034203.
- Z.C. Tiu, M. Suthaskumar, **A. Zarei**, S.J. Tan , H. Ahmad, S.W. Harun (2015). Generation of switchable domain wall and Cubic–Quintic nonlinear Schrödinger equation dark pulse. *Optics & Laser Technology* *73* 127–129
- Rosdin, R. Z. R. R., **Zarei, A.**, Ali, N. M., Arof, H., Ahmad, H., & Harun, S. W. (2015, January). Fundamental and harmonic soliton mode-locked erbium-doped fiber laser using a single-walled carbon nanotubes embedded in poly (ethylene oxide) film saturable absorber. In *International Seminar on Photonics, Optics, and Applications 2014* (pp. 94440I-94440I). International Society for Optics and Photonics.

APPENDIX

A selection of published works are attached in this appendix